MODELLING AND ENERGY EFFICIENCY ANALYSIS OF A SCROLL TYPE AIR MOTOR

Thesis submitted in accordance with the requirements of the University of Liverpool for the degree of Doctor in Philosophy

by

Li Yang

December 2008

ABSTRACT

This thesis presents the development of a comprehensive mathematical model for a scroll air motor, and energy efficiency analysis of a scroll air motor based on the mathematical model.

The mathematical model includes the geometry, thermodynamics, and mechanics of a scroll air motor. Intrinsic equations are used to construct the scrolls. Green's Theorem is used to calculate the chamber cross section areas. Newton's second law of rotational motion is used to calculate the angular speed. First law of thermodynamics and compressible flow in an open control volume are used to calculate the dynamic processes. The model can be used to perform parametric study and optimise the design.

Based on the mathematic model, in conjunction with the definition of air power, the energy efficiency analysis for a scroll air motor is given in this thesis. As the benefit of the unique structure, a scroll air motor is able to utilise both transmission energy and expansion energy carried by compressed air, while a normal pneumatic actuator, such as pneumatic cylinders and vane type air motors, utilises the transmission energy only. And expansion energy takes more than 50% of compressed air energy, if the pressure is greater than 5 bar. The analysis shows that a scroll air motor is highly effective in energy conversion and is able to work at higher

energy efficiency than traditional pneumatic actuators under appropriate conditions.

An experimental system was built to validate the mathematical model and the experimental results are in agreement with those produced by simulation.

The results of the investigations and analysis are used to make recommendations for future study of a scroll type air motor and its energy efficiency.

CONTENTS

LIST OF FIGURES

Number *Page*

ACKNOWLEGEMENT

I would like to express my gratitude to all who gave me the possibility to complete my PhD study. I want to thank Dr. Stephen Mangan, Mr. James W Derby, and Mr. Iain Henshaw from Energetix Group PLC for their support.

I would appreciate my supervisor Dr. Jihong Wang whose stimulating suggestions and encouragement helped me at all the times during the last four years.

I would also like to thank Prof. Q. H. Wu for his help in need.

Finally, I would thank Dr. Lin Jiang and Prof. Philip Moore for their advice on writing this thesis.

SYMBOLS

Symbol	Description	Unit
$\mathbf{A}, \mathbf{B}, \tilde{\mathbf{A}}, \tilde{\mathbf{B}}$	Scroll surfaces	
A	Area	m^2
A_f	Gap area of flank leakage	m^2
A_r	Gap area of radius leakage	m^2
C	Centre of curvature	
C_0	Flow constant	
C_d	Discharge coefficient	
C_k	Calculated constant	
C_p	Specific heat at constant pressure	
C_r	Critical pressure ratio	
C_V	Specific heat at constant specific volume	
$\mathbf{D}$	Orbit of moving scroll	
e	Available energy per unit mass of air at atmospheric temperature	J
E	Energy	J
$\dot{E}$	Energy flux	*watt*
E_{CV}	Energy in control volume	J
$\mathbf{F}$	Force	N
F_s	Static friction	N
F_c	Coulomb friction	N
g	Gravity acceleration	m/s^2
h	Enthalpy of a unit mass of air	J/kg

h_w	Scroll wall thickness parameter	m
$\mathbf{I}$	Moment of inertia	$kg \cdot m^2$
M, m	mass	kg
$\dot{m}_{in}$	Inward mass flow rate	kg/s
$\dot{m}_{out}$	Outward mass flow rate	kg/s
O	Origin of axes	
p	Pressure (absolute)	N/m^2
p_{atm}	Atmospheric air pressure	N/m^2
p_d	Downstream pressure (absolute)	N/m^2
p_e	Exhaust pressure (absolute)	N/m^2
p_s	Air supply pressure (absolute)	N/m^2
p_u	Upstream pressure (absolute)	N/m^2
P	Power	$watt$
P_t	Transmission power of air	$watt$
P_e	Expansion power of air	$watt$
Q	Volumetric flow rate	m^3/s
$\dot{Q}$	Work done to the control volume	J
R	Gas constant	$J/K \cdot kg$
r	Radius of the orbit	m
$\mathbf{r}$	Vector from the axis of rotation to the point on which the force is acting	
s	Length of spiral segment	m
t	time	s
T	Temperature	K
v	Velocity	m/s

U_{CV}	Internal energy of a control volume	J
V	Volume	m^3
V_c	Volume of charge chamber	m^3
V_d	Volume of discharge chamber	m^3
V_e	Volume of exhaust chamber	m^3
V_s	Volume of side/expansion chamber	m^3
W	Work	J
x, y	Horizontal, vertical coordinate	m
x_0	Initial value of horizontal coordinate	m
y_0	Initial value of vertical coordinate	m
z	Height of scroll walls	m
α	Orbit angle of moving scroll	deg
α_d	Start orbit angle of discharge process	deg
α_s	End orbit angle of expansion process	deg
γ	Specific heat	
δ	Thickness of scroll wall	m
δ_f	Flank leakage gap	m
δ_r	Radius leakage gap	m
η	Efficiency	%
κ	Slope of the radius of curvature	
μ	Friction coefficient	
π	Ratio of a circle's circumference to its diameter	
ρ	Radius of curvature	m
ρ_0	Initial value of radius of curvature	m
τ, Γ	torque	Nm

φ, ϕ	Tangential angle of a spiral	deg
ω	Angular speed	deg/ s

ABBREVIATIONS

Symbol	Description
AC	Alternating Current
CASCES	Compressed Air and Supercapacitors Energy Storage
C-E	Compressor-Expander system
DAQ	Data Acquisition
Micro CHP	Micro Combined Heat and Power system
NI	National Instruments
RMS	Root Mean Square value
UPS	Uninterrupted Power Supply
VI	Virtual Instrumentation

Chapter1

Introduction

1.1 Background of the research project

Compressed air, as a kind of clean and safe energy, is widely used in all aspects of modern industry. It is the most common gas used in industry, though nitrogen is occasionally used (Lin-Chen 2001). It is non-hazardous, readily available, can be stored easily and is convenient source of power for a range of machines and tools. Compared with hydraulic and electrical counterparts, pneumatic systems are environment friendly, cleaner, simpler, easier in maintenance and safer. They can work in harsh environments, work without sparks, stall without damages. In food, timber/wood, textile and other industries, where safety considerations, environmental constraints, high duty cycle or relatively low-precision profile following tasks are involved, pneumatic systems are the best choice of power. Nowadays, compressed air systems take up a significant part of the total electricity consumption in manufacturing industry. In 1998, in Japan, pneumatic systems consumed 10% to 20% of the total electricity supplied to factories, reaching 40 billion kilowatt hour (Cai & Kagawa 2001). That was approximately 5% of the national total electricity consumed in Japan (Cai, Kawashima & Kagawa 2006). In 2006, Irish Energy Centre found approximately 10% of all electrical power in industry

is employed in compressing air ('Compressed Air Case Studies' 2006). In 2003, the Energy Institution found compressed air represented over 10% percent of all the industrial electricity consumed. It cost at least 50p per kwh at the point of generation ('Saving Energy in Compressed Air Systems' 2003). In Australia, Champion Compressor claims that around 10 percent of the power generated is used to compress air ('Counting the cost of compressed air' 2006).

Customers are becoming aware that pneumatic actuators are comparatively expensive to operate due to its lower energy efficiency. In fact, energy efficiency of pneumatic actuators is often lower than 20%, which is much lower than its electrical counterparts, 60% (Cai, Kagawa & Kawashima 2002). Users have realised that some irreversible processes, such as air leaks, frictions, pressure losses through dryers, filters, etc as well as improper settings and operation account for energy waste of pneumatic systems. Due to these affects, the end-to-end efficiency of a compressed air driven system is only around 10 percent ('Counting the cost of compressed air' 2006). It is very urgent to improve energy efficiency of pneumatic systems.

There are already some effective methods to save energy in compressed air. Intuitively, most users are making efforts in reducing air consumption of the pneumatic equipments in their plants (Yang et al. 2008a). Reducing leakage is the first option as it counts significant amount of energy in an

industrial compressed air system, sometimes up to 20% - 30% of a compressor output ('Compressed Air Case Studies' 2006). Air audit is used to measure air demand, so that compressors with proper size and proper site layout will be chosen ('Compressed Air Case Studies' 2006) ('Saving Energy in Compressed Air Systems' 2003) ('Counting the cost of compressed air' 2006). Optimal control algorithms provide energy saving methods without modifying hardware of a pneumatic system (Ke et al. 2005; Ke, Wang & Yang 2006). Secondly, using waste heat generated by compressors to supplement or reduce the demand on other forms of heating is feasible ('Saving Energy in Compressed Air Systems' 2003). Thirdly, effective utilisation of the exhaust air by improving drive systems can also save energy. (Yang et al. 2008a) reported by-pass valve control for asymmetric cylinder can save 12-28% in energy and improve control performance of the system.

Beside the above, using pneumatic actuators with high ability of energy conversion such as scroll type air motor is another method to save energy (Gao Xiaojun et al. 2004; Yang, Wang & Ke 2006).

A scroll type air motor, also known as a scroll expander is a relatively new concept for pneumatic actuation. Its unique structure features it many advantages as well as higher energy efficiency than conventional pneumatic actuators, such as cylinders, vane-type air motors, and *etc.* The scroll technique is now mainly and widely implemented in air conditioner

and refrigerator compressors, because its compact design matches the requirements of small, quiet, and highly efficient refrigeration compressors. Recently, the concept was re-invented to air motors. Instead of compressing air to raise pressure, the air motors or expanders release the high pressure air energy to a driving force, which makes it a suitable actuator for electric power generation.

Based on the air motor - generator technology, a new heating system called Micro Combined Heat and Power system (Micro CHP) was introduced by some manufacturers, such as Honda and Climate Energy ('Powergen MicroCHP' 2005) (Mayer 2005) (Crozier & Jones 2002). Micro CHPs are used to generate electric power while heating a house and invert surplus electric power to the grid. It was claimed that up to 95% of available fuel energy can be used (Mayer 2005). British Gas had been testing the system in the UK. It is claimed that people can save £150-200 a year on combined gas and electricity bills, which is about a 20% reduction. Micro CHP system aligns with British government's policy because there are 12 million suitable homes in the UK and the system can help the people to reduce 33 million tones of CO_2 annually. Because the advantages, scroll expanders are ideal drive for Micro CHP generators. Energetix Group introduced their new generation of UPS featuring scroll expander driven generator ('Pnu Power' 2006). Scroll air motors can also be used to recover work in fuel cells (Gao Xiaojun et al. 2004).

Research on energy efficiency of a pneumatic actuator usually involves theoretical and experimental methods. Theoretical approaches can give a general idea and guide experimental activities. Furthermore, theoretical methods are much cheaper and less time consuming. A mathematical model represents a useful tool to "run experiments" under conditions and for scenarios that would be very difficult to create in a real experiment. However, not all physical effects can be counted in theoretical analysis. Experimental investigations are often expensive and time consuming, but offer the advantage of allowing for insight into the "real" performance characteristics of the pneumatic actuator. For a scroll air motor, there is not any publication regarding its energy efficiency analysis.

The objective of the research project described in this thesis was to develop a mathematical model for a scroll air motor and analyse its energy efficiency to find out the reason why scroll air motors are able to transform energy more efficiently than other pneumatic actuators and how working conditions affect its energy efficiency.

1.2 Introduction to scroll type air motors

A scroll air motor, also known as a scroll expander, is a relatively new concept for pneumatic actuation. Its unique structure leads the motors to demonstrate energy transformation in a good manner. In recent years, scroll air motors have been adopted by combined heat and power boilers,

uninterrupted power supplies and some other energy storage systems as a new mechatronic device for energy conversion.

The scroll air motor's geometry is one of the main factors influencing energy efficiency of the scroll air motor. In order to create a mathematical model for a scroll air motor, the geometry of the scroll air motor has to be studied firstly and understood thoroughly. Because a scroll air motor is effectively a scroll air compressor working backwards, the geometric characteristics are same as a scroll air compressor. The most common shape for scroll wraps is the involute of a circle. Two methods were found to parameterise scrolls. One is to parameterise a spiral with involute angle; the other is to use tangential angle. Parametric equation approach were widely used to present scrolls (Bush et al. 1992) (Halm 1997) (Zhu 1994) (Lee & Wu 1995) (Chen 2000) (Liu et al. 1996) (Li 1998) (Li 2000). The second method is also call intrinsic equation method that relates the tangential angle with arc length. When this relation is a function, so that tangential angle is given as a function of arc length, certain properties become easy to manipulate. In particular, the derivative of the tangential angle with respect to arc length is equal to the curvature. Intrinsic equations exist in intrinsic coordinate system which is arguably not a true coordinate system, since it describes points on a curve relative to the curve itself rather than the space in which it belongs, and points not on the curve have no intrinsic coordinates. In this thesis, intrinsic equations are used to

describe spirals and Green's Theorem is used to calculate the volume in a chamber.

An equation specifies a curve in terms of intrinsic properties such as arc length, radius of curvature, and tangential angle instead of with reference to artificial coordinate axes. Intrinsic equations are also called natural equations. It specifies a curve independent of any choice of coordinates or parameterisation. The study of natural equations began with the following problem: given two functions of one parameter, find the space curve for which the functions are the curvature and torsion.

Euler gave an integral solution for plane curves, which always have torsion. Call the angle between the tangent line to the curve and the x-axis the tangential angle, then

$$\phi = \int k(s)\,ds$$

where k is the curvature, s is length of arc. Then the equations

$$k = k(s)$$

$$\tau = 0$$

where τ is the torsion, are solved by the curve with parametric equations

$$x = \int \cos\varphi\, ds$$

$$y = \int \sin\varphi\, ds$$

The equations $k = k(s)$ and $\tau = \tau(s)$ are called the natural or intrinsic equations of the space curve. An equation expressing a plane curve in terms of s and curvature, k, is called a Cesàro equation, and an equation expressing a plane curve in terms of s and ϕ is called a Whewell equation.

The investigation of dynamic behaviour of a scroll air motor is very important for analysing mechanical characteristics and energy efficiency. In order to establish a dynamic model of a scroll air motor, the force from compressed air applying on the scrolls and the motion of the moving scroll have to be studied. It has to be said that establishing a model for the dynamic behaviour of the moving part goes hand in hand with establishing a model for the pneumatic and thermal processes. Dynamic models usually include equations of motion for the moving scroll and taking into account gas forces and friction forces. The motion of a moving scroll is a rigid motion. And the orbit can be described by an intrinsic equation as the scrolls (Gravesen & Henriksen 2001).

A cycle from the inlet of the central chamber to the exhaust generally consists of a number of phases/processes, which are not cascaded. The working phases of a scroll air motor are charging phase, expansion phase, and discharging phase. When the compressed air is connected to the air inlet, the orbiting scroll wobbles. The first phase finishes when the central chamber/charging chamber is divided into three parts with two of them to have compressed air isolated from the air supply. The isolated chambers or

pockets will form the consequent phases, expansion phase and discharging phase.

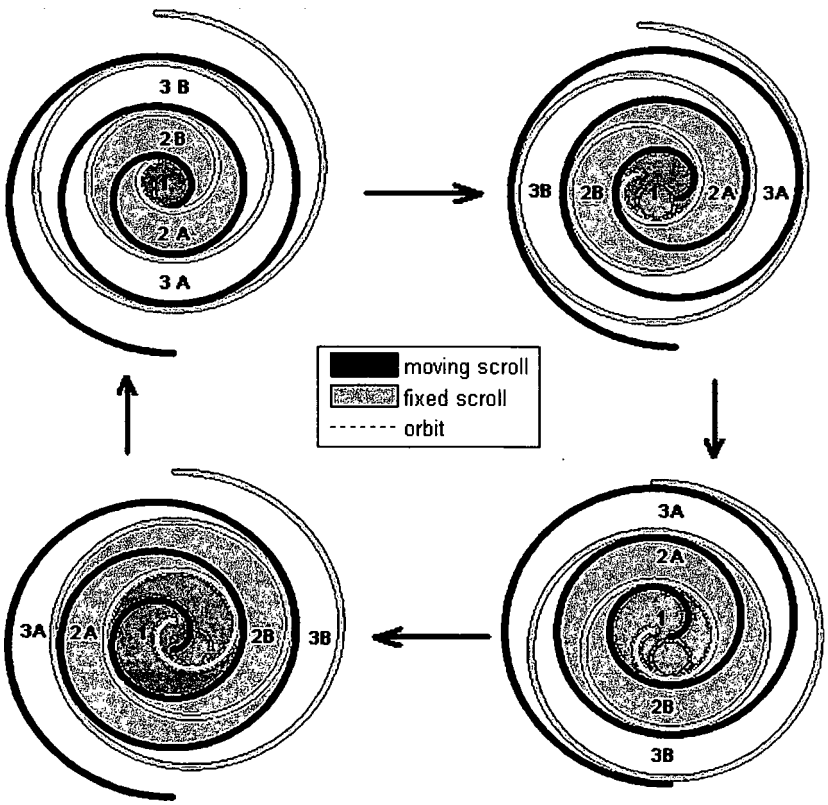

Figure 1.1. Working processes of a scroll air motor

As shown in Figure 1.1, the grey scroll is the fixed scroll and the black one is moving scroll that travels along the orbit anticlockwise when compressed air comes into chamber 1 through the inlet in the centre. Each scroll is fitted to a back plate. As the moving scroll travels along the circle orbit, these two scrolls keep contacting at some points, so that there are even number of crescent chambers. When a scroll air motor is in motion, it

goes successively and repeatedly through the four states shown in the figure following the arrows.

The Charging process starts when compressed air goes into the central chamber of a scroll air motor through the inlet until the central chamber separates into a pair of side chambers. In Figure 1.1, the charging phase starts at the point shown in the upper left diagram of the figure, when compressed air starts entering the central chamber marked "1", the deep grey chamber. There are now four sealed chambers, "2A", "2B", "3A", and "3B". After one quarter of a cycle, the scroll air motor comes to the upper right diagram in, the chamber "1" is getting bigger; chamber "2A", "2B", "3A", and "3B" have rotated anticlockwise and increased in size. It continues through another two quarters of cycle. Then after one complete cycle, the air motor comes back to the diagram in upper right. But the gas started life in chamber "1" is now partially in chamber "2A" and "2B" and got sealed. The inlet was modelled by orifice theory (Wolansky, Nagohosian & Henke 1977). And the dynamics in the central chamber were modelled by behaviours of a control volume.

The expansion process occurs immediately after the charging process. The compressed air is sealed in the pair of side chambers and pushes the moving scroll to move outwards resulting in increase in chamber volume. In Figure 1.1, after the air is sealed in chambers "2A" and "2B" of the upper left diagram, it starts to expand. As the air motor continues through

the second cycle, the air in chamber "2A" and "2B" expand and end up going into chamber "3A" and "3B".

The expansion process can be described by an isentropic process, relating the pressure directly to the expansion chamber volume. However, in the real world, the process is much more complicated than that due to leakage, heat transfer, etc (Halm 1997). Leakage was modelled by air flow through restrictions. The first law of thermodynamics was applied to the expansion chambers in order to calculate the air properties as a function of the orbiting angle.

The discharging process is the last working process for a scroll air motor. It starts when the expansion chambers open to the chamber closed by the housing and connecting to atmosphere via the outlet. Chambers "3A" and "3B" in the two lower diagrams of Figure 1.1 are discharging. This process is the reverse of the charging process, so the equations used in the modelling charging process are appropriate with varying port widths.

Leakage in a scroll air motor can create significant losses. Usually there are two different paths for leakage in a scroll air motor. One is the path formed by a gap between the bottom or the top plate and the scrolls. This kind of leakage is called radial leakage. Another path is formed by a gap between the flanks of the two scrolls and is called flank or tangential leakage. The models used to describe leakage differ from each other in terms of flow

path and flow characteristics assumed. Some models use an isentropic diverging converging nozzle to describe flank leakage flow. It was reported that when the flank clearance exceeded 0.1mm, the volumetric efficiency decreased 87.5% (Tojo 1980). A greater impact of radial leakage than flank leakage was found. The radial leakage was modelled as the flow between two plates. Navier-Stoke equation can also be used to calculate detailed flow field in a clearance (Yong 1994).

Friction is a natural resistance to relative motion between two contacting bodies. It presents in parts with relative motions in every machine. The presence of nonlinear friction forces is unavoidable. In pneumatic actuator systems, friction, both static and dynamic, plays a very important roll. The friction model has been widely studied by numerous researchers, who tried to understand its physics and dynamics (Lin-Chen 2001). It was found that friction might occur at many locations, such as main bearings, crank bearings, sub bearings, moving and fixed scrolls, coupling, shaft etc (Hayano et al. 1988). In fact, friction analysis is very complicated and may be modelled by a forty element equation (Lee & Wu 1995). However the purpose of this research was not to create an accurate model. To simplify the analysis, a simplified friction model introduced by (Lin-Chen 2001) and (Wang et al. 1998) was adopted. It includes kinetic friction and static friction. Furthermore, kinetic friction is more important for the project as it stands for the friction loss when a scroll air motor is running.

Chapter 1 Introduction

Air energy refers to the power transmitted by flowing compressed air. Traditionally, air volume and its flow rate are used to represent air consumption. Although the same method is applicable to hydraulics, it is not appropriate for pneumatics because it is compressible unlike oils. The proposal of air power was introduced by Maolin Cai et al (Cai & Kagawa 2001) (Cai, Kawashima & Kagawa 2006) (Cai, Kagawa & Kawashima 2002). The properties of air power including composition, temperature, kinetic energy and power loss factors are considered. Air power is defined as a property of compressed air using a thermodynamics item, exergy, to derive a general equation. Air power is investigated in terms of the energy conversion for the state change of air. Two parts of air power are defined; transmission power and expansion power, with expansion power usually the larger of the two. Temperature and kinetic energy can generally be neglected when calculating air power.

In this project, the air power proposal was used to calculate air power at inlet and outlet of a scroll air motor to calculate the energy conversion ability of the scroll air motor.

Besides the above, there are some other aspects existing in real life. Such as noise (Ishii et al. 1986) (Ishii et al. 1988) , vibration, fluid dynamics (Rodger & Wanger 1990), etc. The purpose of the project was to explain in general why a scroll air motor has high energy efficiency rather than create

an accurate mathematical model for a scroll air motor. Thus these aspects were ignored in the study.

1.3 Experimental bench

Research on energy efficiency of a scroll type air motor also involves experimental investigation for validation. Unfortunately, only a little experimental information about scroll type air motor has been published. The characteristics of a C-E, Compressor-Expander, system was studied by (Gao Xiaojun et al. 2004), where a scroll air motor was acting as a expander to covert pneumatic energy generated by a compressor into mechanic power output. The output work of the scroll expander was figured out as the differential value of the electric power consumed by the compressor working alone and the power consumed by the C-E system. The comparison of theoretical value and practical value was also given.

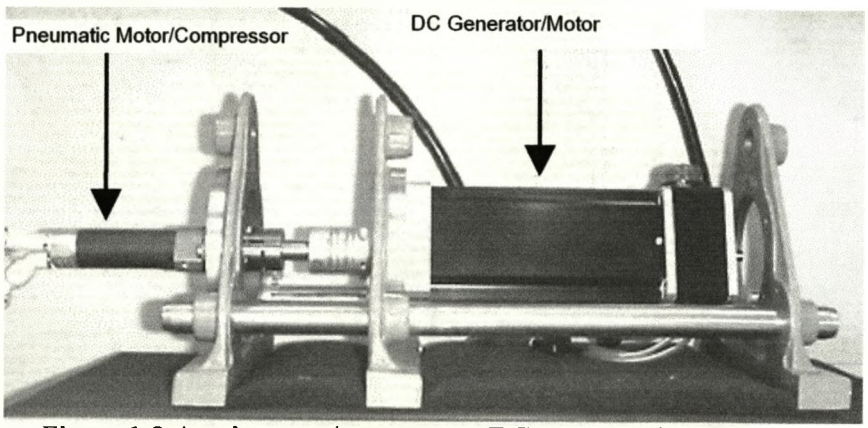

Figure 1.2 An air motor/compressor-DC generator/motor system

Experiments on rotary pneumatic actuators, such as vane type air motor, have been done and published. Optical encoders were used to measure the angular speed of the vane type air motor (Wang et al. 1998) to validate the model of the simplified vane type air motor.

An experiment system of the hybrid Compressed Air and Supercapacitors Energy Storage (CASCES) system, Figure 1.2, was presented to measure the energy efficiency and to implement the Maximum Efficiency Point Tracking algorithm (Lemofouet et al.). The system consists of a vane type air motor/compressor, a DC generator/motor, air storage, and power electric interface. The idea is implemented in the context of an off-line UPS system.

A complex experimental system measuring the dynamic status of the scroll type air compressor used to validate the mathematical model was presented by (Chen 2000). In the system, six pressure transducers, six thermocouples, and a photo-electric position sensor are installed on the fixed scroll to measure the dynamics of the scroll compressor.

1.4 Objectives of the project and contribution

When Energetix group was developing a new generation of environment friendly UPS, among the air motors used in the experiments, it was found that the scroll type air motor had higher energy efficiency than others. The project was inspired by the experiments and the purpose was to analyse the

energy efficiency of a scroll air motor and find out the reason why it is able to transform energy efficiently.

The mathematical model is entirely based on a physical and mechanic basis. The model was validated through experiments. The energy efficiency analysis was based on the model. In details, the following tasks were conducted:

- Develop the mathematical model of a scroll type of air motors, which represents the mechanical structure and the dynamic processes of a scroll motor
    - Describe the scrolls with intrinsic equations
    - Define air motor chambers
    - Calculate volumes of various air motor chambers
    - Analyse effects of wall thickness on the volumes of the chambers and expansion ratio
    - Define working phases
    - Analyse load dynamics and dynamic relationship inside the chambers
    - Implement the mathematical model in Matlab/Simulink environment with a user friendly interface
- Investigate the characteristics of a scroll type air motor and energy efficiency

- Analyse the energy efficiency of a scroll air motor using the model
- Explain how a scroll air motor utilises compressed air energy

- Validate the model through experiments
  - Design and construct the test rig
  - Make a scroll compressor into a scroll air motor
  - Instrument the experimental system
  - Record the data
  - Validate the model

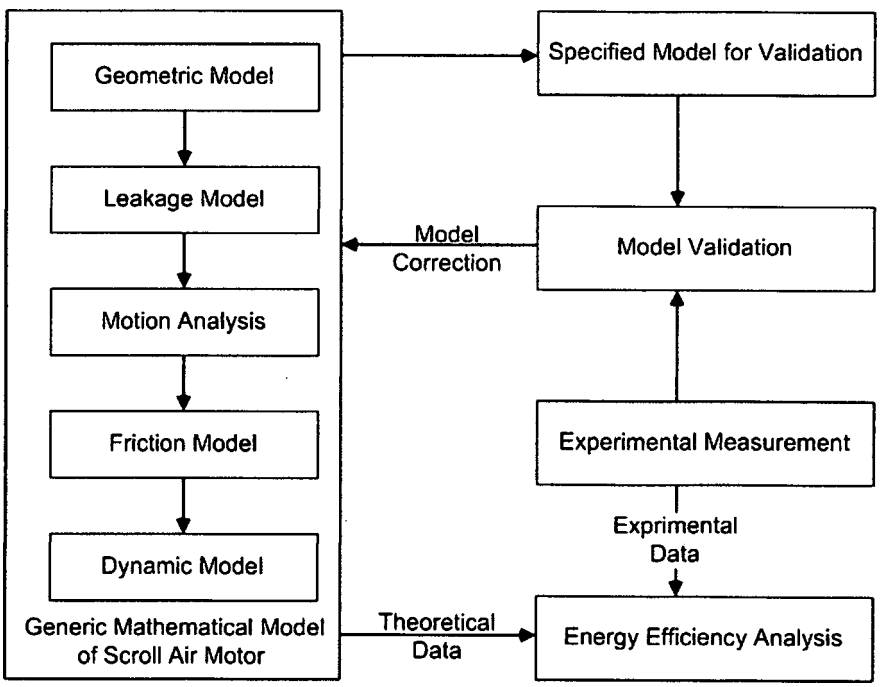

Figure 1.3 Project approach

The approach of the project is shown in Figure 1.3. The mathematical model is comprehensive and generic. It includes geometric model, motion analysis, leakage model, friction model, and dynamic model.

The geometric model includes the physical parameters that greatly affect energy efficiency of a scroll air motor. The shapes of moving scroll and fixed scroll as well as housing and ports are studied in this part. Both fixed and orbiting scrolls are modelled by intrinsic equations, in which the radius of curvature is considered as a function of tangent direction and all relevant geometrical quantities can be described in a closed analytical form. The scroll wall thickness can be either constant or variable, so that the model can be used for parametric study. The volume of a chamber is expressed as a function of the orbiting angle. For a scroll machine, leakage is not negligible. There are two kinds of leakage in a scroll air motor, flank leakage and radial leakage. They were both modelled. Motion analysis considers the motion of the orbiting scroll, so that the force generated by compressed gas is modelled as a function of orbiting angle and air pressure inside the chambers. Friction of a scroll machine is very complicated and may be represented by high order equations. To simplify the analysis, a friction model considering static and kinetic friction was used and modelled.

In order to validate the generic mathematical model of a scroll air motor, a test rig was designed and constructed. The model was specified with the measured parameters of the air motor used for validation.

With the mathematical model and the air power proposal introduced by (Cai & Kagawa 2001), the energy efficiency is analysed.

1.5 Thesis organisation

There are eight chapters in this thesis. The organisation is as follows:

Chapter 1 presents project background and objectives. Statistics of energy consumption by pneumatic devices is given to weigh up the importance of improving energy efficiency of pneumatic systems.

Chapter 2 reviews the history of pneumatic actuator system development and modelling, including basic physics and fundamentals for a pneumatic actuator system.

Chapter 3 presents a mathematical model of a vane type air motor using the theories studied in Chapter 2 as the preparation work for modelling a scroll type air motor.

Chapter 4 describes how to construct the geometry model of a scroll air motor. The scrolls are described with intrinsic equations. The scroll wall thickness can be either constant or variable for parametric study. Green's

Theorem is used to calculate the cross section area of the chambers. The volume of chamber is expressed as a function of the orbiting angle.

Chapter 5 presents the analysis of the dynamics of a scroll air motor, including the leakage model, friction model, and motion analysis. Together with the geometric model given in Chapter 4, the overall model of a scroll air motor comes into being. And the simulation results are also included.

Chapter 6 introduces the definition of air power. Energy efficiency of a scroll air motor is analysed using the definition of air power and the mathematical model.

Chapter 7 describes the experimental system and model validation. The details of the test bench are included. The measurements of the scroll air motor used for validation are given. The experimental data were compared with the simulation results to validate the model.

Chapter 8 is the summary of the project and further discussion based on the results of the project.

Chapter2

Literature Review - Mathematical Modelling of Pneumatic Actuator Systems

The literature review gives an overview of standard pneumatic systems and theoretical modelling of pneumatic systems. The fundamentals of pneumatic actuator systems and fluid dynamic theory are studied.

2.1 Description of pneumatic actuator systems

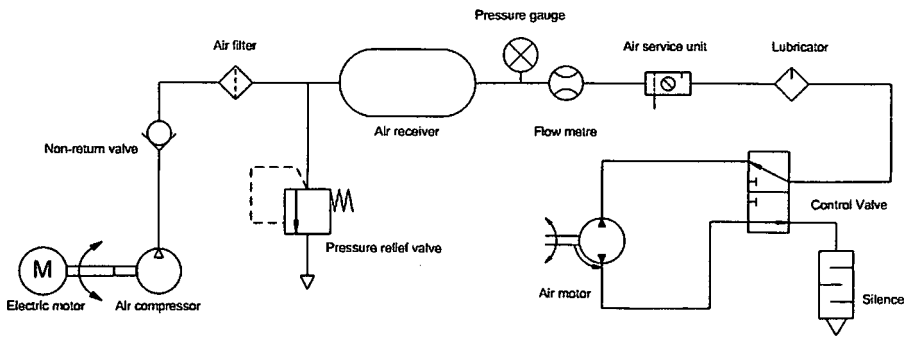

Figure 2.1 A typical pneumatic system layout

A pneumatic actuator system generally consists of compressed air supply, control valves, pneumatic actuators and miscellaneous parts, such as pipes and lubricators. A typical example is shown in Figure 2.1, which includes an air compressor, an air receiver, a proportional control valve, an air motor, and other pneumatic devices.

The components of the pneumatic system in Figure 2.1 can be classified into four groups, compressed air equipment, valves, actuators, and miscellaneous parts.

2.1.1 Compressed air equipment

Most pneumatic systems use compressed air as the operating medium. Compressed air equipment normally includes air compressors, air receivers, and air treatment devices, such as air filters, regulators, etc.

An air compressor is used to generate compressed air. A good quality compressed air supply is very important for a pneumatic system. The compressor increases air pressure by reducing its volume. There are many types of air compressors, such as piston compressors, screw compressors, rotary compressors, and dynamic compressors.

An air receiver is used to store high pressure air, which is generated by the compressor, to provide constant supply pressure and/or flow rate. It is also called air reservoir or air tank.

In order to provide reliable and effective operation of pneumatic systems, the following units are used in a system.

(1) Filter: The air leaving the compressor can be hot, and contains contaminants, such as oil, moisture and dust particles. A filter

separates and collects liquid droplets and solid particles that are present in the air flow through the filter.

(2) Regulator: Generally, the air pressure from the supply is set to be greater than the required. A pressure regulator is used to keep the pressure constant regardless of the flow.

(3) Lubricator: In order to reduce wear and frictional losses, a lubricator adds adequate amount of lubricant to the compressed air before it goes into sliding parts in the system, such as valves, cylinders, air motors.

(4) Service Units: The term service unit is used for the combination of filter, moisture separator, pressure regulator, pressure indicator. Such combinations are frequently required for a pneumatic system.

2.1.2 Control valves

The primary function of valves is to regulate the flow of a fluid, such as gases, fluidized solids, slurries, or liquids, by opening, closing, or partially obstructing various passageways. Additionally, the valve can be used as a power element for the supply of working fluid to the actuator. Valves can be divided into two groups, variable position valve and finite position valve.

A variable position valve can take any position between fully open and closed. It can be used to modulate air flow or pressure. A servo valve is one example in this category. A finite position valve can take a number of discrete positions between fully open and closed positions. An on-off valve is one example of finite position valve.

2.1.3 Actuators

An actuator is a device used to apply force to an object, and hence possible motion of that object (Wolansky, Nagohosian & Henke 1977). Pneumatic actuators have been widely used in applications for applying forces and for positioning, including simple speed control in industrial processes and automation. Pneumatic actuators can be classified in two groups, linear actuator and rotary actuator.

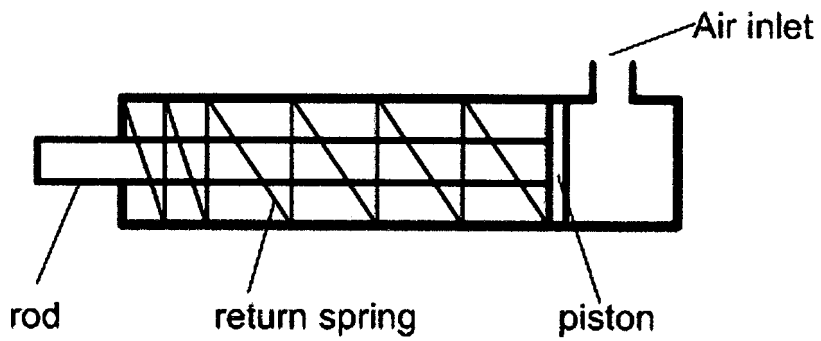

Figure 2.2 Single acting cylinder

Linear actuators are used to move an object or apply a force in a straight line. It is one of the most important types of actuators used in industry. It

can be divided into two types, single-acting cylinders and double-acting cylinders. A single-acting cylinder, Figure 2.2, is only powered for one direction. Compressed gas is applied on only one side of the piston to force the piston to move in one direction, while the other side of the piston is open to the atmosphere. The piston returns back in the other direction by the force of an internal spring or some external force. Double-acting cylinders, Figure 2.3, have similar structure to single-acting ones, but no return springs. Two ports are used as inlet and outlet in turn. Therefore, the cylinder is able to carry out work in both directions.

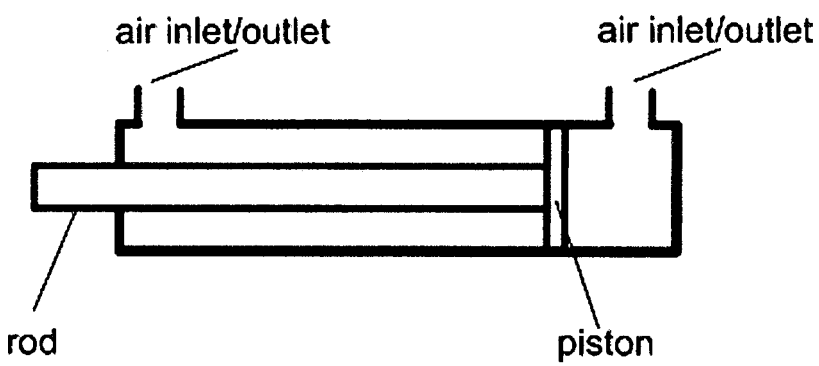

Figure 2.3 Double acting cylinder

Rotary actuators are used to move an object in a particular path. Rotary actuators are the pneumatic equivalent of electric motors. Vane type air motors are an example of rotary pneumatic actuator. So is a scroll type air motor.

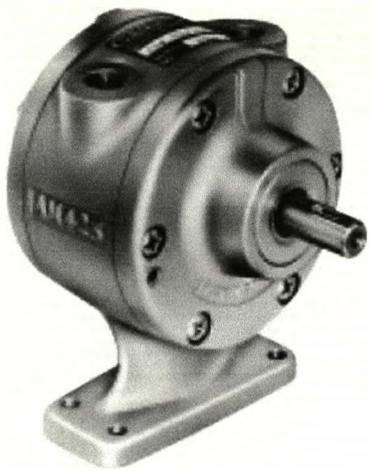

Figure 2.4 GAST 4AM-FRV-13C vane type air motor

2.2 Basic physics for pneumatic actuator systems

2.2.1 Enthalpy, internal energy, and specific heat

A corollary of the first law of thermodynamics states that if a closed system executes a non-cyclic process, then the difference between the heat transfer to the system, Q, and the work done by the system, W, is equal to the change in the internal energy of the system, ΔU, that is

$$Q - W = \Delta U \tag{2.1}$$

The enthalpy H for a mass of fluid in equilibrium is defines (Blackburn, Reethof & Shearer 1960; Dehoff 1993)

$$H = U + pV \tag{2.2}$$

where p and V are the pressure and volume, respectively. Enthalpy can be used to calculate the "useful" work obtainable from a closed thermodynamic system under constant pressure and entropy. It is also a property that is the change of enthalpy between two states depends only on the end states and not upon the process between the states. The specific enthalpy h, the enthalpy for unit mass, is given by

$$h = u + pV_{ss} \tag{2.3}$$

where u is the specific internal energy and V_{ss} is the specific volume.

Having defined internal energy and enthalpy, the specific heat at constant volume, C_v, and the specific heat at constant pressure, C_p, can be defined as (Winnick 1997)

$$\begin{aligned} C_V &= \left.\frac{du}{dT}\right|_{V_{ss}} \\ C_p &= \left.\frac{dh}{dT}\right|_{P} \end{aligned} \tag{2.4}$$

where T is absolute temperature. C_V and C_p have the below relationship.

$$\begin{aligned} C_p &= C_V + R \\ C_p / C_V &= \gamma \end{aligned} \tag{2.5}$$

2.2.2 Total temperature

If a gas has a temperature T when moving at velocity of $\overline{U}$, then the stagnant temperature, or total temperature, T_t. When the gas is brought to rest adiabatically (no heat transfer) is given by

$$T_t = T + \frac{\overline{U}^2}{2C_P} \tag{2.6}$$

2.2.3 Equation of state

The thermodynamic state of a fluid in equilibrium can be determined from knowledge of two independent properties. In general, no simple algebra equation, termed an equation of state, can be found which covers all possible states of a fluid. However, for a perfect gas, such an expression does exist, and the equation of state is (Wolansky, Nagohosian & Henke 1977)

$$\begin{aligned} pV &= mRT \\ pV_{ss} &= RT \end{aligned} \tag{2.7}$$

where R is the gas constant.

2.2.4 Reversible process

If a fluid undergoes a reversible process, then both the fluid and its surroundings can be restored to their original state. This implies that there are no friction effects and the temperature and the pressure difference

between the fluid and the surroundings are infinitesimally small. Although a reversible process is physically impossible, the concept of reversible is used extensively in thermodynamics.

2.2.5 The steady flow energy equation

When there is a steady flow of fluid through a control volume, then the application of the first law of thermodynamics results in the steady flow energy equation. A control volume is any volume of fixed shape and position and is bounded by a control surface across which fluid can flow.

If Q is the heat transfer across the control surface and W is the external work done then the steady flow energy equation for a pure substance (neglecting capillary, electrical, and magnetic effects) is (Goldstein & Goldstein 1993)

$$Q-W=M\Delta(h+\overline{U}^2/2+gZ) \tag{2.8}$$

where g is gravitational acceleration, Z denotes height, and M is the mass of fluid.

When the change of temperature is small, then the change in internal energy is negligible and equation (2.8) can be simplified to give

$$Q-W=M\Delta\left(PV_{ss}+\overline{U}^2/2+gZ\right) \tag{2.9}$$

If both W and Q are zero and there are no energy losses, then equation (2.9) reduces to the Bernoulli equation.

When friction losses occur, this is manifested as a change in the internal energy. For the case where there is steady adiabatic flow in a pipe with friction, equation (2.8) becomes

$$\Delta\left(PV_{ss}+\overline{U}^2/2+gZ\right)=\text{energy loss} \tag{2.10}$$

2.2.6 Compressible flow through an orifice

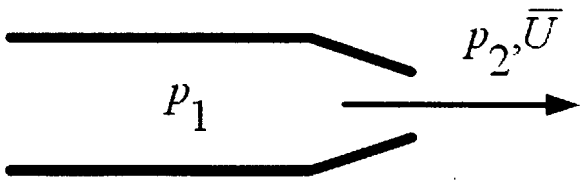

Figure 2.5 Air flow through an orifice

Figure 2.5 illustrates steady flow of compressible flow through a tube or a nozzle. p_1 stands for upstream pressure; p_2 stands for downstream pressure; $\overline{U}$ stands for the air flow speed at the exit of the nozzle. This kind of flow process does not involve work transfer or heat transfer, i.e. $Q=W=0$, and negligible change in height (Andersen 1976). Applying the energy equation to the system, then

$$H_s=H+\overline{U}^2/2 \tag{2.11}$$

H stands for the enthalpy. H_s is the stagnation enthalpy. $\overline{U}^2/2$ is the kinetic energy.

If the fluid is perfect gas, then equation (2.11) can be rewritten using equation (2.4) to give

$$C_P T_s = C_P T + \overline{U}^2/2 \tag{2.12}$$

Because $C_P = C_V + R$ and $C_P/C_V = \gamma$, then the following can be derived $C_P = \gamma R(\gamma - 1)$, γ represents ratio of specific heat, R is gas constant. Thus (2.12) becomes

$$\frac{\gamma R}{\gamma - 1} T_s = \frac{\gamma R}{\gamma - 1} T + \overline{U}^2/2 \tag{2.13}$$

Assuming the fluid is isentropic (reversible adiabatic, or, no heat would be gained or lost during an isentropic process) (Kane & Sternheim 1980), and then it stands that

$$\begin{aligned} &\frac{p_2}{p_1} = \left(\frac{\rho_2}{\rho_1}\right)^{\gamma} = \left(\frac{T_2}{T_1}\right)^{\gamma} \\ &p_1 = \rho_1 R T_1 \\ &p_2 = \rho_2 R T_2 \end{aligned} \tag{2.14}$$

So, from (2.13), it can be derived that

$$\overline{U} = \sqrt{\frac{2\gamma}{\gamma - 1} R T_1 \left[1 - \left(\frac{p_2}{p_1}\right)^{\frac{\gamma-1}{\gamma}}\right]} \tag{2.15}$$

If the velocity is assumed to be uniform across the section, the mass flow rate through a restriction is given by

$$\dot{M} = \rho A \overline{U} \tag{2.16}$$

where A is the cross section area of the restriction.

From equations (2.13) through (2.16),

$$\dot{M} = \frac{p_1}{\sqrt{T}} A \sqrt{\frac{2\gamma}{R(\gamma-1)}\left[\left(\frac{p_2}{p_1}\right)^{\frac{2}{\gamma}} - \left(\frac{p_2}{p_1}\right)^{\frac{\gamma+1}{\gamma}}\right]} \tag{2.17}$$

To obtain the pressure ratio corresponding to the maximum mass flow rate, differentiate (2.17) with the respect to p_2 / p_1 and set the derivative equal to zero. This gives the critical pressure ratio c_r (Wolansky, Nagohosian & Henke 1977):

$$c_\gamma = \left(\frac{p_2}{p_1}\right)_{c_\gamma} = \left(\frac{2}{\gamma+1}\right)^{\frac{\gamma}{\gamma+1}} \tag{2.18}$$

Substituting this value into equation (2.15) gives the critical velocity

$$\overline{U}_{c_r} = \sqrt{\gamma RT} \tag{2.19}$$

This is the equation for the speed of sound at temperature T. It indicates that, for a given value of total pressure and temperature, the maximum

mass flow that can be passed through any area occurs at the local speed of sound. Under maximum flow conditions, sonic velocity is attained at the throat of the nozzle. If the backpressure is reduced below the critical pressure, then there is no increase in mass flow and the nozzle is said to be chocked.

Substituting equation (2.19) into equation (2.17) gives the critical mass flow rate:

$$\dot{M}_{c_r} = \frac{p_1 A}{\sqrt{T}} \sqrt{\frac{\gamma}{R}\left(\frac{2}{\gamma+1}\right)^{\frac{\gamma+1}{\gamma-1}}} = c_0 \frac{p_1 A}{\sqrt{T}} \tag{2.20}$$

where

$$c_0 = \sqrt{\frac{\gamma}{R}\left(\frac{2}{\gamma+1}\right)^{\frac{\gamma+1}{\gamma-1}}} \tag{2.21}$$

Dividing equation (2.17) by equation (2.20), the following can be derived:

$$\begin{aligned} \frac{\dot{M}}{\dot{M}_{c_r}} &= \left[\frac{2}{\gamma-1}\left(\frac{\gamma+1}{2}\right)^{\frac{\gamma+1}{\gamma-1}}\right]^{\frac{1}{2}} \left[\left(\frac{p_2}{p_1}\right)^{\frac{2}{\gamma}} - \left(\frac{p_2}{p_1}\right)^{\frac{\gamma+1}{\gamma}}\right]^{\frac{1}{2}} \\ &= c_k \left[\left(\frac{p_2}{p_1}\right)^{\frac{2}{\gamma}} - \left(\frac{p_2}{p_1}\right)^{\frac{\gamma+1}{\gamma}}\right]^{\frac{1}{2}} \end{aligned} \tag{2.22}$$

where $c_k = \left[\frac{2}{\gamma-1}\left(\frac{\gamma+1}{2}\right)^{\frac{\gamma+1}{\gamma-1}}\right]^{\frac{1}{2}}$.

Then

$$\dot{M} = c_0 c_k \frac{p_1 A}{\sqrt{T}} \left[\left(\frac{p_2}{p_1} \right)^{\frac{2}{\gamma}} - \left(\frac{p_2}{p_1} \right)^{\frac{\gamma+1}{\gamma}} \right]^{\frac{1}{2}} \tag{2.23}$$

Equation (2.23) is strictly valid at any point in a flowing gas.

2.2.7 Mathematical model of a three way spool gas servo valve

Equation (2.23) is commonly used to describe the characteristics of gas flow through nozzles, orifices and valves. It is correct provided that the total pressure, total temperature, and static pressure are known at some area in the restriction across which the velocity is constant.

Assuming supply and exhaust pressures are constant, then each port of the control valves acts like a standard orifice. Hence, p_1, p_2 and T in equation (2.23) can be considered as p_u, p_d and T_u respectively. According to standard orifice theory, the mass flow rate through a valve orifice takes the form (Andersen 1976; Blackburn, Reethof & Shearer 1960; Burrows & Webb 1967; Wang et al. 1998)

$$\dot{M} = c_d c_0 X_{\max} X p_u \tilde{f}(p_r) / \sqrt{T_u} \tag{2.24}$$

where $p_r = p_u / p_d$

$$\tilde{f}(p_r)=\begin{cases} 1 & \frac{p_{atm}}{\max(p_u)} < p_r < c_r \\ c_k\left(p_r^{2/\gamma} - p_r^{(\gamma+1)/\gamma}\right)^{1/2} & c_r < p_r < 1 \end{cases} \quad (2.25)$$

It can be shown that the function $\tilde{f}(p_r)$ and its derivative are continuous with respect to p_r.

For a valve component, the inputs to the valve are supply pressure and valve displacement. The output is the mass flow rate. A three way spool valve contains a pressure port, an exhaust port, and a device port (Figure 2.6 a). p_s and p_e are pressure of air supply and exhaust, respectively. X is the valve spool displacement. The arrow indicates the positive direction of the spool displacement. The pressure port connects to an air supply. The device port connects to an actuator, such as cylinders. When the valve is closed, there is no air flow through the valve. When it is open and in charging status, compressed air goes from air supply through the valve to charge the actuator (Figure 2.6 b). Now, the spool displacement is a positive value. If the valve is in discharging status, air in the actuator goes through the valve to atmosphere (Figure 2.6 c). In this status, spool displacement is a negative value.

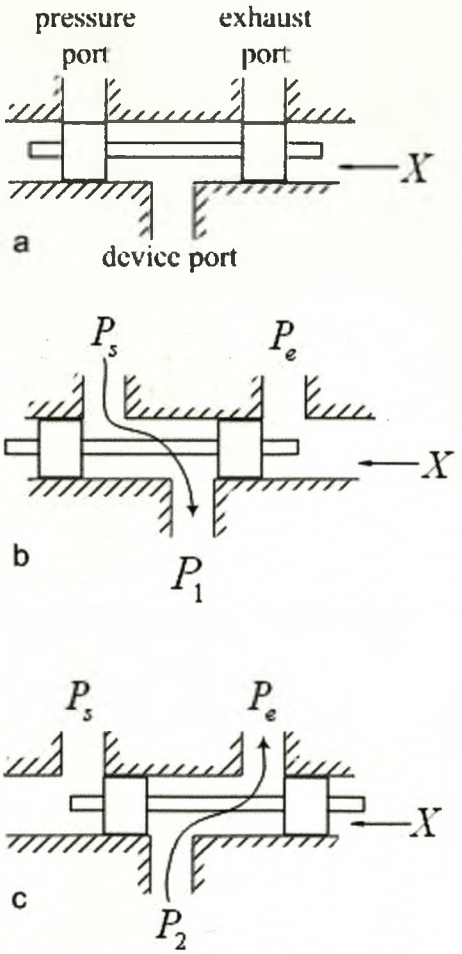

Figure 2.6 Diagram of a three-way proportional valve.

When it is charging a chamber with constant supply pressure (Figure 2.6 b), $p_u = p_s$, $p_d = p_1$, $p_r = p_1 / p_s$. Thus, equation (2.24) becomes

$$\dot{M} = c_d c_0 X_{\max} X p_s \tilde{f}(p_r) / \sqrt{T_s} \tag{2.26}$$

where

$$\tilde{f}(p_r)=\begin{cases}1 & \dfrac{p_{atm}}{\max(p_u)}<p_r<c_r\\ c_k\left(p_r^{2/\gamma}-p_r^{(\gamma+1)/\gamma}\right)^{1/2} & c_r<p_r<1\end{cases}$$

Introducing a reference mass flow rate, assuming p_s is constant and $p_s >> p_1$, so $p_r = 1$, then

$$\dot{M}_{\max}=c_d c_0 X_{\max} X_{\max} p_s \tilde{f}(p_r)/\sqrt{T_s} \tag{2.27}$$

Then equation (2.24) can be converted to dimensionless form as shown below

$$\begin{aligned}\frac{\dot{M}}{\dot{M}_{\max}}&=\frac{X}{X_{\max}}\tilde{f}(p_r)\\ &=\chi\tilde{f}(p_r)\end{aligned} \tag{2.28}$$

When it is exhausting a chamber with constant exhaust pressure (Figure 2.6 c), $p_u = p_2$, $p_d = p_e$, $p_r = p_e / p_2$.

$$\begin{aligned}\frac{\dot{M}}{\dot{M}_{\max}}&=\frac{X}{X_{\max}}\frac{p_2}{p_s}\tilde{f}(p_r)\\ &=\chi\frac{p_2}{p_s}\tilde{f}(p_r)\end{aligned} \tag{2.29}$$

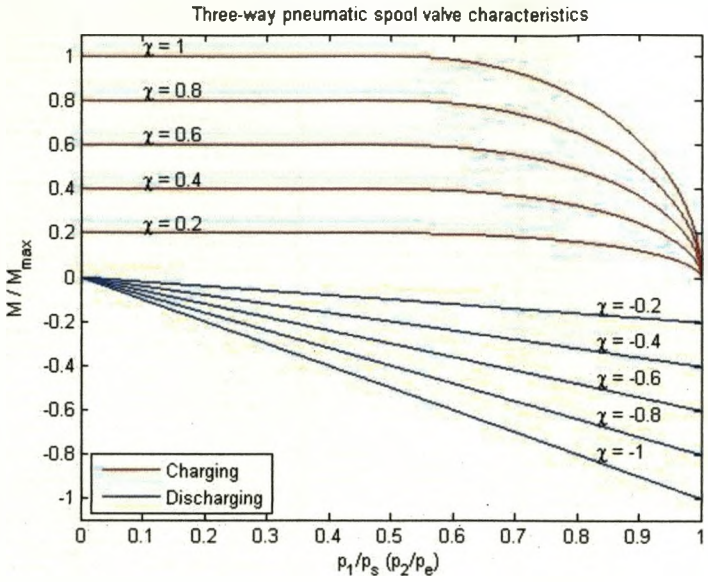

Figure 2.7. Three-way pneumatic spool valve characteristics

Figure 2.7 shows the characteristics when a chamber is being charged, where p_s is a constant of $6\times10^5(Pa)$ and the valve displacement is positive. When a chamber is being discharged, where p_e is a constant of $1x10^5$ Pascal and the valve displacement is negative.

For compressible flow, gas, through a given orifice there is a definite maximum value for the mass flow rate and it occurs when the ratio of the downstream to upstream pressure reaches a value of 0.528 (c_r).

When the ratio is less than c_r, the nozzle is said to be chocked, and the value of the pressure at which this occurs is known as the critical pressure.

When chocked flow occurs the fluid is moving at the speed of sound at the throat of the nozzle, where the throat is defined as the minimum cross-sectional area of the nozzle. Any further reduction in the downstream pressure will not propagate to the nozzle since flow travels at sonic velocity.

When flow is exhausting through the valve to the atmosphere, the characteristics are represented by straight lines, after a small initial curved portion. In the straight-line region, flow is chocked, but as the upstream pressure is increased the flow through the valve increases.

2.2.8 Mathematical model of a control volume

For a control volume, the inputs are mass flow rate from the valve and the volume of the chamber, and the output is the pressure of the chamber. The model for the mass flow into a chamber can be obtained from the energy conservation equation for the control volume bounded by the walls. According to the first law of thermodynamics, the control volume energy is given by $C_V \rho V T$, where ρ is the air density, C_V is the specific heat of air at constant volume, V is chamber volume and T is air temperature. Assuming the air flowing into the control volume to be an adiabatic process of a perfect gas, the change in energy due to the mass transfer equals (Blackburn, Reethof & Shearer 1960; Wolansky, Nagohosian & Henke 1977)

$$\frac{d}{dt}(C_V \rho V T) = \dot{m} C_p T - p\dot{V} \tag{2.30}$$

$\dot{m}C_pT$ is the change in internal gas energy, and $p\dot{V}$ is the work done by the control volume. According to standard practice, the gas kinetic energy term can be neglected since it is small.

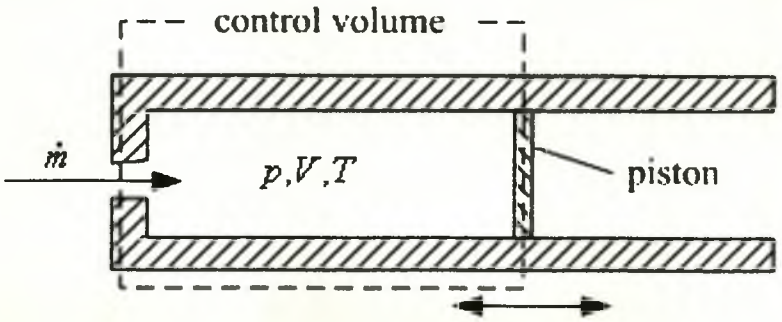

Figure 2.8 Diagram of a control volume

For an ideal gas, the state equation is $p = R\rho T$, where ρ can be cancelled by substituting the equation into equation (2.30). Then it becomes

$$\dot{m} = \frac{p}{C_p T}\frac{dV}{dt} + \frac{1}{\gamma R T}\frac{d}{dt}(pV) \tag{2.31}$$

where γ is the ratio of specific heats for air at the temperature T. For perfect gas

$$\frac{1}{R} = \frac{1}{C_p} + \frac{1}{\gamma R} \tag{2.32}$$

Thus the mass flow rate

$$\dot{m} = \frac{\left(p\dot{V} + \dot{p}V/\gamma\right)}{RT} \tag{2.33}$$

From equation (2.33), the state function of the control volume pressure can be derived as

$$\dot{p} = \frac{\left(\dot{m}RT - p\dot{V}\right)}{V}\gamma \tag{2.34}$$

From equation (2.34), it can be seen that the pressure change of a control volume is a function of its volume, gas temperature, and the mass flow rate.

2.3 Summary

Pneumatic fundamentals and modelling of a pneumatic actuator system are studied in this chapter. The theories and equations mentioned are used to describe the dynamics inside a scroll air motor in the following chapters.

Chapter3

Mathematical Model of a Vane Type Air Motor

A mathematical model of a vane type air motor was studied using the knowledge introduced in Chapter 2 as preparation work before studying the scroll type air motor.

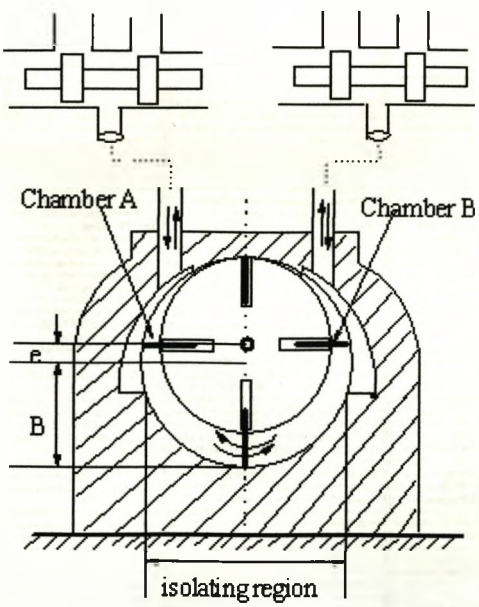

Figure 3.1. A vane type air motor with four vanes

A typical vane type air motor with four vanes is schematically shown in Figure 3.1. The rotating element is a slotted rotor that is mounted on a driving shaft. Each slot of the rotor is fitted with a freely sliding rectangular vane. The rotor and vanes are enclosed in the housing, the

inner surface of which is offset from the drive shaft axis. When the rotor is in motion, the vanes tend to slide outward due to centrifugal force. The distance that the vanes slide is limited by the shape of the rotor housing. The vane in the isolating region divides the volume inside the air motor into two parts, Chamber A and Chamber B with four sections. There is a port on Chamber A and Chamber B respectively. The two ports may be alternatively used as inlet and outlet, thus providing rotation in either direction. The symbol e in the figure stands for eccentricity. B stands for the radius of the housing.

Depending on the flow direction, it can rotate in the way of either clockwise or anticlockwise. For example, if the port on the left of the air motor connects to air supply, and Chamber B is open to atmosphere, when compressed air goes into Chamber A, the air pressure in Chamber A is greater than that in Chamber B. The difference of air pressure generates forces on the vane in the isolating region providing the torque required to rotate the shaft. Hence, the rotor will turn counter clockwise. Each vane, in turn enters the isolating region and the rotor turns continuously. The potential energy of the compressed air is thus converted into mechanical energy in the form of rotary motion and torque. The air is exhausted to atmosphere with reduced pressure level comparing with the pressure at the inlet. The shaft of the motor is connected to the unit to be actuated.

3.1 Geometry structure of a vane type air motor

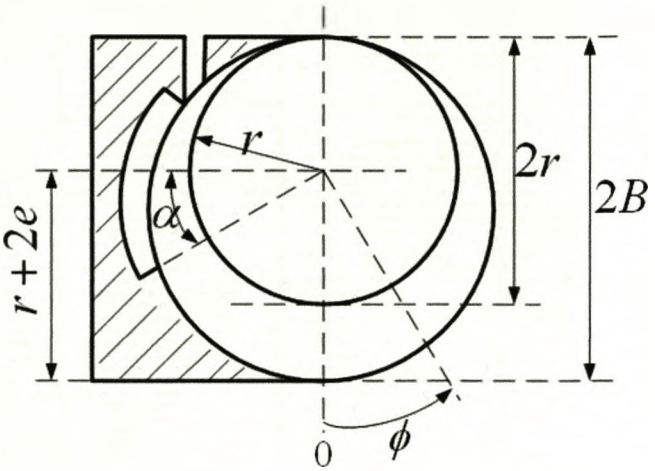

Figure 3.2 Simplified vane motor structure

In order to carry out a basic analysis, a simplified structure is introduced in Figure 3.2, where B is the radius of motor body (housing), e is the eccentricity, r is the rotor radius, α is the angle between the lower end of the connecting slot and the horizon, ϕ is the motor rotating angle.

As shown in Figure 3.1 and Figure 3.2, when Chamber A is the drive chamber, assuming the pressure in the isolated area is the same as the pressure in the drive chamber and that the volume of the isolated area, Vm, belongs to the drive chamber. Then the motor is driven by the torque difference between the drive chamber and the exhaust chamber.

Assuming the rotor is tangent to the housing at the top of the rotor (point A), then the torque that drives the rotor should be produced by the pressures applying on the vane, known as valid vane, that is next to, in the

opposite direction of rotation, the latest vane that has passed the critical point from the driving chamber into the exhaust chamber.

The symbol ϕ stands for motor rotating angle. If the initial condition is $\phi = 0$, when Chamber A is the drive chamber, the range of ϕ should be $[0, +\infty)$. When Chamber B is the drive chamber, the range of ϕ should be $[0, -\infty)$. In the computations, such ranges cannot be employed, because a valid vane only travels in the range of $[\frac{\pi}{2} - \alpha - \frac{2\pi}{n}, \frac{\pi}{2} - \alpha)$, where n is the number of vanes. Hence, the angle between the balance point and the valid vane is the valid angle, denoted by ϕ_{valid}. The angle is the base of the further analysis.

The relationship between ϕ and ϕ_{valid} is given by

$$\begin{aligned} \phi_{valid} &= \phi, \phi \in [0, \frac{\pi}{2} - \alpha) \\ \phi_{valid} &= \phi - \frac{2\pi}{n}, \phi \in [\frac{\pi}{2} - \alpha, \frac{\pi}{2} - \alpha + \frac{2\pi}{n}] \end{aligned} \tag{3.1}$$

and

$$\phi_{valid} = \frac{\pi}{2} - \alpha - \frac{2\pi}{n} + rem\left(\phi - \frac{\pi}{2} + \alpha, 2\pi / n\right) \tag{3.2}$$

where

$$\phi \in \left(\frac{\pi}{2} - \alpha + \frac{2\pi}{n}, +\infty \right)$$

$rem\left(\phi - \frac{\pi}{2} + \alpha, 2\pi / n \right)$ stands for the remainder of $\frac{\phi - \frac{\pi}{2} + \alpha}{\frac{2\pi}{n}}$

n stands for the number of vanes

The working radius measured from the rotor centre of a drive vane is given by

$$x_a = e\cos\phi_{valid} + \sqrt{B^2 - e^2 \sin^2 \phi_{valid}} \tag{3.3}$$

3.2 Drive torque and load dynamics

The drive torque is determined by the difference of the torque acting on the drive vane. Assuming the length of the lever arm is

$$\frac{1}{2}(x_a + r) \tag{3.4}$$

Then drive torque is given by

$$\begin{aligned} M &= (p_a - p_b)(x_a - r)(x_a + r)L/2 \\ &= (p_a - p_b) \\ &\bullet \left(e^2 \cos 2\phi_{valid} + 2Be\cos\phi_{valid} + B^2 - r^2\right)\frac{L}{2} \end{aligned} \tag{3.5}$$

M strands for the drive torque. p_a stands for the pressure in Chamber A. p_b stands for the pressure in Chamber B. L is the vane active length in the axial direction.

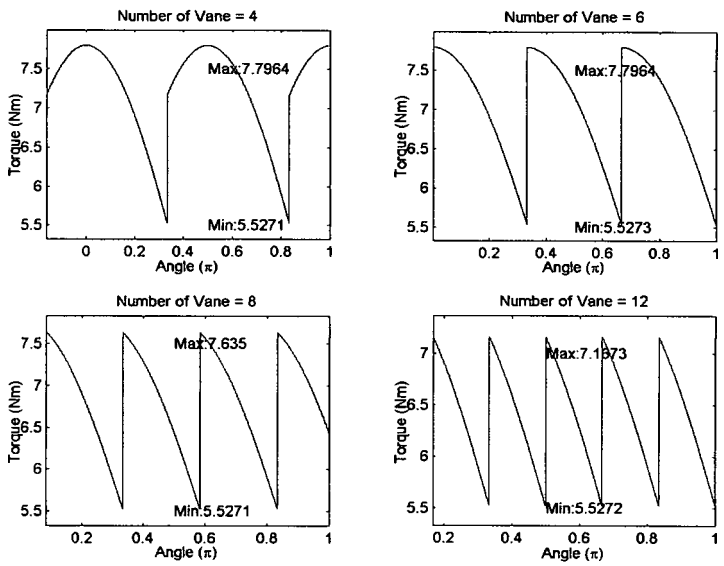

Figure 3.3 Dynamic drive torque

Figure 3.3 shows the relation between dynamic drive torque and the number of vanes with the geometric parameters of $L = 44.5mm$, $B = 36.5mm$, $e = 4mm$, $r = B - e$ and the pressure difference on a drive vane is 6 bar. From the figure, it can be seen that increasing the number of vanes results in less maximum torque and shorter period. Meanwhile, the minimal torque remains same. That can be explained such that the maximal

torque occurs where the valid angle is $\frac{\pi}{2}-\alpha-\frac{2\pi}{n}$, and the minimal torque occurs where the valid angle is $\frac{\pi}{2}-\alpha$.

The value of torque rises sharply and immediately after the trough points, i.e. the curves are not continuous at these points. This is caused by the assumption that a vane does not generate any torque immediately after it passes the critical point until the next period. However, that is not true in real life. Fourier approximation can be used to make it continuous (Wang et al. 1998).

Applying Newton's second law of angular motion to the actuation system, the dynamic behaviour of the system can be expressed by the following equation:

$$M - M_c S(\dot{\phi}) - M_f \dot{\phi} = J\ddot{\phi} \tag{3.6}$$

M_c stands for stiction coefficient. M_f stands for kinetic friction coefficient. M stands for the drive torque, $\dot{\phi}$ stands for angular velocity. $\ddot{\phi}$ stands for angular acceleration. And $S(\dot{\phi})$ is described as below,

$$S\left(\dot{\phi}\right)=\begin{cases}1 & \dot{\phi}=0\\ sign(\dot{\phi})\delta_c(0\le\delta_c<1) & \dot{\phi}\neq 0\end{cases}$$

3.3 Volumes of drive and exhaust chamber

Assuming the initial condition is $\phi = 0$ (Figure 3.2), the initial volumes of both drive and exhaust chambers are the same and described by

$$V_0 = \frac{1}{2} L(B^2 - r^2)\pi \tag{3.7}$$

When Chamber A is the drive chamber and $e^2 Sin^2\varphi << B^2$ holds, the control volumes of the drive exhaust chambers, respectively, are described by

$$\begin{aligned} V_a &= V_0 + \frac{1}{2} L \int_0^{\phi - j\frac{\pi}{2}} x_a^2 - r^2 d\ddot{\phi} \\ &= \frac{L}{2}\left(B^2 - r^2\right)\left[\pi + \left(\phi - j\frac{\pi}{2}\right)\right] \\ &\quad + \frac{1}{4} L e^2 \sin 2\left(\phi - j\frac{\pi}{2}\right) + LBe \sin\left(\phi - j\frac{\pi}{2}\right) \end{aligned} \tag{3.8}$$

$$V_b = V_0 - \int_0^{\phi - j\frac{\pi}{2}} \frac{1}{2} L(x_a{}^2 - r^2) d\tilde{\phi}$$

where

$$\phi \in [-\alpha + j\frac{\pi}{2}, -\alpha + (j+1)\frac{\pi}{2}) \quad and \quad j = 0,\ \pm 1,\ \pm 2,\ .....\pm \Re$$

The derivatives of V_a and V_b are

$$\dot{V}_a = \frac{dV_a}{dt} = \tilde{V}_a \frac{d\phi}{dt} = \tilde{V}_a \dot{\phi} \quad \text{and} \quad \dot{V}_b = \frac{dV_b}{dt} = \tilde{V}_b \frac{d\phi}{dt} = \tilde{V}_b \dot{\phi}$$

where

$$\tilde{V}_a = \frac{dV_a}{d\phi} = \left[\frac{1}{2}L(B^2 - r^2) + \frac{1}{2}Le^2 Cos\phi + LBeCos(\phi - j\frac{\pi}{2})\right]$$

$$\tilde{V}_b = -\tilde{V}_a$$

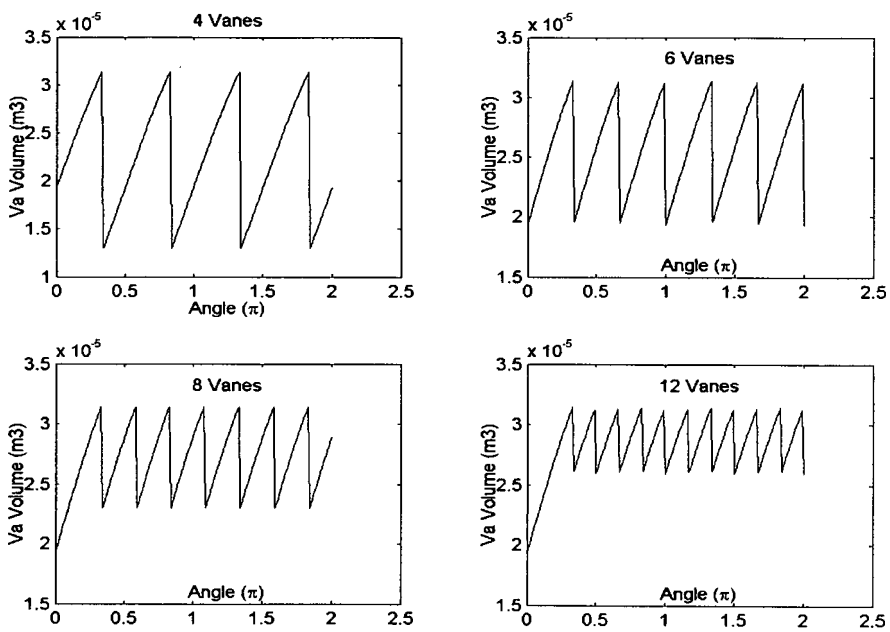

Figure 3.4 Dynamic volumes of Chamber A

From equations (3.8), it can be seen that V_a , V_b are periodic and discontinuous functions.

Figure 3.4 shows the dynamic volume of the driving chamber with different number of vanes. It shows that as the number of vanes increases, the range of volume change narrows.

3.4 Dynamic relationship within the control chambers

When the changes in each control chamber occur, the relationships between mass flow rates ($\dot{m}_a$, $\dot{m}_b$) and the change of both pressure ($\dot{p}_a$, $\dot{p}_b$) and volume ($\dot{V}_a$, $\dot{V}_b$) in the actuator control chambers have the following forms:

$$\begin{aligned} \dot{m}_a &= \left(p_a \dot{V}_a + V_a \dot{p}_a / \gamma\right)\left(RT\right) \\ \dot{m}_b &= \left(p_b \dot{V}_b + V_b \dot{p}_b / \gamma\right)\left(RT\right) \end{aligned} \tag{3.9}$$

In conjunction with compressible flow through a restriction, equation (2.23), and equation (3.9), the following expressions are derived, showing the pressure changes in the chambers.

$$\begin{aligned} \dot{p}_a &= \frac{\dot{V}_a \gamma}{V_a} p_a + \frac{\gamma}{V_a} RTC_d C_0 A_a X_a f\left(p_a, p_s, p_e\right) \\ \dot{p}_b &= \frac{\dot{V}_b \gamma}{V_b} p_b + \frac{\gamma}{V_b} RTC_d C_0 A_a X_a f\left(p_b, p_s, p_e\right) \end{aligned} \tag{3.10}$$

3.5 State function for the vane type air motor

Choosing system state variables $x_1 = \phi$, $x_2 = \dot{\phi}$, $x_3 = p_a$, $x_4 = p_b$ and control input variables $u_1 = X_a$, $u_2 = X_b$, the state functions of the air motor system shown in Figure 3.2 are

$$\dot{x}_1 = x_2 \tag{3.11}$$

$$\dot{x}_2 = -\frac{1}{J} M_c S(x_2) - \frac{M_f}{J} x_2 + \frac{1}{2J} L\left(e^2 \cos 2x_1 + 2eB\cos x_1 + B^2 - r^2\right)(x_3 - x_4)$$

$$\dot{x}_3 = -\frac{\dot{V}_a(x_1)}{V_a(x_1)} k x_3 x_4 + \frac{k}{V_a(x_1)} RTC_d C_0 A_0 f(x_3, p_s, p_e) u_1$$

$$\dot{x}_4 = -\frac{\dot{V}_a(x_1)}{V_a(x_1)} k x_3 x_4 + \frac{k}{V_a(x_1)} RTC_d C_0 A_0 f(x_4, p_e) u_2$$

3.6 Step response of the model

Figure 3.5 shows the step response of the whole system in 0.2 second.

The parameters of the system are:

$n = 4$, $M_c = 0.5N$, $M_f = 0.09Ns$, $L = 44.5mm$, $B = 36.5mm$, $e = 4mm$, $r = B - e$, $J_1 = 6.08\times10^{-4} kgm^2$, $J_2 = 2.69\times10^{-4} kgm^2$, $J = J_1 + J_2$, $T_s = 293K$, $\alpha = \pi/6$, $k = 1.4$, $C_d = 0.8$, $C_0 = 0.0404$, $A_a = A_b = 0.004m$, $R = 287J/(kgK)$, $p_s = 6bar$

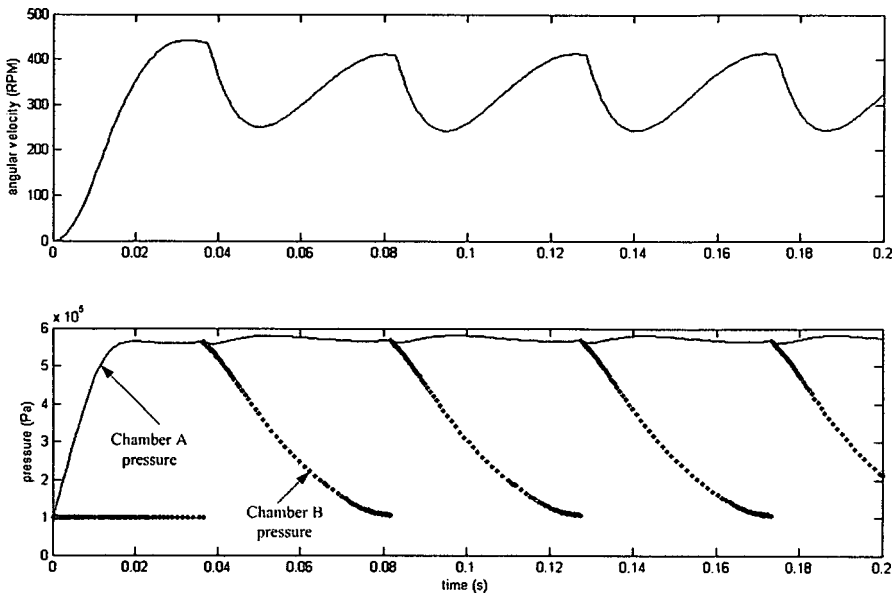

Figure 3.5 Simulation results based on the model

The initial state is $x_1 = 0, x_2 = 0, x_3 = 1bar, x_4 = 1bar$. The curves represent the response for 36% valve open input at $t = 0$. The upper plot shows the angular speed response of the vane type air motor. The value increases rapidly at the start and oscillates in steady state, where the drive torque, equation (3.5), oscillates as the dynamics of air pressures in the chambers, equation (3.8), the length of the lever arm, equation (3.4), and the area of the drive vane. The period of angular speed oscillation is that of the drive torque. The lower plot shows the air pressure in the chambers. The pressure in Chamber A is slightly below the supply pressure consistently. The pressure in Chamber B steps up to the value of the pressure of Chamber A periodically, as a vane goes into the Chamber B from the isolation area. After that, the pressure in Chamber B decreases as the

compressed air exhausts into the atmosphere. The structure of a vane type air motor determines that the compressed air in Chamber B does not push a vane to output torque and make positive effect to utilise air power. From the figure, the exhaust pressure in Chamber B drops from 5.5 bar to 1 bar. Expansion power takes more than 50% of compressed air energy when the pressure is greater than 5 bar (Cai & Kagawa 2001), so the majority of the energy is wasted. A vane type air motor does not transform energy efficiently.

3.7 Summary

Mathematical modelling a pneumatic actuator system, a vane type air motor, is studied in this chapter. The mathematical model for a vane type air motor is developed as the first step of preparation for the development of the mathematical model of the scroll air motor. From the simulation results, it can be seen that the air pressure in the exhaust is still high. Due to the structure of a vane type air motor, it only utilises transmission power of compressed air energy, which accounts for less than half of compressed air energy when the pressure is greater than 5 bar. According to the definition of air power, the energy efficiency of a vane type air motor is low. Further energy efficiency analysis of pneumatic actuators is given in Chapter 6, where the statement in this chapter is explained further.

Chapter4

Mathematical description of the scroll geometry

In order to derive a mathematical model of a scroll air motor, it is essential to understand its mechanical structure, physical characteristics, and pneumatic features. The first step towards fully understanding scrolls is to study its geometric characteristics. In this chapter, the mechanical structure of a scroll is studied in terms of geometry, which is one of main factors influencing its operating efficiency. The fundamental curve to construct a scroll is a spiral. Spirals are studied firstly using intrinsic equations. Then the motion of a scroll air motor is analysed followed by definition of charge chamber, expansion chamber, and discharge chamber. Finally, the mathematical descriptions of cross section areas and volumes of different chambers are derived as functions of the orbiting angle. As the moving scroll orbits, the volume of a crescent chamber changes. The volume of a chamber in a scroll air motor is calculated using the Green Theorem. How the volume of a chamber changes with respect to the orbiting angle will be discussed corresponding to different scroll profiles.

The cross section of a scroll-type air motor is shown in Figure 4.1 which illustrates the relationship between the fixed scroll and the moving scroll.

A scroll-type air motor, in general, consists of a moving scroll, a fixed scroll, housing, bottom plate and a cam. The fixed scroll is fixed on the bottom plate. The air inlet is at the centre of the bottom plate. The moving scroll is fixed on the cam. The scroll geometry could be involute, Archimedean spiral, or hybrid curves (Tojo 1980) (Tischer & Utter 1985) (Richardson 1989) (Caillat, Weatherston & Bush 1988) (Etemad, Yannascoli & Hatzikazakis 1989).

4.1 Mathematical description of the geometry of a spiral

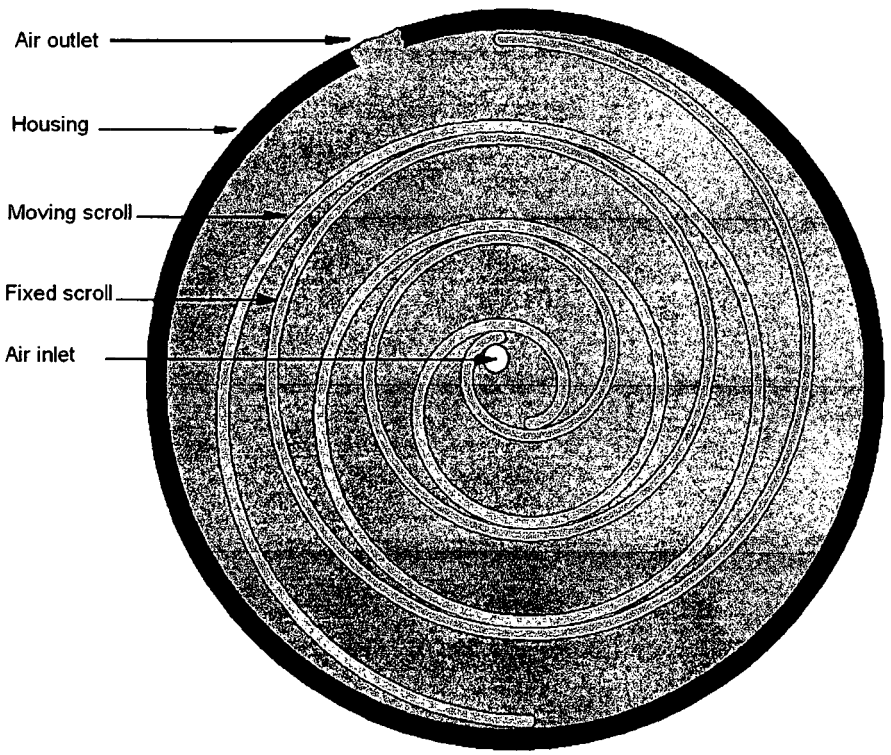

Figure 4.1 Cross section of a scroll air motor to demonstrate its mechanism

Intrinsic coordinates is a coordinate system which defines points upon a

curve partly by the nature of the tangents to the scroll curve at that point. A point is given as (s,φ) where s is the length of the curve from a set point (often the origin) and φ is the angle which the tangent to the scroll curve at that point makes with the x-axis; $s = f(\varphi)$ is the intrinsic equation of the curve.

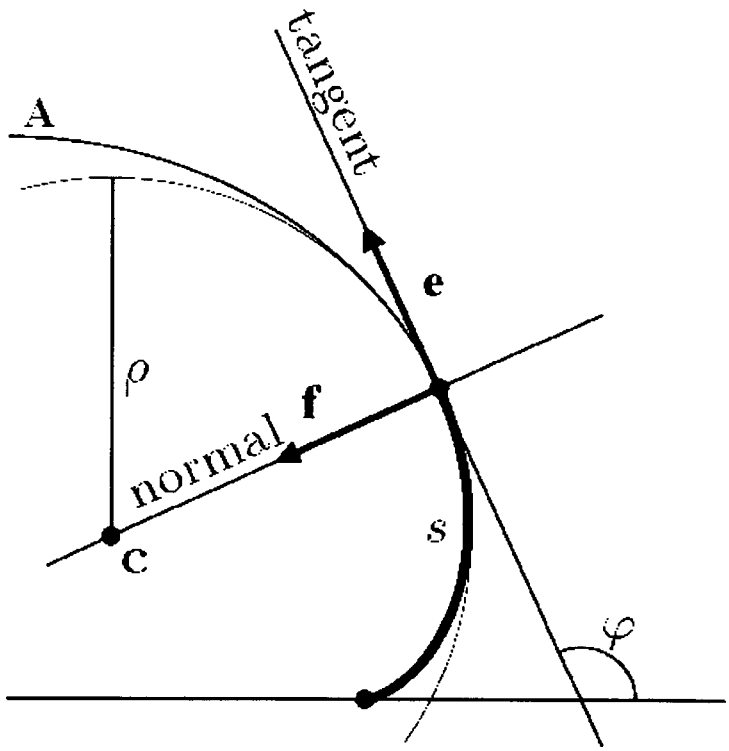

Figure 4.2. Basic geometry of a spiral

This coordinate system may break down entirely when straight lines are considered. A spiral is the fundamental geometry curve of the scroll considered in this study. A circular spiral is shown in Figure 4.2, in which

φ is the tangential angle of a point on the spiral **A**. Tangential angle is the angle from the horizon to the tangent line at a point on a curve. s is the arc length of the bold section, $\mathbf{e}(\varphi)$ is the unit tangent vector at the point whose tangential angle is φ on the spiral, $\mathbf{f}(\varphi)$ is the unit normal vector at the point, $\mathbf{f}(\varphi)$ and $\mathbf{e}(\varphi)$ are a pair of orthonormal frame, ρ is the radius of the curvature, C is the centre of the curvature.

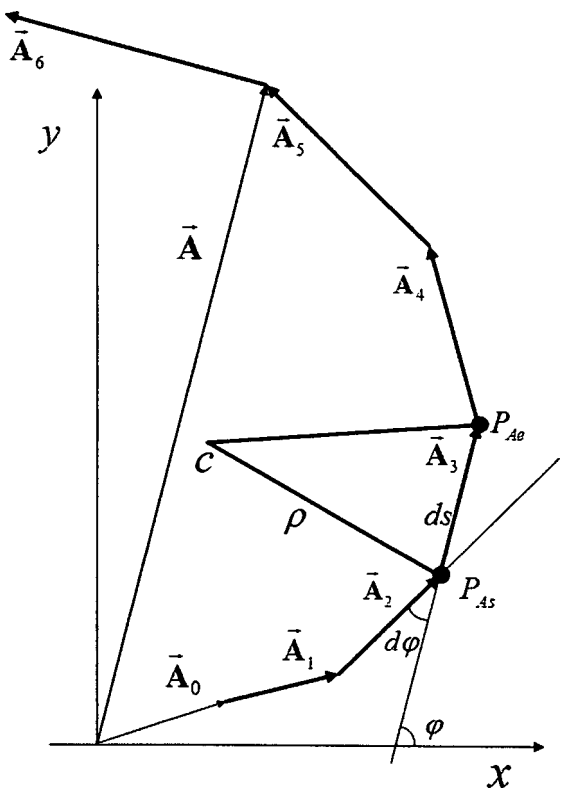

Figure 4.3. Vector approximation to the scroll

For further analysis, the scroll geometry is mapped on to an x-y coordinate system. If the curve is broken down into smaller segments, then each segment is approximately a line segment (see Figure 4.3). This sequence of

line segments are denoted by $\overrightarrow{\mathbf{A}_i}$ and each segment is a vector. Hence any point on the curve can be expressed by the sum of the vectors, i.e. $\overrightarrow{\mathbf{A}} = \sum_{i=1}^{n} \overrightarrow{\mathbf{A}_i}$ (if the vectors are represented in magnitude and direction by the side of a polygon, the sum of the vectors is represented in magnitude and direction by the line segment used to close the polygon.)

As shown in Figure 4.3, if $d\varphi$ is small enough, ds will tend to zero, i.e., while $d\varphi \to 0$, $ds \to 0$. Then the lengths of two adjacent radiuses of curvature, $\overline{cP_{As}}$ and $\overline{cP_{Ae}}$ are almost equal to each other. Let ρ stand for the length of the radius of curvature, then the relationship of $d\varphi$, ds and ρ is

$$\begin{aligned} ds &= \frac{d\varphi}{2\pi} \cdot 2\pi\rho \\ \Rightarrow \rho &= \frac{ds}{d\varphi} \end{aligned} \tag{4.1}$$

and

$$d\mathbf{A} = ds \cdot \mathbf{e}(\varphi)$$

So

$$\mathbf{A}(\varphi) = \int_0^{\varphi} d\mathbf{A} du \tag{4.2}$$

and

$$\frac{d\mathbf{A}}{d\varphi} = \frac{ds}{d\varphi} \cdot \mathbf{e}(\varphi) = \rho(\varphi) \cdot \mathbf{e}(\varphi)$$

Thus equation (4.2) becomes

$$\mathbf{A}(\varphi) = \int_0^{\varphi} \rho(u)\mathbf{e}(u)du$$

$\mathbf{e}(\varphi)$ can be defined as $\mathbf{e}(\varphi) = (\cos\varphi, \sin\varphi)$ so $\mathbf{f}(\varphi) = (-\sin\varphi, \cos\varphi)$. Therefore,

$$\mathbf{A}(\varphi) = \int_0^{\varphi} (\rho(u)\cos u, \rho(u)\sin u)du \tag{4.3}$$

If the initial point of the spiral is at $\mathbf{A}_0 = (x_0, y_0)$ and $\rho = \rho_0 + k\varphi$, equation (4.3) can be written as:

$$\mathbf{A}(\varphi) = \mathbf{A}_0 + \int_0^{\varphi} ((\rho_0 + \kappa u)\cos u, (\rho_0 + \kappa u)\sin u)du \tag{4.4}$$

After performing integration on equation (4.4), the horizontal and vertical position of any point on the spiral can be identified by:

$$\begin{aligned} x_A(\varphi) &= x_0 + (\rho_0 + \kappa\varphi)\sin\varphi + k\cos\varphi - \kappa \\ y_A(\varphi) &= y_0 - (\rho_0 + \kappa\varphi)\cos\varphi + \kappa\sin\varphi + \rho_0 \end{aligned} \tag{4.5}$$

$\varphi \in [0, \varphi_s]$

Equation (4.5) is the function of the tangential angle to represent a spiral. In order to describe a scroll with variable wall width, it must be discussed

piecewise. A scroll with variable wall width will be studied later in this chapter.

4.2 Relationship between the fixed and moving scrolls

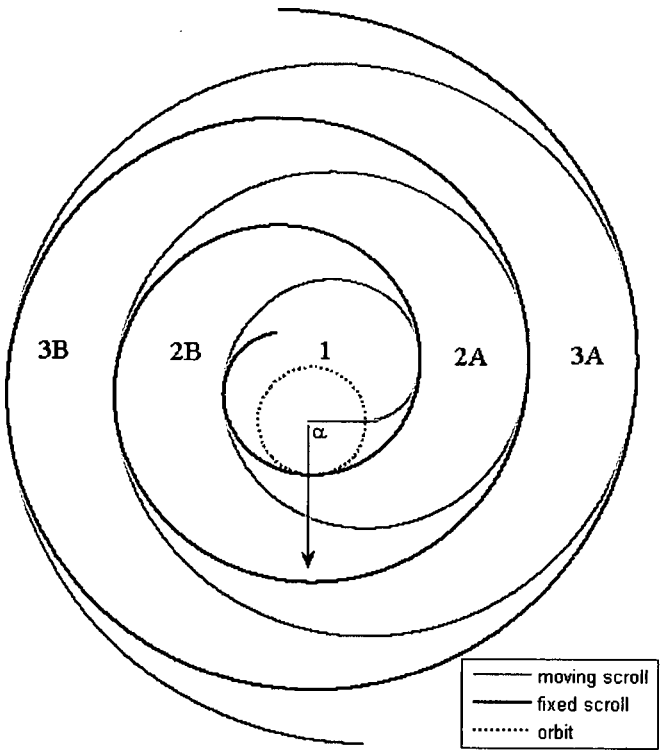

Figure 4.4. A diagram of a simplified representation for the relationship of the fixed scroll and the moving scrolls

Figure 4.4 shows a simplified scroll structure for both fixed and moving scrolls with three-wraps, which form an air motor. In this design, both the moving scroll and the fixed scroll are circle involutes. The grey scroll represents the moving scroll; the black one shows the fixed scroll; the dashed circle in the centre is the orbit along which the moving scroll wobbles; α the orbiting angle that indicates the location of the moving

scroll. In this design, both the moving and fixed scrolls are circle involutes. The orbiting angle varies at a period of 2π . The chamber marked "1" is the chamber located in the central position, where the inlet is located,

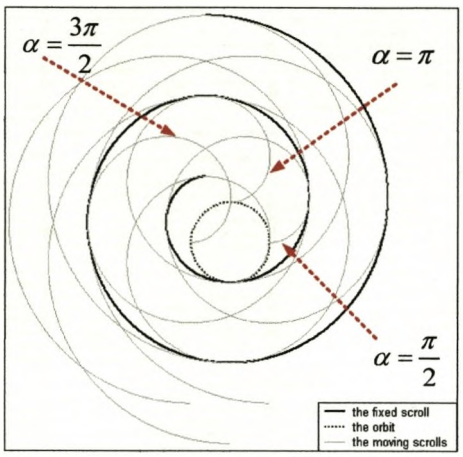

a

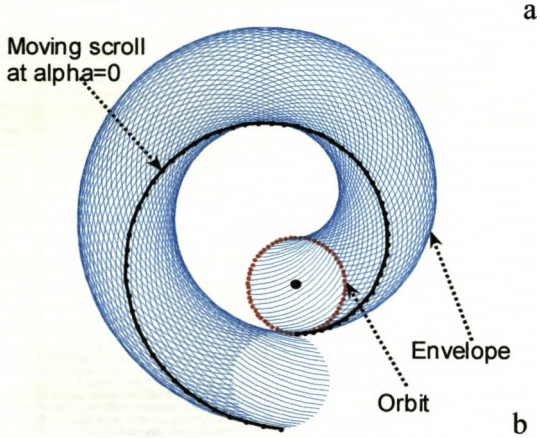

b

Figure 4.5. A family of spirals

called central chamber. The chambers marked with "2A", "2B", "3A" and "3B" are two pairs of sealed crescent side chambers. Side chambers are located at the side of the central chamber. A scroll air motor, normally, have only one central chamber, but a certain pairs of side chambers. The mathematical analysis conducted here is based on this diagram without

considering wall thickness. However, the wall thickness parameterisation will be given in later sections.

When a scroll air motor is operating, the moving scroll moves anticlockwise along the orbit. If we project some moments during one cycle onto one single figure, it is easy to see that the moving scroll forms a family of curve, and the fixed scroll is the envelope of the family (Figure 4.5).

If the orbit is define as:

$$\mathbf{D} = -r\mathbf{f} = r(\sin\alpha, \cos\alpha) \tag{4.6}$$

and the equation for the moving scroll is $\mathbf{A}(\varphi)$, then the family of the moving scroll is

$$\mathbf{A}(\varphi,\alpha) = \mathbf{A}(\varphi) + \mathbf{D}(\alpha) \tag{4.7}$$

The second parameter, α, indicates the position of the moving scroll. The range of α is determined by the number of wraps of the scrolls. If $\varphi \in [0, \varphi_{end}]$, then $\alpha \in [0, \varphi_{end} - 2\pi]$. As the motion is rigid, α does not affect the shape of the moving scroll. $\mathbf{A}(\varphi,\alpha)$ and $\mathbf{A}(\varphi)$ both refer to the moving scroll in the thesis.

From equation of the spiral, equation (4.5), and the equation of the orbit, equation (4.6), equation (4.7) becomes

$$\begin{aligned} x_A(\varphi,\alpha) &= x_0 \\ &\quad + (\rho_0 + \kappa\varphi)\sin\varphi + \kappa\cos\varphi - \kappa + r\sin\alpha \\ y_A(\varphi,\alpha) &= y_0 \\ &\quad - (\rho_0 + \kappa\varphi)\cos\varphi + \kappa\sin\varphi + \rho_0 - r\cos\alpha \end{aligned} \tag{4.8}$$

$\varphi \in [0, \varphi_s]$

Equation (4.8) gives the coordinate of a point on the moving scroll at the tangential angle φ, when the orbit angle is α.

While a scroll moves along its orbit, a curve enveloping the family of the moving scroll curves is formed as shown in Figure 4.5. This envelope forms the fixed scroll curve, which is tangent to the family of the moving scroll curves at each point. To derive the fixed scroll mathematical model, the following definitions and theorem are required (Carmo 1976).

Definition 2.1.

With the parameters $\nu \in S_1 \subset \Re$, and $\upsilon \in S_2 \subset \Re$, for a smooth family of parameterised curves $\{z_\upsilon(\nu)\}$, $(\nu,\upsilon) \mapsto Z(\nu,\upsilon) = (X,Y) : S_1 \times S_2 \to \Re^2$, the singular set of $Z(\nu,\upsilon)$ is the set of the points defined by

$$\left|\frac{\partial(X,Y)}{\partial(\nu,\upsilon)}\right| = \begin{vmatrix} \dfrac{\partial X}{\partial \nu} & \dfrac{\partial X}{\partial \upsilon} \\ \dfrac{\partial X}{\partial \nu} & \dfrac{\partial X}{\partial \upsilon} \end{vmatrix} = 0$$

So the singular set is given by $\dfrac{\partial Z}{\partial \nu}$ and $\dfrac{\partial Z}{\partial \upsilon}$ are parallel.

Definition 2.2.

An envelope of the smooth family of parameterised curves is a curve $\mu \mapsto \Gamma(\mu): S_3 \to \Re^2$ ($S_3 \subset \Re$) which satisfies:

i) for each μ, $\Gamma(\mu)$ lies on the curve $\nu \mapsto z_\upsilon(\nu)$ indeed $\Gamma(\mu) = z_{\upsilon(\mu)}(\nu(\mu))$, and

ii) at $\Gamma(\mu)$, the tangent vectors $\Gamma'(\mu)$ and $z'_{\upsilon(\mu)}(\nu(\mu))$ are parallel, where S_3 is an interval, and $\mu \mapsto \nu(\mu): S_3 \to S_1$ and $\mu \mapsto \upsilon(\mu): S_3 \to S_2$ are smooth functions.

Theorem 2.1.

The curve $\mu \mapsto \Gamma: S_3 \to \Re^2$, given by $\Gamma(\mu) = z_{\upsilon(\mu)}(\nu(\mu))$, is an envelope of the smooth family $\{z_\upsilon(\nu)\}$ of curves, if and only if, $(\nu(\mu), \upsilon(\mu))$ belongs to the singular set of $Z(\nu, \upsilon)$ for each μ.

For the moving scroll at a particular orbit angle α, the fixed scroll $\mathbf{B}(\phi)$ touches the moving scroll $\mathbf{A}(\varphi, \alpha)$, that is. From Definitions 2.1 and 2.2 and Theorem 2.1, the procedure for determining an envelope is 1) compute the singular set of $Z(\lambda, t)$; 2) choose a suitable parameter u, which parameterises the singular set.

Following the steps specified above, the envelope of the family of moving scrolls can be obtained in the following way. The singular set is given by

$$\begin{vmatrix} \dfrac{\partial x_A(\varphi,\alpha)}{\partial\varphi} & \dfrac{\partial x_A(\varphi,\alpha)}{\partial\alpha} \\ \dfrac{\partial y_A(\varphi,\alpha)}{\partial\varphi} & \dfrac{\partial y_A(\varphi,\alpha)}{\partial\alpha} \end{vmatrix} = 0$$

That is

$$\begin{vmatrix} (\rho_0+\kappa\varphi)\cos\varphi & r\cos\alpha \\ (\rho_0+\kappa\varphi)\sin\varphi & r\sin\alpha \end{vmatrix} = 0$$

Then

$$\begin{aligned} &(\rho_0+\kappa\varphi)\cos\varphi\cdot r\sin\alpha-(\rho_0+\kappa\varphi)\sin\varphi\cdot r\cos\alpha=0 \\ &\Rightarrow(\rho_0+\kappa\varphi)\sin(\varphi-\alpha)=0 \\ &\Rightarrow\alpha=\varphi+n\pi \end{aligned} \tag{4.9}$$

where n is an arbitrary integer. For the envelope, choose $\phi=\alpha$ and replace φ by the variable ϕ in the moving scroll equation. The equations for the envelope $\mathbf{B}(\phi)=(x_B,y_B)$ are:

$$\begin{aligned} x_B(\phi+n\pi) &= x_0+(\rho_0+\kappa(\phi+n\pi))\sin(\phi+n\pi) \\ &\quad +\kappa\cos(\phi+n\pi)-\kappa+r\sin(\phi+n\pi) \\ y_B(\phi+n\pi) &= y_0-(\rho_0+\kappa(\phi+n\pi))\cos(\phi+n\pi) \\ &\quad +\kappa\sin(\phi+n\pi)+\rho_0-r\cos(\phi+n\pi) \end{aligned} \tag{4.10}$$

with $\phi\in(\phi_0,\phi_s)$.

Equation (4.10) indicates that the moving scroll touches the fixed scroll at the points $\varphi=\phi+n\pi$. The value of n should be chosen to satisfy $n\geq 0$.

In order to reduce the number of symbols, ϕ is replaced by φ thereafter. The equations describing the fixed scroll are:

$$\begin{aligned} x_B(\varphi+n\pi) &= x_0 + (\rho_0 + \kappa(\varphi+n\pi))\sin(\varphi+n\pi) \\ &\quad + \kappa\cos(\varphi+n\pi) - \kappa + r\sin(\varphi+n\pi) \\ y_B(\varphi+n\pi) &= y_0 - (\rho_0 + \kappa(\varphi+n\pi))\cos(\varphi+n\pi) \\ &\quad + \kappa\sin(\varphi+n\pi) + \rho_0 - r\cos(\varphi+n\pi) \end{aligned}$$

As $\varphi \geq 0$ and $\varphi + n\pi \geq 0$, they range in the same domain. In order to simplify the equation, let $n = 0$, then the equation becomes

$$\begin{aligned} x_B(\varphi) &= x_0 + (\rho_0 + \kappa\varphi)\sin\varphi \\ &\quad + \kappa\cos\varphi - \kappa + r\sin\varphi \\ y_B(\varphi) &= y_0 - (\rho_0 + \kappa\varphi)\cos\varphi \\ &\quad + \kappa\sin\varphi + \rho_0 - r\cos\varphi \end{aligned} \tag{4.11}$$

and

$$\mathbf{B}(\varphi) = (x_B, y_B)$$

4.3 Description of the wall thickness of scrolls

Two symmetrical scrolls assembled in a scroll air motor are offset by 180 degrees and in conjugacy. The relations governing the conjugacy of the two scrolls have the following features:

1) Each point on one scroll surface has only one mating point on the other scroll surface. The moving scroll contacts the fixed scroll at certain points determined by equation (4.11).

2) The tangent vectors at the two conjugate points are parallel to each other and normal to the direction of the offset of the two wrap centres.

From equations (4.8) and (4.11), knowing one side of the moving scroll $\mathbf{A}(\varphi,\alpha)$ and the orbit $\mathbf{D}(\alpha)$, one can get its mating side on the fixed scroll $\mathbf{B}(\varphi)$. By reflecting $\mathbf{A}(\varphi,0)$ and $\mathbf{B}(\varphi)$ in a suitable point respectively, we have the other side of the moving scroll $\widetilde{\mathbf{B}}(\varphi-\pi)$ and $\widetilde{\mathbf{A}}(\varphi+\pi,0)$.

$$\mathbf{A}(\varphi,0)\mapsto\widetilde{\mathbf{B}}(\varphi-\pi) \text{ and } \mathbf{B}(\varphi)\mapsto\widetilde{\mathbf{A}}(\varphi+\pi,0)$$

As shown in Figure 4.6, $\mathbf{A}(\varphi,0)$ is one side of the moving scroll, and $\mathbf{B}(\varphi)$ is its mating side on the fixed scroll. The dashed spiral, $\widetilde{\mathbf{A}}(\varphi+\pi,0)$, is the other side of the moving scroll and the reflection of $\mathbf{B}(\varphi)$. The spiral marked with dash and dots, $\widetilde{\mathbf{B}}(\varphi-\pi)$, is the other side of the fixed scroll and the reflection of $\mathbf{A}(\varphi,0)$. The dotted sections are inner ends of the scrolls. They can be simply described as the extensions of $\widetilde{\mathbf{A}}(\varphi+\pi,0)$ and $\mathbf{B}(\varphi)$ as mentioned in (Gravesen & Henriksen 2001) and (Gravesen, Heneiksen & Howell 1998), or as studied in (Lee & Wu 1995) (Liu et al. 1996) and (Yanagisawa et al. 1990). In this thesis, the dotted sections are considered as extensions of the scroll walls. The extension on $\widetilde{\mathbf{A}}(\varphi+\pi,0)$

has the tangential angle range of $[0,\pi]$, the extension on $\mathbf{B}(\varphi)$ has the tangential angle of $[-\pi,0]$.

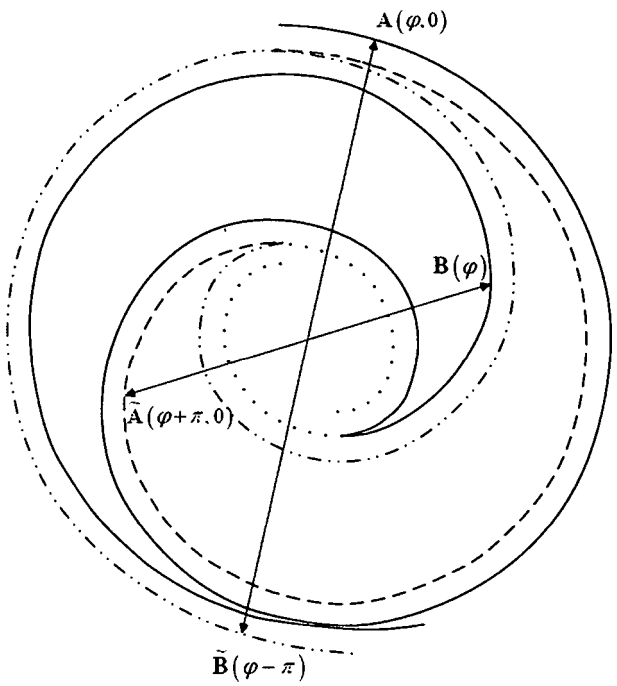

Figure 4.6 A pair of scrolls in conjugacy

Suppose that the radius of the orbit is r, the scroll wall thickness is δ, the description of the other side of each scroll is:

$$\widetilde{\mathbf{A}}(\varphi+\pi,0)=\mathbf{A}(0,0)+\mathbf{A}(\pi,0)+\delta\cdot\mathbf{f}(\pi)-\mathbf{B}(\varphi) \tag{4.12}$$

$$\widetilde{\mathbf{B}}(\varphi-\pi)=\mathbf{A}(0,0)+\mathbf{A}(\pi,0)+\delta\cdot\mathbf{f}(\pi)-\mathbf{A}(\varphi,0) \tag{4.13}$$

So far, two sides of a scroll are discussed, but the two sides are not connected. The inner end of a scroll is considered as a half circle of the

diameter of δ (Figure 4.7). The outer end of a scroll is considered as a line connecting two outer end points of both sides of the scroll.

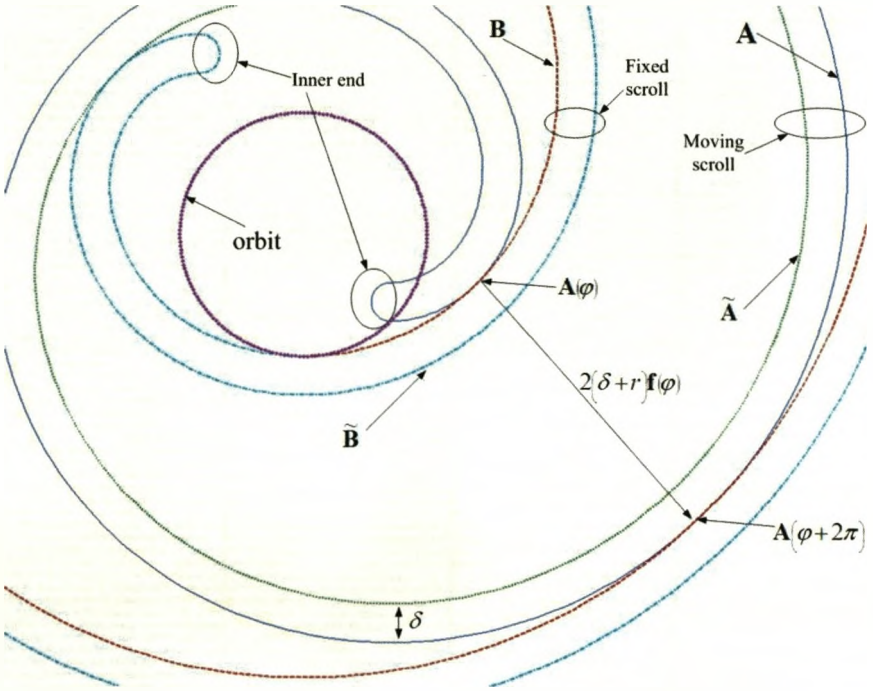

Figure 4.7. Scroll with constant wall width and wall thickness constant definition

4.4 Scrolls with constant wall thickness

In Figure 4.7, $\mathbf{A}$ and $\tilde{\mathbf{A}}$ are the two sides of the moving scroll; $\mathbf{B}$ and $\tilde{\mathbf{B}}$ are the two sides of the fixed scroll; r denotes the radius of the orbit; δ stands for the thickness of the wall. $\mathbf{A}$ and $\mathbf{B}$ are a pair of mating sides, which touch each other at some points while the scroll type air motor is running; $\tilde{\mathbf{A}}$ and $\tilde{\mathbf{B}}$ are the other pair of mating sides. Thus

$$\mathbf{A}(\varphi + 2\pi) - \mathbf{A}(\varphi) = -2(r + \delta)\mathbf{f}(\varphi) \tag{4.14}$$

where $\mathbf{f}(\varphi)$ is the unit normal vector at $\mathbf{x}(\varphi)$.

From (4.5) and (4.14), the wall thickness constant can be derived as

$$\kappa = \frac{r + \delta}{\pi} \tag{4.15}$$

It is the distance between two points on a scroll surface, whose tangential angles have the difference of 2π. The unit of κ is metre. Equation (4.15) is a condition that should be satisfied in designing a scroll with intrinsic functions and constant wall thickness, otherwise the mating relationship will not be there.

4.5 Scrolls with variable wall thickness

Equation (4.15) is the definition for wall constant for scrolls with constant wall thickness δ. In fact, many scroll air motors are designed to have variable wall thickness distributed along scrolls. For a scroll compressor, variable wall width may result in higher compression ratio, while, for a scroll air motor, that may result in higher expansion ratio. The volume of scroll air motor chambers will be discussed later in this chapter. In the case of variable scroll wall width, k in equation (4.15) is defined as a profile function. When a scroll with variable wall thickness is considered, equation (4.15) becomes

$$\kappa = \frac{r + \delta + h_w}{\pi} \tag{4.16}$$

h_w is the scroll wall thickness parameter in metres. The value of h is constrained by the condition which ensures the scroll is physically feasible (Gravesen & Henriksen 2001) (Gravesen, Heneiksen & Howell 1998).

In order to ensure a scroll air motor is physically feasible, the following conditions (sufficient) must be satisfied:

- One of the scrolls does not have any self intersection
- The moving scroll can orbit freely in a circle with radius r, i.e., the two scrolls must not overlap each other

The first condition is secured if ρ is a strictly increasing function (Gravesen & Henriksen 2001).

Further conditions that ensure the moving scroll can orbit freely are:

- $d\left(\mathbf{A}(\varphi), \tilde{\mathbf{A}}(\varphi)\right) = d\left(\mathbf{B}(\varphi), \tilde{\mathbf{B}}(\varphi)\right) = \delta + h/2$
- $d\left(\mathbf{A}(\varphi,\alpha), \mathbf{B}(\varphi)\right) \in [0, r]$
- $d\left(\tilde{\mathbf{B}}(\varphi), \tilde{\mathbf{A}}(\varphi,\alpha)\right) \in [0, r]$

$d(.,.)$ means the distance between two points.

As mentioned earlier in this chapter, the scroll must be defined piecewise in the case of variable scroll wall thickness.

The piecewise form of equation (4.5) is:

$$\begin{aligned} x_A(\varphi_2) &= x_1 + \kappa(\cos\varphi_2 - \cos\varphi_1) + \rho_1(\sin\varphi_2 - \sin\varphi_1) \\ &\quad + \kappa\sin\varphi_2(\varphi_2 - \varphi_1) \\ y_A(\varphi_2) &= y_1 + \kappa(\sin\varphi_2 - \sin\varphi_1) + \rho_1(\cos\varphi_1 - \cos\varphi_2) \\ &\quad + \kappa\cos\varphi_2(\varphi_2 - \varphi_1) \end{aligned} \tag{4.17}$$

The piecewise form of equation (4.11) is

$$\begin{aligned} x_B(\varphi_2) &= x_1 + \kappa(\cos\varphi_2 - \cos\varphi_1) + \rho_1(\sin\varphi_2 - \sin\varphi_1) \\ &\quad + \kappa\sin\varphi_2(\varphi_2 - \varphi_1) + r(\sin\varphi_2 - \sin\varphi_1) \\ y_B(\varphi_2) &= y_1 + \kappa(\sin\varphi_2 - \sin\varphi_1) + \rho_1(\cos\varphi_1 - \cos\varphi_2) \\ &\quad + \kappa\cos\varphi_2(\varphi_2 - \varphi_1) + r(\cos\varphi_1 - \cos\varphi_2) \end{aligned} \tag{4.18}$$

φ_1 stands for the tangential angle of the start point of the scroll surface piece. φ_2 stands for the tangential angle of a point on the scroll surface piece. ρ_1, x_1, y_1 represent radius of curvature, horizontal coordinate, and vertical coordinate at the start point of the spiral, respectively.

The way to create a scroll surface with variable wall thickness is:

1. Find out the breakpoints on a scroll surface according to the scroll wall thickness profile. Then break the scroll surface into spiral pieces.

2. Determine the start point and end point of the piece.

3. Create one side of the scroll, **A**, with equation (4.17). Create the mating surface, **B**, with equation (4.18).

4. Calculate the other side of the scroll, $\tilde{\mathbf{A}}$, with equation (4.12).

For example, given the range of the tangent angle $\varphi \in [\varphi_{start}, \varphi_{end}]$, the initial value of radius of curvature, radius of the orbit, the value of δ, and the scroll wall thickness profile:

$$h_w = \begin{Bmatrix} h_{w\_1} & \varphi \in [\varphi_{breakpoint\_1}, \varphi_{breakpoint\_2}] \\ \dots \quad mm & \dots \\ h_{w\_n} & \varphi \in [\varphi_{breakpoint\_n}, \varphi_{breakpoint\_n+1}] \end{Bmatrix}$$

$\varphi_{breakpoint\_1} = \varphi_{start}$, $\varphi_{breakpoint\_n+1} = \varphi_{end}$, $n = 1,2,3,\dots$, a point on side **A** of the moving scroll can be described by substitute the parameters into equation (4.17). Then the equation becomes

$$\begin{aligned} x_A(\varphi_i) &= x_{breakpoint\_i} + \kappa_i(\cos\varphi_i - \cos\varphi_{breakpoint\_i}) \\ &\quad + \rho_{breakpoint\_i}(\sin\varphi_i - \sin\varphi_{breakpoint\_i}) \\ &\quad + \kappa_i \sin\varphi_i(\varphi_i - \varphi_{breakpoint\_i}) \\ y_A(\varphi_i) &= y_{breakpoint\_i} + \kappa_i(\sin\varphi_i - \sin\varphi_{breakpoint\_i}) \\ &\quad + \rho_{breakpoint\_i}(\cos\varphi_{breakpoint\_i} - \cos\varphi_i) \\ &\quad + \kappa_i \cos\varphi_i(\varphi_i - \varphi_{breakpoint\_i}) \end{aligned}$$

$i = 1,..,n$, φ_i stands for the tangent angle of a point between the points of the tangent angles of $\varphi_{breakpoint\_i}$ and $\varphi_{breakpoint\_i+1}$, κ_i stands for the wall

thickness constant in the range, $\rho_{breakpoint\_i}$ is the radius of curvature at the point of the tangent angle $\varphi_{breakpoint\_i}$.

The mating surface of **A**, **B**, can be calculated with the same method. Then the other side of the scroll, $\widetilde{\mathbf{A}}$, can be calculated. The points on the whole scroll are then derived.

How does variable scroll wall thickness affect the geometry of a scroll air motor will be discussed further later in this chapter.

4.6 Definitions of scroll chambers

In order to analyse the dynamics of a scroll air motor, the chambers of a scroll air motor are defined based on their functions, according to the working processes, charge chamber, expansion chamber, and discharge chamber. As shown in Figure 4.8, different air motor chambers are referred to with numbers. The charge chamber, which connects to the inlet port directly, is labelled chamber "1". Compression chambers "2A" and "2B" develop from chamber "1" after the orbiting angle of 2π. After a revolution, chamber "2A" becomes expansion chamber "3A", and chamber "2B" becomes expansion chamber "3B". As the expansion chambers open up to discharge region, chamber "3A" becomes chamber "4A" and chamber "3B" becomes chamber "4B". In the figure, the volume expansion chambers of "2A" and "2B" are of the period of 2π. The period of volume

of chambers "3A" and "3B" is $\alpha_s = \varphi_{end} - 2\pi$, as after the orbit angle $\alpha = \alpha_s$ the expansion chambers next to the discharge chambers become into discharge chambers. The end of expansion process is also the start of discharge process, so the start orbit angle of discharge process $\alpha_d = \alpha_s$. This definition will be adopted through the thesis and it can be applied to scrolls with more number of wraps.

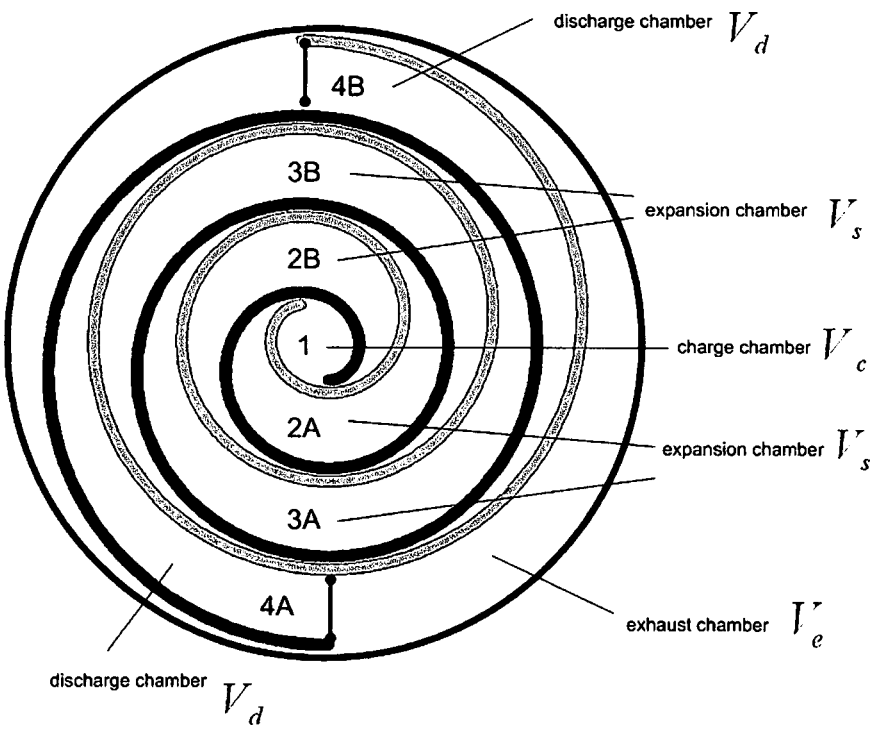

Figure 4.8. Definition of scroll air motor chambers

From Figure 4.8, the expansion chambers/side chambers, V_s, are sealed by the moving scroll and the fixed scroll. The charge chamber, V_c, is unsealed and connects to the air supply directly. Also the discharge chambers are not

sealed and merge into the area between the scrolls and the housing wall, V_e, on which the exhaust port is. V_e is worked out by subtracting the volume enclosed by the housing with the sum of volume of other chambers.

Comparing to the expansion chambers, the dynamics of charge chamber and discharge chamber are more complex as the charge and discharge chambers are not sealed. The charge chamber can be considered as a variable volume with fixed orifice to the air supply.

The discharge chambers can be considered as variable volumes with variable openings (Chen 2000). In Figure 4.8, V_d represents the volume of a discharge chamber at certain of orbit angle, α_d, after the discharge process has started. The chamber volume at that angle is defined as the height of the scroll multiplied with the area enclosed by the fixed and moving scroll and a line segment starting from the end tip of the moving scroll inner side and normal to the fixed scroll outer side.

4.7 Volume calculation of the scroll chambers

Green's Theorem gives the relationship between a line integral around a simple closed curve and a double integral over the plane region bounded by a closed curve.

Theorem 2.2. Green's Theorem

Let C be a positively oriented, piecewise smooth, simple, closed curve and let D be the region enclosed by the curve. If P and Q have continuous first order partial derivatives on D then,

$$\oint_C P dx + Q dy = \iint_D \left(\frac{\partial Q}{\partial x} - \frac{\partial P}{\partial y} \right) dA$$

Green's theorem can be used to calculate areas. The area of region D is

$$\iint_D dA = \frac{1}{2} \oint_C x dy - y dx$$

For a plane curve specified parametrically as $(x(t), y(t))$, the above equation becomes

$$\iint_D dA = \frac{1}{2} \oint_C (xy' - yx') dt \tag{4.19}$$

In Figure 4.9, at the orbiting angle $\alpha = 0$ the moving scroll and the fixed scroll contact each other at $\mathbf{A}(\alpha + 2n\pi, \alpha)$ and $\mathbf{B}(\alpha + 2n\pi)$ $(n = 0,1,2,3\cdots)$. There is one central chamber and two side chambers shown in Figure 4.9. As given in equations (4.8) and (4.11), the boundaries of the chambers have been parameterised in the formation of equation (4.5). And the parameter, φ, is simply increasing/decreasing on a piecewise smooth boundary, which is positively oriented. Then Green's Theorem is applicable to calculate the area of a closed scroll chamber.

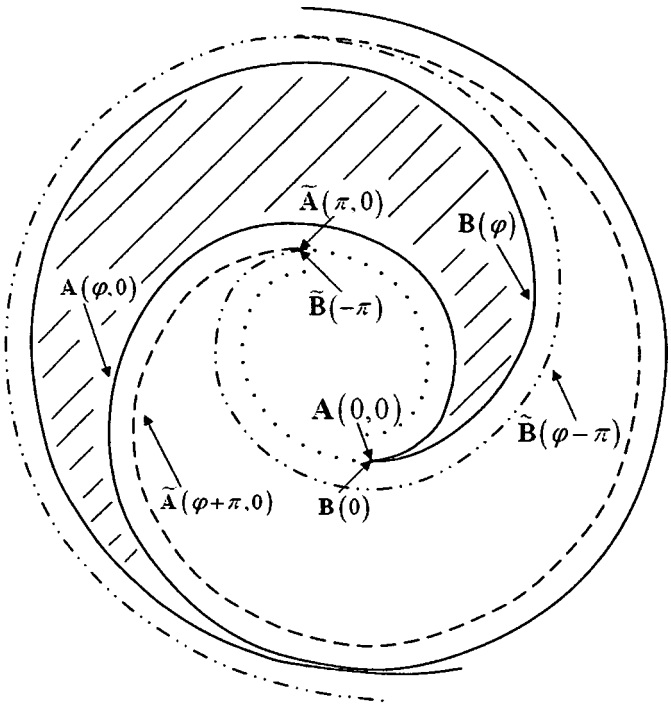

Figure 4.9. The areas bounded by the scrolls

At the orbit angle of α, the bottom area of a scroll chamber can be calculated by a line integral along its positively orientated boundaries. And the bottom area times the height of the scroll wall gives the volume of the scroll chamber. For a side chamber bounded with **A** and **B**, the start and end tangent angles are $\varphi = \alpha + 2n\pi$ and $\varphi = \alpha + 4n\pi$ $(n = 0,1,2,3,...)$ respectively, where n indicates $(n+1)^{th}$ pair of side chamber. Then the volume is expressed by equation (4.20), where $\alpha \in [0,2\pi]$ stands for the orbit angle, φ stands for the tangential angle, z stands for the height of the scrolls. The volume changes with the period of 2π.

$$\begin{aligned} V_s(\alpha,n) = -\frac{1}{2}z\int_{\alpha+4n\pi}^{\alpha+2n\pi} -y_{\mathrm{A}}(\varphi_{\mathrm{A}})d(x_{\mathrm{A}}(\varphi_{\mathrm{A}})) \\ + x_{\mathrm{A}}(\varphi_{\mathrm{A}})d(y_{\mathrm{A}}(\varphi_{\mathrm{A}})) \\ + \frac{1}{2}z\int_{\alpha+2n\pi}^{\alpha+4n\pi} -y_{\mathrm{B}}(\varphi_{\mathrm{B}})d(x_{\mathrm{B}}(\varphi_{\mathrm{B}})) \\ + x_{\mathrm{B}}(\varphi_{\mathrm{B}})d(y_{\mathrm{B}}(\varphi_{\mathrm{B}})) \end{aligned} \tag{4.20}$$

Volume calculation is more complicated for a scroll air motor with variable wall thickness. For a pair of side chambers, the volume of one chamber is equal to that of the other one, so instead of calculating the volume twice, calculating the volume of a side chamber regarding the orbit angle as the moving scroll travels along the orbit can investigate the dynamic geometric change of a scroll air motor.

As mentioned early, in the case of variable scroll wall thickness, a scroll must be discussed piecewise in order to calculate the volume with the Green's Theorem. For a chamber has the boundaries of $\mathbf{A}(\varphi \mid \varphi \in [\alpha+2n\pi, \alpha+4n\pi])$ and $\mathbf{B}(\varphi \mid \varphi \in [\alpha+2n\pi, \alpha+4n\pi])$, each boundary may need to be divided into a number of boundary pieces according to the orbit angle and the wall thickness profile.

For the boundary of $\mathbf{A}(\varphi \mid \varphi \in [\alpha+2n\pi, \alpha+4n\pi])$ with a number of wall thickness profile breakpoints in the range of $\varphi \in [\alpha+2n\pi, \alpha+2n\pi]$, given the breakpoints $\varphi_{breakpoint\,1}$, $\varphi_{breakpoint\,2}$, ..., $\varphi_{breakpoint\,j}$, and $\varphi_{breakpoint\,1} = \alpha+2n\pi$, $\varphi_{breakpoint\,n} = \alpha+4n\pi$,

then the boundary is divided into the pieces of, $\mathbf{A}\lfloor\varphi_{breakpoint\,1},\varphi_{breakpoint\,2}\rfloor$, ..., $\mathbf{A}\lfloor\varphi_{breakpoint\,j-1},\varphi_{breakpoint\,j}\rfloor$.

Similarly, for the boundary of $\mathbf{B}(\varphi \mid \varphi \in [\alpha+2n\pi,\alpha+4n\pi])$, the boundary pieces are: $\mathbf{B}\lfloor\varphi_{breakpoint\,1},\varphi_{breakpoint\,2}\rfloor$, $\mathbf{B}\lfloor\varphi_{breakpoint\,1},\varphi_{breakpoint\,2}\rfloor$, ..., $\mathbf{B}\lfloor\varphi_{breakpoint\,j-1},\varphi_{breakpoint\,j}\rfloor$.

Then piecewise form of side chamber volume equation is

$$V_s(\alpha,n)=\frac{1}{2}z\sum_{i=1}^{j-1}\left(-V_{partA}+V_{partB}\right) \tag{4.21}$$

and

$$V_{partA}=\int_{\varphi_{breakpoint\,i}}^{\varphi_{breakpoint\,i+1}}-y_{\mathbf{A}}(\varphi_{\mathbf{A}})d(x_{\mathbf{A}}(\varphi_{\mathbf{A}}))+x_{\mathbf{A}}(\varphi_{\mathbf{A}})d(y_{\mathbf{A}}(\varphi_{\mathbf{A}}))$$

$$V_{partB}=\int_{\varphi_{breakp\,i}}^{\varphi_{breakpoint\,i+1}}-y_{\mathbf{B}}(\varphi_{\mathbf{B}})d(x_{\mathbf{B}}(\varphi_{\mathbf{B}}))+x_{\mathbf{B}}(\varphi_{\mathbf{B}})d(y_{\mathbf{B}}(\varphi_{\mathbf{B}}))$$

V_{partA} is the line integral along a positively oriented boundary piece on the boundary of $\mathbf{A}(\varphi \mid \varphi \in [\alpha+2n\pi,\alpha+4n\pi])$, while V_{partB} stands for the line integral along a positively oriented piece on the boundary of $\mathbf{B}(\varphi \mid \varphi \in [\alpha+2n\pi,\alpha+4n\pi])$. $i=1,2,..,j-1$. $\varphi_{breakpoint\,i}$, $\varphi_{breakpoint\,i+1}$ are the start and the end point tangential angles of the boundary piece respectively. For scrolls with constant wall thickness, there is no breakpoints on one of the boundaries, and the tangential angle of the start

point is the orbit angle, and the tangential angle of the end point is the orbit angle plus 2π.

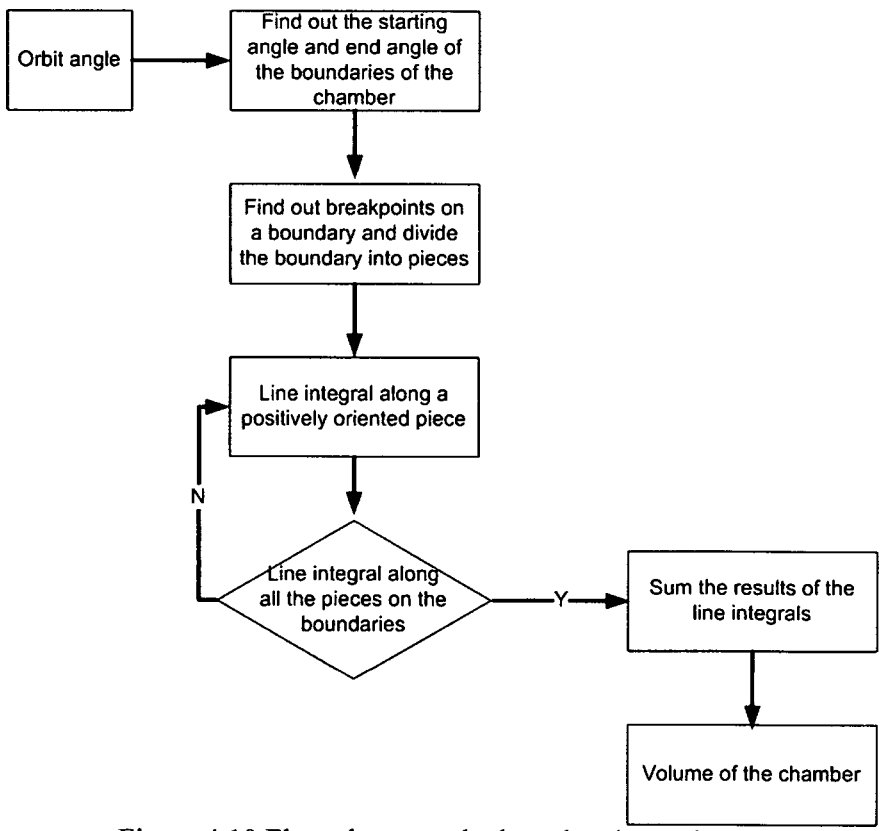

Figure 4.10 Flow chart to calculate chamber volume

Figure 4.10 shows the flow chart for calculating the volume of a side chamber using equation (4.21). First, with the orbit angle, the start and end point tangential angles of one boundary are known. The start point tangential angle is equal to the orbit angle plus $2n\pi$, and the end point tangential angle is equal to the orbit angle plus $4n\pi$. From the start, end point tangential angles of the boundary, and the scroll wall thickness profile, the breakpoints can be found out. The breakpoints are the

breakpoints of wall thickness profile between the start and the end points of a boundary. Then the boundaries are divided into a number of pieces with the breakpoints, and the start and end point tangential angles of each boundary piece are determined. Substituting the start and end point tangential angles of a piece and the initial values of radius of curvature of this piece, the line integral can be calculated. After calculating line integral along every boundary piece on the boundaries, the sum of the integrals is the cross section area of the chamber. Multiplying the area by the scroll wall height, the volume of the side chamber is worked out.

In order to calculate the change of pressure in the expansion chamber as the orbit angle processes, the derivative of the expansion chamber volume with respect to the orbit angle needs to be calculated as well. The differentiation of equation (4.21) yields:

$$\dot{V}_s(\alpha,n) = -\frac{1}{2} z \sum_{i=1}^{j-1} \left(x_{\mathrm{A}} y'_{\mathrm{A}} - y_{\mathrm{A}} x'_{\mathrm{A}} + x_{\mathrm{B}} y'_{\mathrm{B}} - y_{\mathrm{B}} x'_{\mathrm{B}} \right)$$

Similarly, with Green's Theorem, the volumes of the central chamber and the discharge chamber can be calculated.

The volume of the exhaust chamber is calculated by:

$$V_e(\alpha) = z\pi\phi_{backplate}{}^2 / 4 - V_c - 2*(V_s + V_d + V_{scroll})$$

where $\phi_{backplate}$ is the inner diameter of the housing, V_{scroll} is the volume of a scroll wall, which can be calculated using the method described.

4.8 Simulation results of the geometric model

The scroll air motor used for the experiment has the following parameters: $\rho_0 = 9.5mm$, $r = 5.5mm$, $\delta = 4.5mm$, $z = 3.32mm$, $\varphi \in [0,3.5\pi]$, $\phi_{backplate} = 112mm$. Simulation results are given using these parameters. The results summarise the geometric model developed in this chapter, which is the key output of the study.

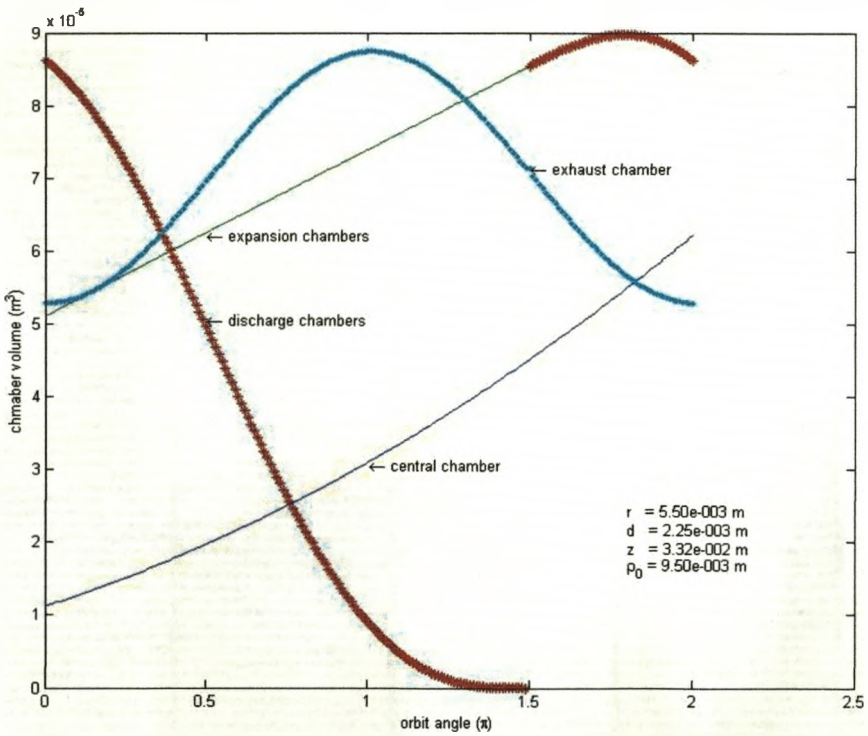

Figure 4.11 Chamber volumes of a scroll air motor through a shaft revolution

Substituting the parameters into the equations of the chamber volumes, how the chamber volumes change through a shaft revolution, $\alpha \in [0,2\pi]$, is shown in Figure 4.11. The volume of the central chamber changes in the period of 2π. And the period starts from $\alpha = 0$. Because the tangential angle $\varphi \in [0,3.5\pi]$, the expansion chambers exists only for the first orbit angle of 1.5π of one entire shaft revolution.

The volumes of two expansion chambers are added together. The expansion process starts at $\alpha = 0$ and ends at the orbit angle of 1.5π, as after $\alpha = 1.5\pi$ the first pair of side chambers are not sealed and become the discharge chambers. The discharge process starts at $\alpha = 1.5\pi$. The volume of the discharge chambers changes at the period of 2π. Same as the expansion chambers, the volumes of two discharge chambers are added together.

In one period, the final value of the expansion chamber is equal to the initial value of the discharge chamber volume, while the initial volume of the expansion chambers is less than the final value of the central chamber volume. As the orbiting angle increases from zero to 2π, the volume of the central chamber increases from $11.5mm^3$ to $63mm^3$. Then, the majority of the central chamber seals and becomes the expansion chambers, while the central chamber goes back to the start of it life. The volume of the expansion chambers increases through its period

consistently. Because the scroll wall thickness is constant, it increases linearly. The discharging phase starts immediately after the expansion phase, where $\alpha = 1.5\pi$. The volume of the discharge chambers increases at the start and reaches the peak value of $89mm^3$. Then it decreases. The discharging phase ends in next shaft revolution and the final value is zero. When the orbiting angle is between 1.5π and π, there is not any expansion chambers.

From Figure 4.11, the volumetric expansion ratio and displacement can also be worked. The minimum chamber volume is $11.5mm^3$ and the maximum value is $89mm^3$. The displacement is $87.5mm^3/revolution$, which matches the specification value of $85.7mm^3/revolution$. The expansion ratio is 8.8. In fact expansion ratio is very important parameter that affects how much a scroll air motor can utilise expansion power. This will be discussed in Chapter 6.

Figure 4.12 shows the derivatives of the chamber volumes. The derivative of the central chamber volume increases throughout it period. The derivative of the expansion chamber volume does not change as the expansion chamber volume increases linearly throughout its period. The derivative of the discharge chamber volume decreases from the start of its period, where $\alpha = 1.5\pi$. It becomes negative after the volume reaches the maximum value.

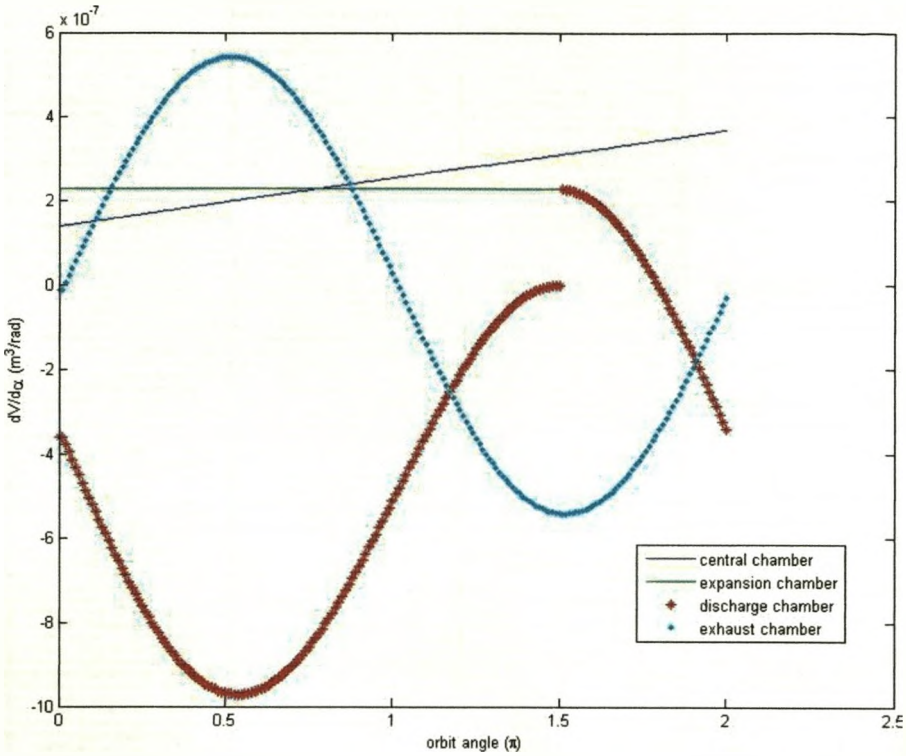

Figure 4.12 Chamber volume derivatives through a shaft revolution

4.9 Summary

The geometry of a scroll air motor is analysed in this chapter. The equations for the scrolls are given in the form of intrinsic equation. Scroll wall thickness is discussed. And chamber volume calculation is given as a function of the orbiting angle. The mathematical description of the geometry of a scroll air motor is given in generic form, so that parameter studies can be conducted to find optimised geometry parameters. The dynamics of a scroll air motor is studied in next chapter.

Chapter5

Air Dynamics in a Scroll Air Motor

In last chapter, the geometry of a scroll air motor is analysed. The equations of the orbit, the moving scroll, and the fixed scroll are given. Based on the equations, the volumes of the chambers are expressed as the functions of the orbit angle. In order to create a mathematical model of a scroll air motor, the dynamic behaviours must be studied. Modern state function models require state variables. This chapter explains how to choose state variables according to the structure of a scroll air motor and its motion behaviour. The main forces applying on the scrolls are analysed. The leakage model is given. With this analysis, the mathematical model of a scroll air motor is presented with simulation results.

5.1 Choosing control volume

In fluid mechanics, a control volume is a mathematical abstraction employed in the process of creating mathematical models of physical processes. In an inertial frame of reference, it is a fixed volume in space through which the fluid flows. The surface enclosing the control volume is referred to as control surface. At steady state, and in the absence of work

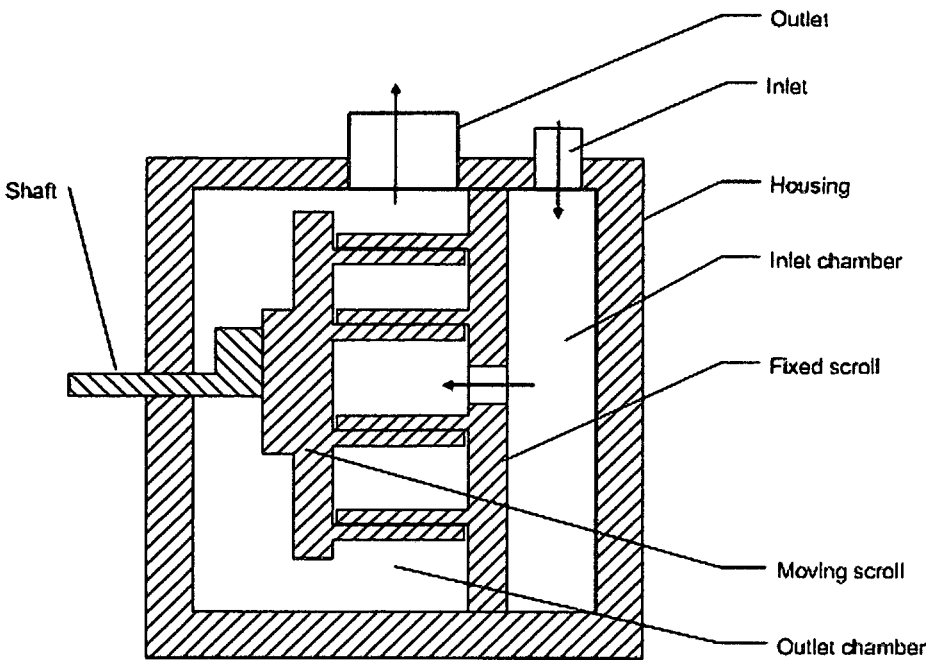

Figure 5.1. Cross section of a scroll air motor and air flow direction

and heat transfer, a control volume can be thought of as an arbitrary volume in which the mass and the enclosed energy of the fluid remain constant. As fluid moves across the control volume, this implies that the mass entering the control volume is equal to the mass leaving the control volume. The same rule applies to the energy.

For a scroll air motor, before compressed air goes into the chambers formed by the moving and fixed scroll, it stays in the inlet chamber for a very short term. And then, it goes into work chambers, which are formed by moving and fixed scroll, to push the moving scroll by expanding itself. Finally, the air reaches the outlet chamber and goes out through the outlet.

Figure 5.1 gives cross section of a scroll with names of the parts and the direction of air flow is indicated by the arrows.

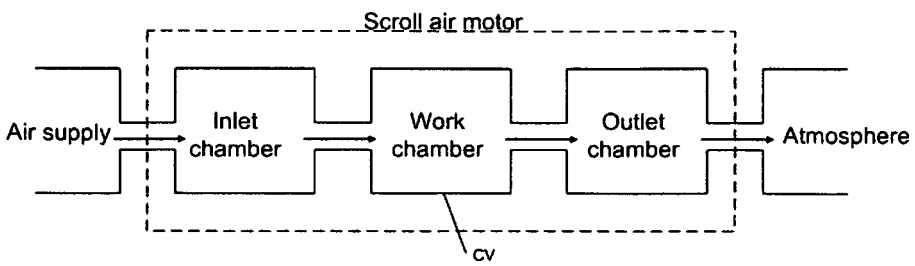

Figure 5.2. Diagram of single control volume method

Control volume method is employed to create the mathematical model. It is natural to study how to choose appropriate control volume before we create the model.

Methods of choosing control volume for scroll machines were studied by (Zhu 1994) (Bo 1995) (Gao 1997) (Li 1989). There are mainly three methods to choose control volume described in these documents.

5.1.1 Single control volume method

Single control volume method is the simplest way to create the model. In Figure 5.2, chambers formed by the moving and fixed scrolls are modelled as one work chamber, CV, which is the only control volume. And the inlet and outlet chambers are considered ideal chambers, in which the thermal status of air does not change, i.e., the status of air in the inlet chamber is same as that in the air supply; and the status of air in the outlet chamber is same as that of atmosphere. As the arrows indicated, compressed air goes

into the work chamber through inlet chamber without changing status. After the work chamber is sealed, the compressed air expands to release energy.

The advantage is that it is easy to create the model with low computer load, so it is suitable for less advanced computers. However this method results in a rough simulation and big difference with experimental data.

5.1.2 Three control volume method

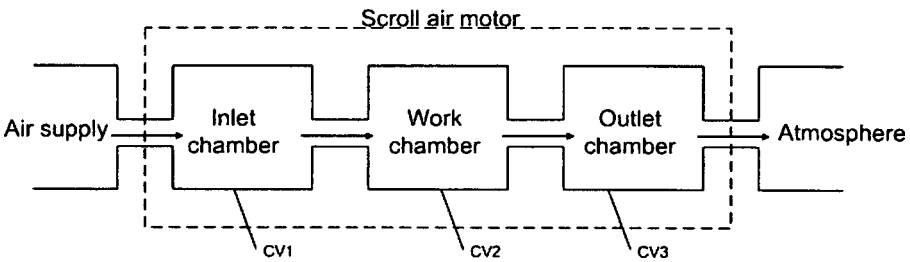

Figure 5.3. Diagram of three control volume method

In three control volume method, Figure 5.3, in addition to single control volume method, inlet chamber and outlet chamber are considered as control volumes. Therefore, there are three control volumes, CV1, CV2, and CV3.

The difference between single control volume and three control volume is that both inlet and outlet chambers are not ideal chambers. Compressed air from air supply goes into inlet chamber with changes in its status, and the status of air in outlet chamber is not same as that of atmosphere. The

system is now cascaded by these three control volumes and heat transfer exists among them.

Three-control-volume method is more complicated than single control volume method and presents more accurate simulation results.

5.1.3 Multi-control volume method

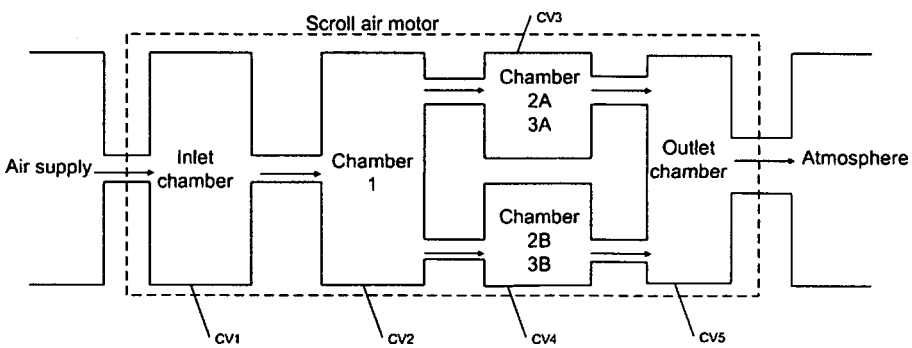

Figure 5.4. Diagram of multi control volume method

In order to have an insight into a scroll air motor, we consider it as a multi-control-volume object. By combining Figure 4.4 and Figure 5.1, Figure 5.4 gives the diagram of choosing control volumes. Further to three control volume method, multi control volume method divides the work chamber in Figure 5.3 into three parts. Chamber 1 is central chamber of a scroll air motor, which connects to inlet chamber. Chamber 2A, 2B, 3A, 3B are side chambers formed by moving and fixed scrolls. Compressed air goes through inlet chamber, and chamber 1, and then it is divided into parts. After that, these two parts merge in outlet chamber and let out into atmosphere. In this thesis, two paired side chambers are considered

symmetric in both mechanical and thermal terms. However, in fact, due to different shape change between fixed and moving scrolls caused by compressed air, the volumes of two paired side chambers are different resulting in different thermal characteristics. Apart from shape change caused by air pressure, other unbalanced mechanical forces also make mechanical and thermal progresses of two paired side chambers uneven.

The advantage of the multi-control volume method is that we can study the dynamic processes deeply. A control volume is a study object. The status of compressed air inside every chamber of a scroll air motor can be simulated.

5.2 Equations describing the thermodynamics in the chambers

Change of pressure, mass of compressed air in any of the chambers described in last chapter with respect to the orbit angle α can be calculated from an equation based on the first law of thermodynamics for an open control volume in conjunction with an air mass balance and equation of state. The first law of thermodynamics for an open volume can be written as:

$$\frac{dE_{CV}}{dt} = \dot{Q} + \dot{W} + \sum \dot{m}_{in}\left(h + \frac{v^2}{2} + gz\right)_{in} - \sum \dot{m}_{out}\left(h + \frac{v^2}{2} + gz\right)_{out} \tag{5.1}$$

E_{CV} is the total energy of the control volume, Q is the work done to the control volume, W is the work done by the control volume, m stands for the mass, h is the specific enthalpy, v is the velocity, g is the gravity acceleration, z is the height.

Neglecting kinetic and potential energies, the total energy of the control volume E_{CV} reduces to its internal energy U_{CV}, then the left side of equation (5.1) can now be transformed into a more useful form as

$$\frac{dE_{CV}}{dt} = \frac{dU_{CV}}{dt} = m\frac{du}{dt} + u\frac{dm}{dt} \tag{5.2}$$

As $du = C_V dT + \left[T\left(\frac{\partial p}{\partial T}\right)_V - p\right]dV$ and $u = h - pV$, the equation above can be written as

$$\frac{dU_{CV}}{dt} = mC_V\frac{dT}{dt} + T\left(\frac{\partial p}{\partial T}\right)_V\left(\frac{dV}{dt} - v\frac{dm}{dt}\right) - p\frac{dV}{dt} + h\frac{dm}{dt} \tag{5.3}$$

Assuming uniform pressure and temperature across each control volume, the work term on the right side of equation (5.1) can be written as:

$$\dot{W} = -p\frac{dV}{dt}$$

p stands for the air pressure, V stands for the volume.

Thus the first law of thermodynamics for the open control volume becomes

$$mC_V \frac{dT}{dt} + T\left(\frac{\partial p}{\partial T}\right)_V \left(\frac{dV}{dt} - v\frac{dm}{dt}\right) + h\frac{dm}{dt}$$
$$= \dot{Q} + \sum \dot{m}_{in} h_{in} - \sum \dot{m}_{out} h_{out}$$

Let ω stand for the angular speed, and $\omega = \frac{d\alpha}{dt}$, the equation above becomes

$$\frac{dT}{d\alpha} = \frac{1}{mC_V}\left\{-T\left(\frac{\partial p}{\partial T}\right)_V \left[\frac{dV}{dt} - \frac{v}{\omega}\left(\dot{m}_{in} - \dot{m}_{out}\right)\right]\right\} + \frac{\dot{Q}}{\omega} - \sum \frac{\dot{m}_{in}}{\omega}\left(h - h_{in}\right) \tag{5.4}$$

The air mass conversation for the control volume is

$$\frac{dm}{d\alpha} = \frac{\sum \dot{m}_{in} - \sum \dot{m}_{out}}{\omega} \tag{5.5}$$

The air state equation is also needs for thermodynamics calculation of the control volume. And the equation of state has the form of

$$\frac{pV}{T} = nR \tag{5.6}$$

R is the gas contant.

Equation (5.4) represents the derivative of the temperature in the control volume with respect to the orbit angle. The thermodynamics of a scroll air motor chamber can be calculated with these equations as a function of the orbit angle α. In order to calculate the air mass flow rate, the theory of compressible flow through a restriction is required.

5.3 Mass air flow in scroll chambers

According to working processes, the chambers formed with the scrolls of a scroll air motor can be divided into three categories, charge chamber, expansion chamber, and discharge chamber. As discussed at the start of this chapter, multi control volume method is used to construct the mathematical model of the scroll air motor. In order to calculate mass air flow in each chamber, how air flows through an air motor needs to be investigated.

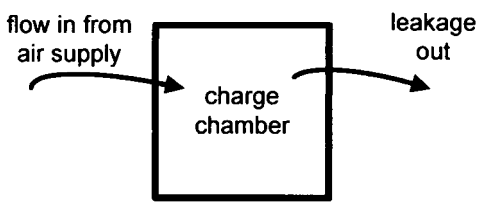

Figure 5.5 Air flow of the charge chamber

The compressed air goes into the charge chamber at the centre of a scroll air motor and pushes the moving scroll to expand itself. As the volume of the charge chamber increases, the pressure should reduce. In order to analysis thermodynamics more efficiently, the air supply is assumed strong enough to keep the pressure at a fixed value. Due to imperfect mechanical surfaces, there are leakages between chambers. As the air supply is connected to the charge chamber directly, the air pressure in the charge chamber is always higher than other chambers of a scroll air motor when the air motor is running, so there is no leakage flowing into the charge

chamber. And the only air flow towards the charge chamber is from the air supply. The air flow of the charge chamber is shown in Figure 5.5.

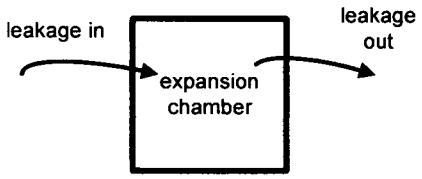

Figure 5.6 Air flow of an expansion chamber

Ideally, an expansion chamber is closed and sealed, which means the amount of air mass inside an expansion chamber is constant through its life. However, in reality due to the gaps between either the two scrolls and one scroll base and one scroll wall, leakages are inevitable. As shown in Figure 5.6, for an expansion chamber, the inward air flow includes leakage from the charge chamber or a more inner expansion chamber if there is more than one pair of expansion chambers. The air flow going out of the chamber is the leakage to the discharge chamber or a more outer expansion chamber, where the pressure is lower.

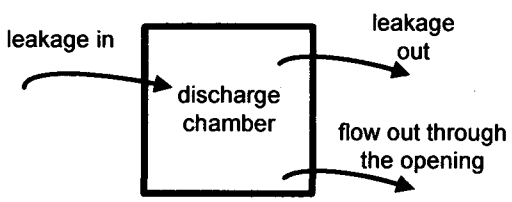

Figure 5.7 Air flow of a discharge chamber

For a discharge chamber, the inward air flow is from the expansion chamber next to it. As a discharge chamber is not closed, the outward flows include leakage and the air flow through the opening (Figure 5.7).

The model of compressible air flow through restrictions will be used in this thesis to calculate the flow rate though a scroll air motor.

$$\dot{M} = \frac{p_1}{\sqrt{T_1}} A \sqrt{\frac{2\gamma}{R(\gamma-1)}\left[\left(\frac{p_2}{p_1}\right)^{\frac{2}{\gamma}} - \left(\frac{p_2}{p_1}\right)^{\frac{\gamma+1}{\gamma}}\right]} \qquad (5.7)$$

$\dot{M}$ is the mass flow rate, p_1 is the upstream pressure, p_2 is the downstream pressure, γ is ratio of specific heat, R is gas constant, T_1 is upstream temperature, A is the area of the flow. This flow is restricted by the critical pressure ratio described by the equation below for choked flow conditions.

$$p_2 / p_1 = \left(\frac{2}{\gamma+1}\right)^{\frac{\gamma}{\gamma-1}}$$

5.4 Leakage flows

For a scroll mechanism, ideally, moving scroll and fixed scroll contact each other perfectly while it is working. In reality, it is not practically feasible to machine them accurately enough. Thus leakage is not negligible, as it may lead to low energy efficiency. In order to make the model properly represent a scroll air motor, leakage must be counted in.

There are mainly two types of leakage in a scroll air motor (Gao Xiaojun et al. 2004). One is radial leakage, which goes through a clearance between the base plate of a scroll and the top of the other scroll wall. The other type of leakage is flank leakage, which goes through a clearance between flanks of two scrolls. These two kinds of leakage are illustrated in Figure 5.8. z is the height of the scroll walls, δ_f is the gap width of flank leakage, δ_r is the gap width of radial leakage.

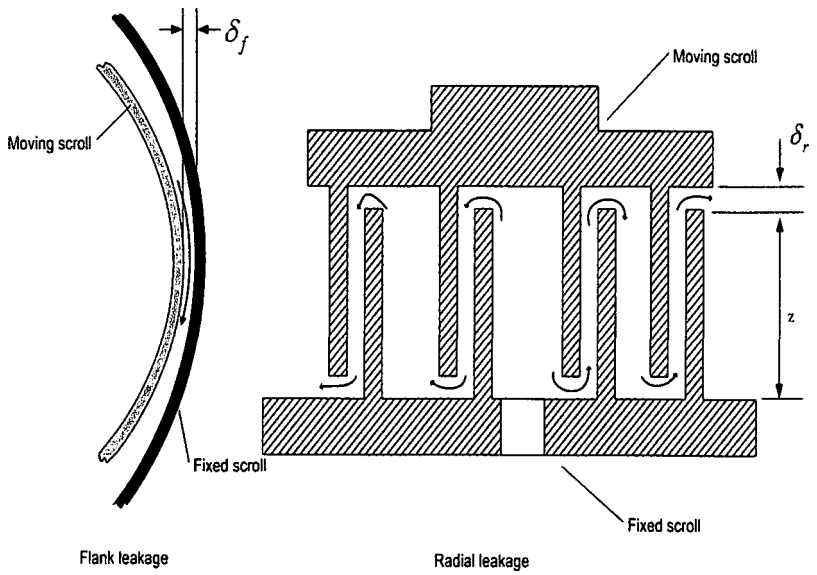

Figure 5.8. Flank leakage and radial leakage

In order to calculate the leakage from a high pressure chamber to one with lower pressure, radial leakage and flank leakage are modelled with the flow equation for isentropic flow of a compressible ideal gas, equation (5.7).

5.4.1 Flank leakage

For flank leakage, the effective area of the gap is

$$A_f = z\delta_f \tag{5.8}$$

z stands for the scroll wall height.

In reality, the gap width is not constant. It can be modelled as a function of the ratio of suction pressure and discharge pressure for a scroll compressor (Chen 2000). It is suggested that the flank gap width is around $10\mu m$ (Li 1998), and this value will be used in this thesis.

5.4.2 Radial leakage

Radial leakage is more complicated than flank leakage. For a side chamber, there are a flow in wall and a flow out wall. The gap length varies as the moving scroll orbits.

Figure 5.9 illustrates the air flow of a side chamber. The arrows indicate the direction of air flow.

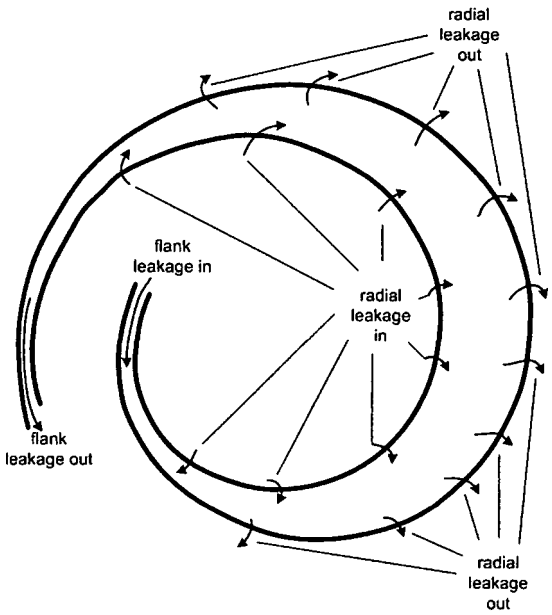

Figure 5.9. Leakage air flow diagram for a side chamber

As mentioned above, there is a flow in wall and a flow out wall for a side chamber. However, the wall segments between a pair of side chambers can be considered as balanced segments, i.e. the air pressure on both sides of the segment are equal, so that there is no air flow cross the segment. Figure 5.10 shows the radial leakage segments in a scroll air motor. The wall segments between the chambers "xA" and "xB" are balanced and can be ignored when calculating radial leakage. Radial leakage flows cross a leakage segments from a high pressure chamber to a chamber with lower pressure next to the high pressure chamber, when the scroll air motor is running. The number of radial leakage segments is even, i.e. half of them are on the moving scroll and the other half are on the fixed scroll. At the

orbit angle α, the radial leakage segments on the moving scroll are $[2n\pi+\alpha,(2n+1)\pi+\alpha]$; the radial leakage segments on the fixed scroll are $[(2n-1)\pi+\alpha,2n\pi+\alpha]$, $(n=0,1,2,...)$. Because of the geometric symmetricity of the scrolls, the length of leakage segments on the moving scroll is equal to accordant leakage segments on the fixed scroll.

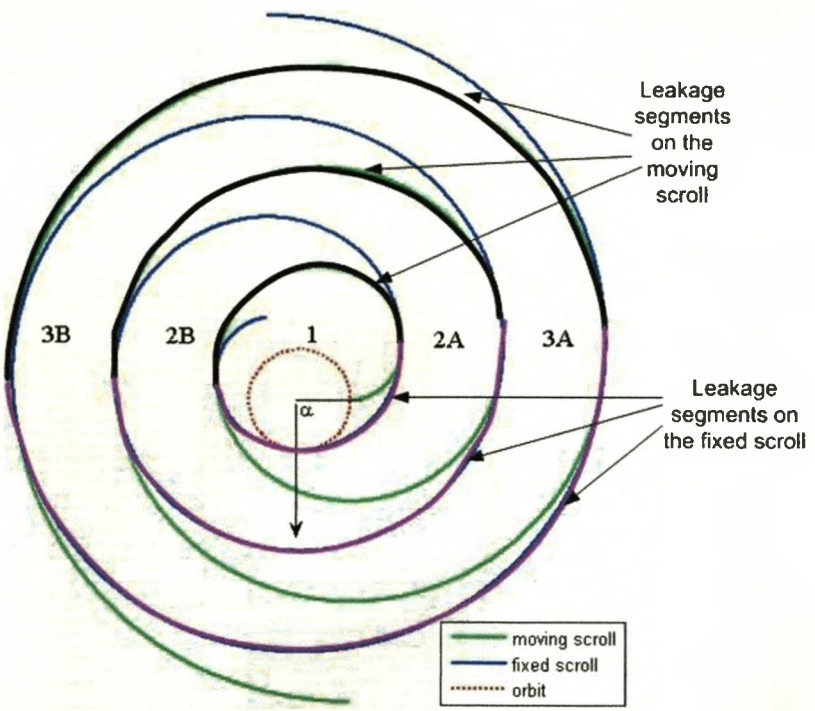

Figure 5.10 Radial leakage segments in a scroll

The length of a radial leakage segment is calculated by

$$s_r = \int_{\varphi_1}^{\varphi_2} \rho d\varphi \tag{5.9}$$

φ_1 is the start tangential angle of the segment; φ_2 stands for the end tangential angle of the segment.

For radial leakage, the effective air flow area for the in flowing gas, A_{r_in} is different from that for out flowing gas, A_{r_out}.

$$\begin{aligned} A_{r\_in} &= s_{r\_in}\delta_r \\ A_{r\_out} &= s_{r\_out}\delta_r \end{aligned} \tag{5.10}$$

s_{r_in} and s_{r_out} are gap lengths of the effective air flow areas for in flowing and out flowing gas respectively. They are both functions of the tangential angle.

Gaps are not constant in the real world, due to imperfect machining, friction, overturning moment and other factors. It is given that, for a scroll compressor, gap sizes are functions of operating conditions (Chen et al. 2002) (Chen 2000). To simplify our analysis, we assume that all parts are rigid objects and their shapes cannot be changed. It is suggested in (Zhu 1994) that radial gap is around $\delta_r = 20\mu m$.

5.5 Motion Analysis of Scrolls

In this section, the motion of the moving scroll is analysed. In order to find the torque, the direction of the sum pressures apply on driving segment(s) of the moving scroll, the lever arm of force and the direction of the motion at a time must be found out. The moving scroll **A** is described by equation (4.8). When a scroll air motor is in motion, every particle on the moving scroll is moving along a orbit with the radius of r. Thus at a moment of t,

the direction of the motion, i.e. the direction of velocity, is the tangent to the point of $\mathbf{D}(\alpha(t))$. The driving torque can be considered as a force for rotation. The rotational analogues of force, mass and acceleration are torque, moment of inertia and angular acceleration respectively. It is known that the torque can be defined as the cross product:

$$\boldsymbol{\tau} = \mathbf{r} \times \mathbf{F}$$

where $\boldsymbol{\tau}$ is torque, $\mathbf{r}$ is the vector from the axis of rotation to the point on which the force is acting, $\mathbf{F}$ is the force vector. By applying Newton's Second Law of rotational motion:

$$\boldsymbol{\tau} = \mathbf{I}\mathbf{a} \tag{5.11}$$

where $\boldsymbol{\tau}$ is the sum of all torques acting on a particle, $\mathbf{I}$ is the moment of inertia and $\mathbf{a}$ is the angular acceleration. Because the moving scroll can only move along the circular orbit in either clockwise or anticlockwise direction, the sum of torque should point to the same direction as the angular acceleration.

The direction of effective pressure (sum of the pressures) is that of the velocity. Since the motion is circular, the length of the lever arm is equal to the radius of the orbit, r.

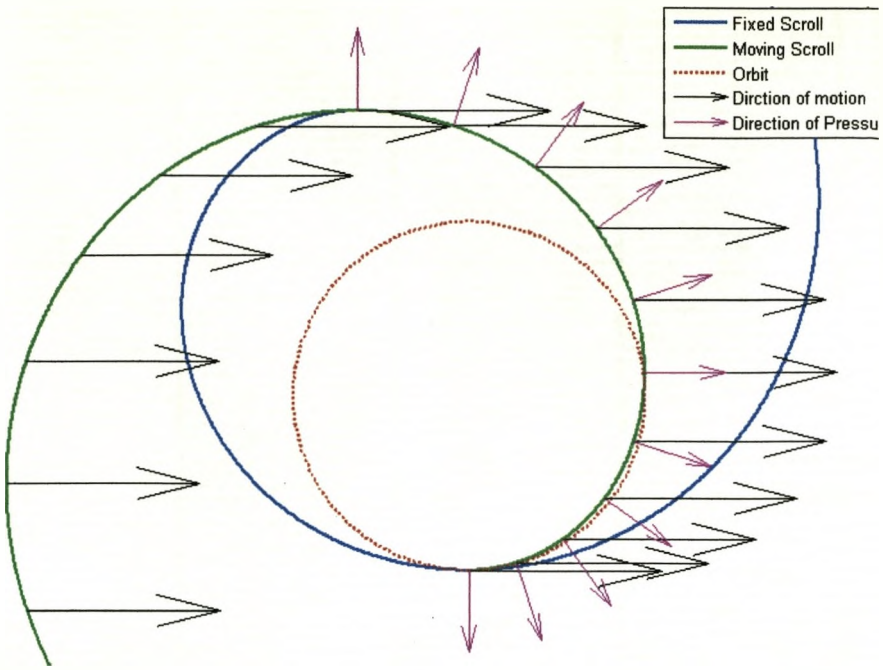

Figure 5.11. Relationship between the direction of motion and direction of effective pressure

In Figure 5.11, the blue spiral represents the fixed scroll, the red spiral represents the moving scroll, the greater arrows are the direction of the movement at this moment, and the smaller arrows stand for the directions of the sum pressures at the points. Thus the sum force on a point can be obtained by:

$$d\mathbf{F} = z\mathbf{p}ds\cos\theta \tag{5.12}$$

where z is the depth of the scroll, ds is the arc length, and θ is the angle between the direction of movement and that of the pressure at a particle, which can be calculated by $\theta = \varphi - \frac{\pi}{2} - \alpha$.

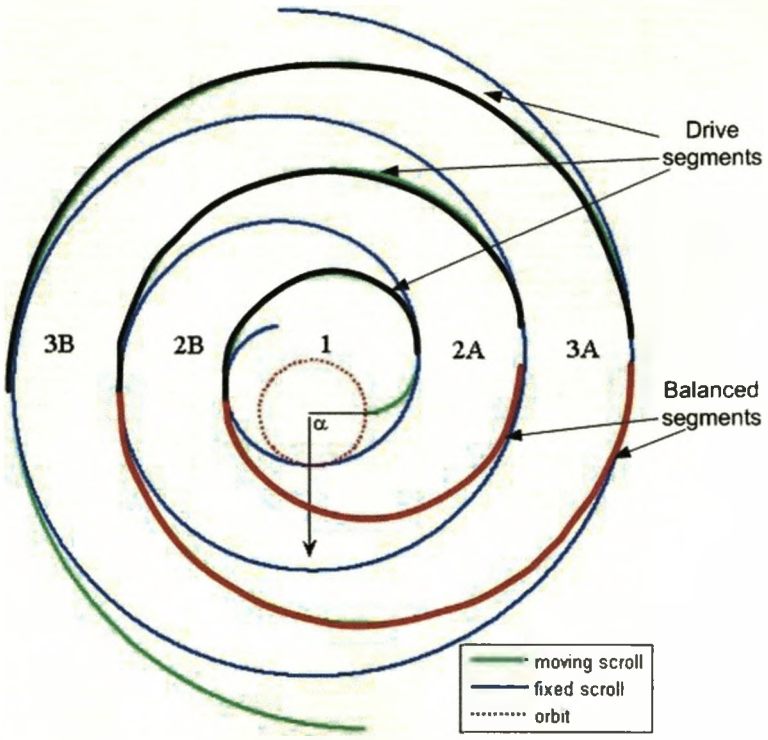

Figure 5.12. Drive segments and balanced segments

While a scroll air motor is moving, two chambers of a pair of side chambers are identical, so some segments of the moving scroll are balanced by the pressures in the identical chambers, while some segments on the moving scroll are drive segments, which generate torque.

In Figure 5.12, chamber 2A and 2B are identical, and the air pressure in 2A equals that in 2B. Same pressures apply on the scroll segment on the moving scroll between chamber 2A and 2B, so the force sum on this scroll segment is zero, i.e. this segment balanced. The pressure in Chamber 3B is lower than that in Chamber 2A, so the force sum on the scroll segment

between Chamber 2A and Chamber 3B is greater than zero pointing outwards. This scroll segment is a drive segment. From the above, at orbit angle α , the drive segments are $\varphi \in [\alpha + 2n\pi, \alpha + (2n+1)\pi]$, $0 \le n \le$ the number of side chamber pairs $+1$. There is only one driving segment for each pair of side chambers. Therefore, the sum of air force is that of the air forces on all drive segments.

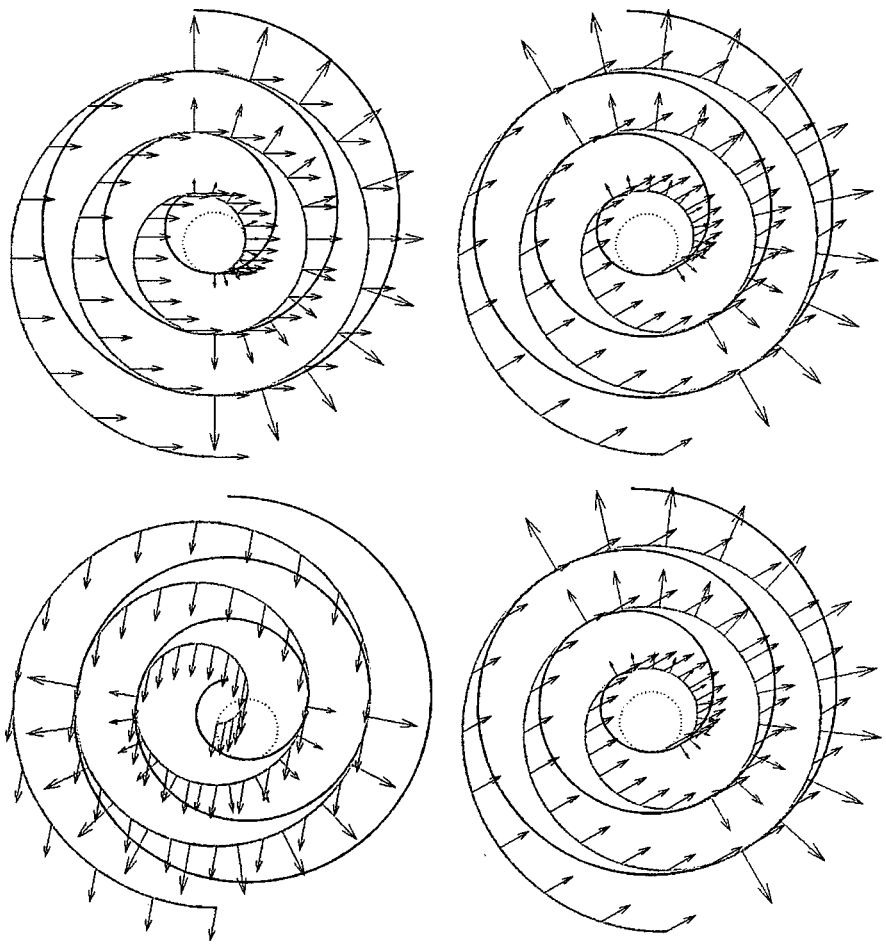

Figure 5.13. Diagrams indicating direction of motion and direction of force at different orbiting angles

At the orbiting angle α, the drive segments on the moving scroll are:

$$\begin{aligned} &\varphi \in [\alpha + 2n\pi, \alpha + (2n+1)\pi] \\ &n = 0,1,.., \text{and } 2n\pi + \alpha \le \varphi_{end} \end{aligned} \tag{5.13}$$

φ_{end} is the maximum tangential angle of the moving scroll. From equations (5.11), (5.12) and (5.13) the drive force applied on a drive segment is

$$\mathbf{F} = z\mathbf{p}\int_{\alpha+2n\pi}^{\alpha+2n\pi+\pi}(\rho_0 + \kappa u)\cos\left(u - \frac{\pi}{2} - \alpha - 2n\pi\right)du \tag{5.14}$$

ρ_0 is the radius of curvature at tangential angle $2n\pi + \alpha$.

After integration, equation (5.14) becomes

$$\mathbf{F} = z\mathbf{p}(2\rho_0 + 2\kappa\alpha + (4n+1)\kappa\pi) \tag{5.15}$$

The torque generated on a drive segment by the drive force is

$$\boldsymbol{\tau} = zr\mathbf{p}(2\rho_0 + 2\kappa\alpha + (4n+1)\kappa\pi) \tag{5.16}$$

The torque generated by a scroll air motor is the sum of the torques on all drive segments.

Figure 5.13 shows the direction of motion and the direction of force at the orbiting angle $\alpha = 0^\circ$ (upper left), $\alpha = 30^\circ$ (upper right), $\alpha = 50^\circ$ (lower right), $\alpha = 110^\circ$ (lower left).

5.6 Mass flow rate calculation

The mass flow rate of a scroll air motor is calculated as the amount of mass that charges the charge/central chamber divided by the time it takes for one entire revolution. Therefore, the mass flow rate is of the form of

$$\dot{m} = m_c \cdot \omega / (2\pi) \tag{5.17}$$

$\dot{m}$ stands for the average mass flow rate, m_c stands for air mass in the charge chamber at a steady flow rate, ω stands for the angular speed.

5.7 Overall model of scroll air motor dynamic processes

To give a mathematical model of a simplified scroll air motor, some assumptions must be made: the compressed is ideal gas, there is no static friction, no heat transfer, surrounding temperature is constant, and the supply pressure is constant.

Based on the description in last three chapters, i.e. orifice theory, equation (2.17), mathematical model of a control volume, equation (2.33) and (2.34), the orbit, equation (4.7), the geometry model of a scroll air motor, equation (4.20), Newton's second law of motion, equation (5.11) , the force analysis, equations (5.14) and (5.16), leakage model, equation (5.7), (5.8) and (5.10), a state-space model of a scroll-type air motor.

$$\dot{\omega} = \tau_{drive} - \tau_f - \tau_{load} \tag{5.18}$$

$$\dot{p}_i = f\left(\dot{V}_i, V_i, \dot{m}_{i\_in}, \dot{m}_{i\_out}, p_i, p_{i\_in}, p_{i\_out}\right) \tag{5.19}$$

The system can be considered as a cascaded connection of two non-linear systems. Equation (5.18) represents the mechanical part of the model, where $\dot{\omega}$ stands for the angular speed, τ_{drive} stands for the drive torque generated by compressed air, τ_f stands for the friction, and τ_{load} stands for torque load. Equation (5.19) represents the air dynamic part of the system, where $\dot{p}_i$ stands for the derivative of instantaneous air pressure in each chamber, $\dot{V}_i$ stands for the derivative of instantaneous volume of the chamber, V_i stands for the instantaneous volume of the chamber, $\dot{m}_{i\_in}$ stands for the mass flow rate into the chamber, $\dot{m}_{i\_out}$ stands for the mass flow rate going out of the chamber, $\dot{p}_i$ stands for the instantaneous pressure of the chamber, $\dot{p}_{i\_in}$ stands for the upstream pressure of the inward air flow, $\dot{p}_{i\_out}$ stands for the downstream pressure of the outward air flow.

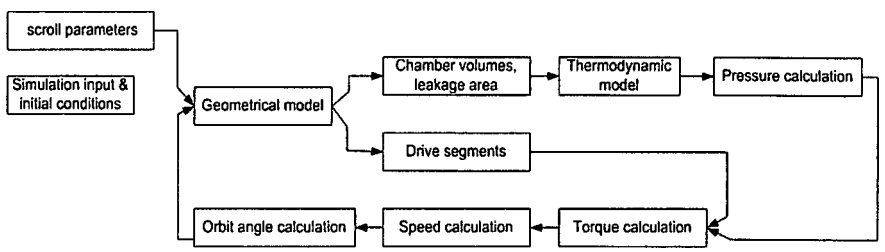

Figure 5.14 Flowchart of the model

Figure 5.14 shows the flowchart of the mathematical model of the scroll air motor. It can be seen that the torque calculation and thermodynamics calculation are both based on the geometrical model, whose inputs are the orbit angle and scroll parameters.

The scroll air motor used for the experiment has the following parameters: $\rho_0 = 9.5mm$, $r = 5.5mm$, $\delta = 4.5mm$, $\varphi \in [0,3.5\pi]$. Then the state variables are x_1 : orbiting angle, x_2 : angular speed, x_3 : pressure in the centre/charge chamber, x_4 : pressure in the expansion chambers, x_5 : pressure in the discharge chambers, x_6 : pressure in the exhaust chamber.

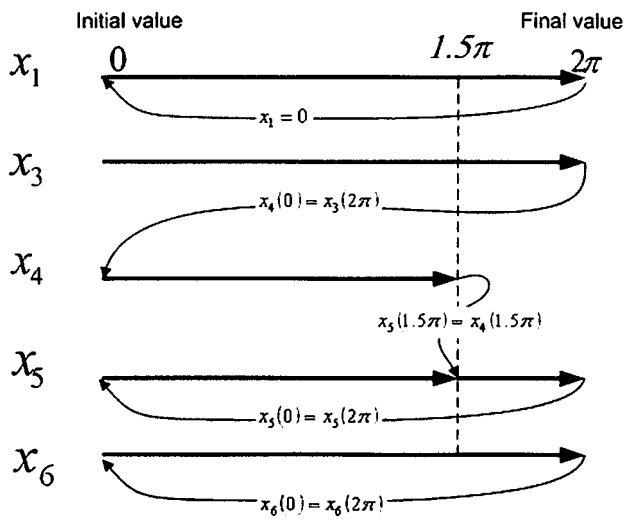

Figure 5.15 Diagram of states shifting

In order to solve the dynamic system, a method called states shifting must be introduced. As it shown in Figure 5.15, x_1 : orbiting angle, x_3 : pressure

in the centre/charge chamber, x_4: pressure in the expansion chambers, x_5: pressure in the discharge chambers. x_6: pressure in the exhaust chamber. The curves between the state variables show the transition behaviours. As a shaft revolution equals 2π, a scroll air motor runs repeatedly at the period of 2π. Compressed air goes into the scroll-type air motor. The first chamber it reaches is the central/charge chamber. As the air motor runs, at $x_1 = 2\pi$, a certain mass of compressed air is sealed in the expansion chambers. The initial value of x_4 is the final value of x_3. At the orbit angle $\alpha = \alpha_e = \alpha_d = 1.5\pi$, the expansion chambers become discharge chambers, the arrowed curve between x_4 and x_5 indicates the state transition. The value of x_5 at the orbit angle 0 is equal to that at the orbit angle 2π. x_6 is of the period of 2π, and its initial value at orbit angle of 0 equals its final value at the orbit angle of 2π. The principal of state shifting is that the state variation of a certain mass of compressed air is observed as it travels from the central chamber through the side chambers to the outlet. If there are N pairs of expansion chambers, at every $x_1 = 2\pi$ (Figure 5.15), the pressure of the n^{th} chamber becomes the pressure of the $(n+1)^{th}$ chamber and then the air motor goes into another cycle.

5.8 The simulation result

The simulation result of a step response of the mathematical model with the following parameters is shown in this section. The results of different conditions, i.e., different supply pressure, different load, will be given in Chapter 7.

The parameters of the model are:

$M_f = 0.09$; $p_s = 3.5$ bar ; $p_{atm} = 1$ bar ; $T = 293$ K ; $R = 287$ J/K kg ;

$J = 12.77 \times 10^{-4}$ Ns^2 /(m Rad) ; $r = 6.33 \times 10^{-3}$ m ; $\rho_0 = 5.17 \times 10^{-3}$ m ;

$z = 10 \times 10^{-3}$ m ; $X = X_{\max} = 3 \times 10^{-3}$ m ; $z = 3.32mm$, $\varphi \in [0, 3.5\pi]$,

$\phi_{backplate} = 112mm$; $\delta = 4.5mm$

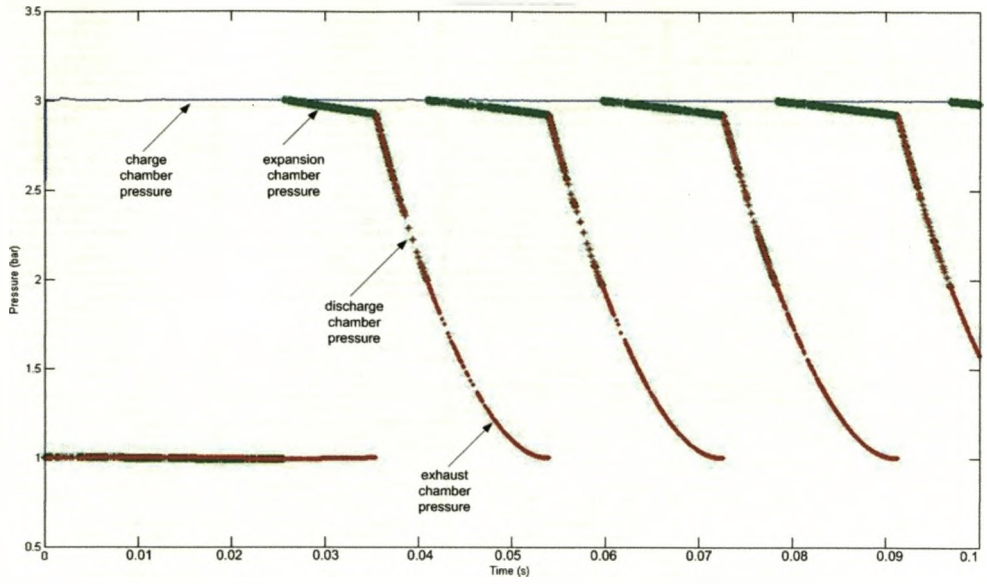

Figure 5.16. Simulation result showing pressure states in chambers of a scroll air motor

Figure 5.16 shows how the pressure inside a scroll-type air motor responses to a step input, $X = 3\times10^{-3}$ m, at time equals zero. The initial pressure in any chamber is 1 bar, and the value of initial orbit angle is zero. From the figure, the pressure in the central/charge chamber keeps nearly constant at the supply pressure. The compressed air pushes the moving scroll to orbit. It can be considered as a quasi-static process, where transmission power of compressed air is utilised. As the compressed air goes into the expansion chambers, the pressure decreases from 3 bar to 2.85 bar as the volume of the side chambers expand and the effect of leakage. The slope of the pressure is nearly constant. This can be explained using the simulation result in Figure 4.12, where the derivative of the

expansion chambers' volume is a constant. Furthermore, the expansion process can be considered isothermal. According to the ideal gas law that the product of air pressure and its volume is a constant where the temperature does not change, the rate pressure change is constant. However, due to the leakage flows, the rate of change is not exactly a constant during the expansion process. In the discharge chambers, the pressure drops more quickly than it does in the expansion chambers as the result of discharging into the exhaust chamber. It can be seen that the exhaust pressure is very low. Expansion power of compressed air is utilised as the compressed air flows through the expansion and discharge chambers.

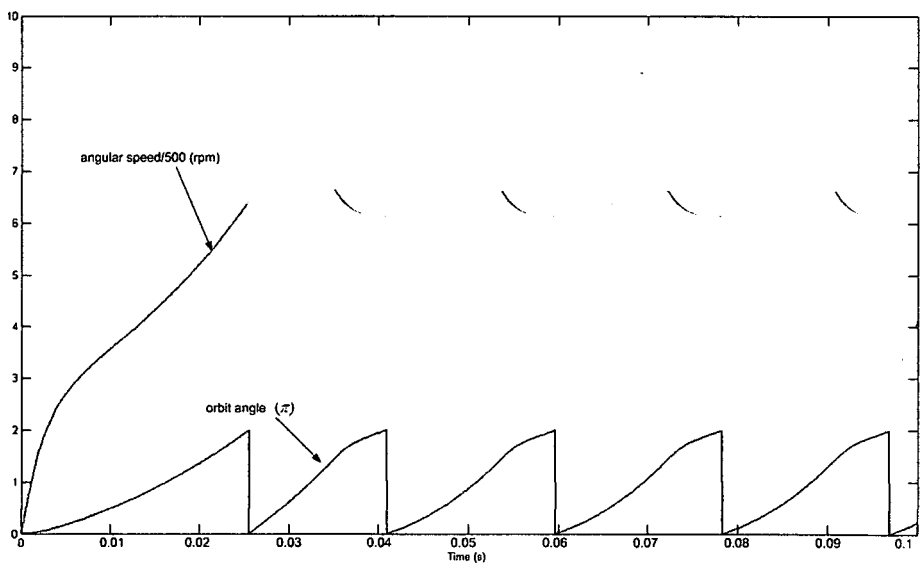

Figure 5.17 Simulation results of orbit angle and angular speed

Figure 5.17, shows the simulation result of the orbit angle and angular speed response of the step input. The orbit angle changes from zero to 2π periodically. The instantaneous value of the angular speed changes at the same frequency of the orbit angle. It increases from when the orbit angle equals zero and reaches the peak when the orbit angle equals 1.5π. Then it decreases until the orbit angle goes back to zero. From Figure 4.11 and Figure 5.16, it can be seen that if the orbiting angle is between 1.5π and π, there is not any expansion chambers. Furthermore, the compressed air in the discharge chambers flows into the exhaust chamber during this period. These result in a rapid drop in drive torque. Then the angular speed decreases.

Figure 5.18 shows angular speed responses with three supply pressure inputs. When the supply pressure is 4 bar, the steady state angular speed is around 3200 rpm; when the supply pressure is 5 bar, the steady state angular speed is around 4150 rpm; when the supply pressure is 6 bar, the steady state angular speed is around 5100 rpm. It can be seen that higher supply pressure will lead to higher angular speed at steady state and shorter rising time.

Figure 5.19 presents the relationship between rotating speed and supply pressure using the mathematical model and the parameters introduced in Chapter 4 and 5. The rotating speed increases up to 3000 rpm as the supply

pressure increases from atmospheric pressure to 3 bar. From the simulation result, it can be seen that the angular speed of scroll air motor at steady state is linear against the supply pressure input.

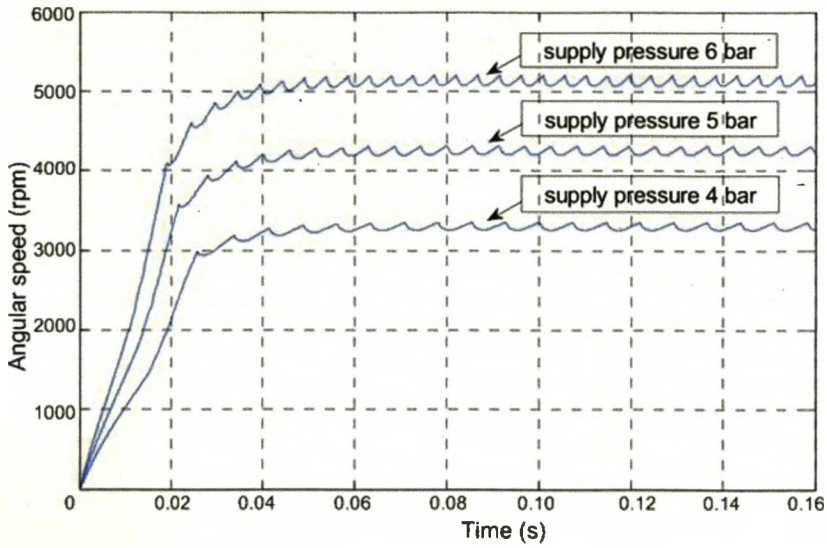

Figure 5.18 Angular speed responses with different supply pressure inputs

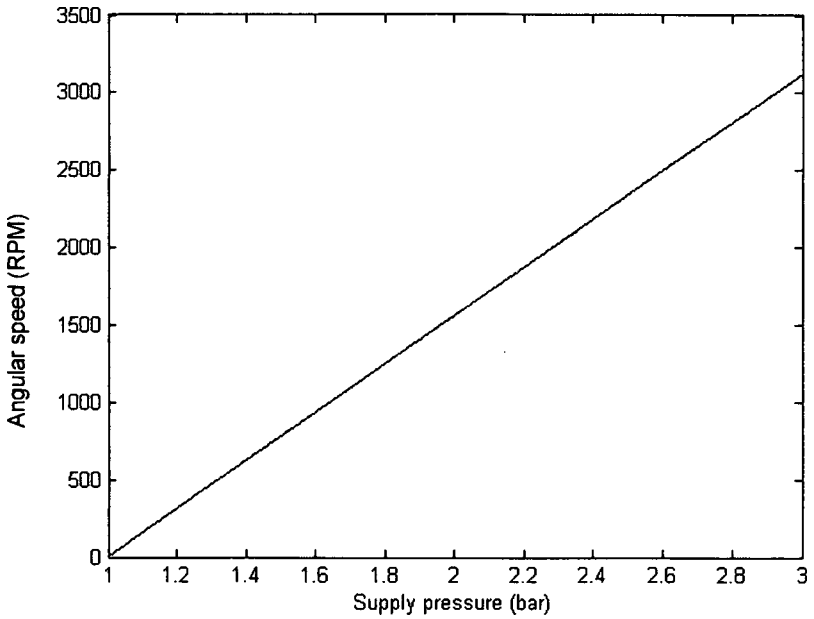

Figure 5.19. Simulation result of supply pressure v.s. angular speed without load

5.9 Summary

The dynamics of a scroll air motor is analysed in this chapter. The models for leakage, friction, force, torque, and the chambers are given to develop the mathematical model for a scroll air motor together with the geometric model introduced in Chapter 4. Individual processes within the air motor chambers have been identified and the models for these processes were developed. The model uses the first law of thermodynamics for open control volumes to calculate the instantaneous air state as a function of the orbiting angle. The simulation results of step response are given, from which the air pressure changes inside the chambers can be seen. This is important to understand and analyse the energy efficiency of a scroll air

motor. Simulation results for different conditions will be given in Chapter 7, where the model is validated.

Chapter6

Energy Transformation of a Scroll Air Motor and Energy Efficiency Comparison between a Scroll Air Motor and a Vane Type Air Motor

As a scroll air motor is a pneumatic actuator to convert pneumatic energy into mechanical energy, in order to analyse energy efficiency of a pneumatic actuator, the energy characteristics of compressed air should be studied first. This chapter continues to theoretic study of air energy including the definition air energy and composition of air energy. Energy efficiency analysis of a scroll air motor is conducted using the mathematical model presented in the previous chapters. The energy conversion ability a vane type air motor is also analysed and its energy efficiency had been compared with the scroll air motor. The analysis shows that the scroll air motor is more energy efficient than the vane type air motor.

Chapter 6 Energy Transformation of a Scroll Air Motor and Energy Efficiency Comparison between a Scroll Air Motor and a Vane Type Air Motor

6.1 Energy carried by air

There was no method to calculate the power consumed by air flow until the concept, called air power, was proposed by (Cai, Kawashima & Kagawa 2006). The term, energy represents the work-producing potential that can be extracted from a substance. For compressed air, the potential is its available energy. It is the maximum work that can be extracted from air as it undergoes a reversible process from a given state to the atmospheric state on the surrounding of the atmosphere. From (Cai, Kagawa & Kawashima 2002), when the air temperature is equal to atmospheric temperature, the available energy per unit mass of air can be expressed by

$$e = \frac{pV}{m} \ln \frac{p}{p_{atm}} \tag{6.1}$$

p is the air pressure, V stands for air volume, m stands for the air mass. From equation (6.1), it can be concluded that p has to be greater or equal to the atmospheric pressure p_{atm} so that the available energy exists. And if p is equal to p_{atm}, e is equal to zero. That means air conveys available energy if and only if its pressure is greater than p_{atm}.

The air power can be defined by:

$$P = \dot{M}RT\left[\ln\frac{p}{p_{atm}} + \frac{\gamma}{\gamma-1}\left(\frac{T}{T_{atm}} - 1 - \ln\frac{T}{T_{atm}}\right)\right] \tag{6.2}$$

$\dot{M}$ stands for mass flow rate of air, R stands for the gas constant, T stands for air temperature, γ stands for specific heat ratio. When the air temperature is equal to atmospheric temperature, i.e., $T = T_{atm}$, air power can be calculated by

$$P = \dot{M}RT_{atm}\ln\frac{p}{p_{atm}} = p\dot{Q}\ln\frac{p}{p_{atm}} \tag{6.3}$$

$\dot{Q}$ stands for volumetric flow rate.

Air power consists of two parts (Cai, Kawashima & Kagawa 2006). One is transmission power that represents pushing power from the upstream to the downstream. Pneumatic cylinders normally utilise this part only. However, compressed air contains not only transmission power, but also, because of compressibility of air, expansion power. Even when the upstream air inlet is shut off, the compressed air inside the chambers can still carry on the work by expanding. Thus another significant part of air power is expansion power that shows the work ability by air expansion.

Assuming there is no friction of leakage, the ideal processes of consuming compressed air energy in shown in Figure 6.1. In part (a), the cylinder is charged with the compressed air and the supply pressure is p_s. The piston

is pushed by the supply pressure from the position A to B and drives the load. During this process, the supply pressure is constant and the drive chamber is open to the compressed air source. Then the transmission energy of compressed air is doing work. In (b) part of the figure, the air inlet is shut, and the compressed air sealed inside the chamber expands until the piston enters balanced condition. During this process, the expansion energy pushes the piston from the position B to C and output work. The pressure-volume diagram of the charge and expansion processes is shown in the (c) part of the figure.

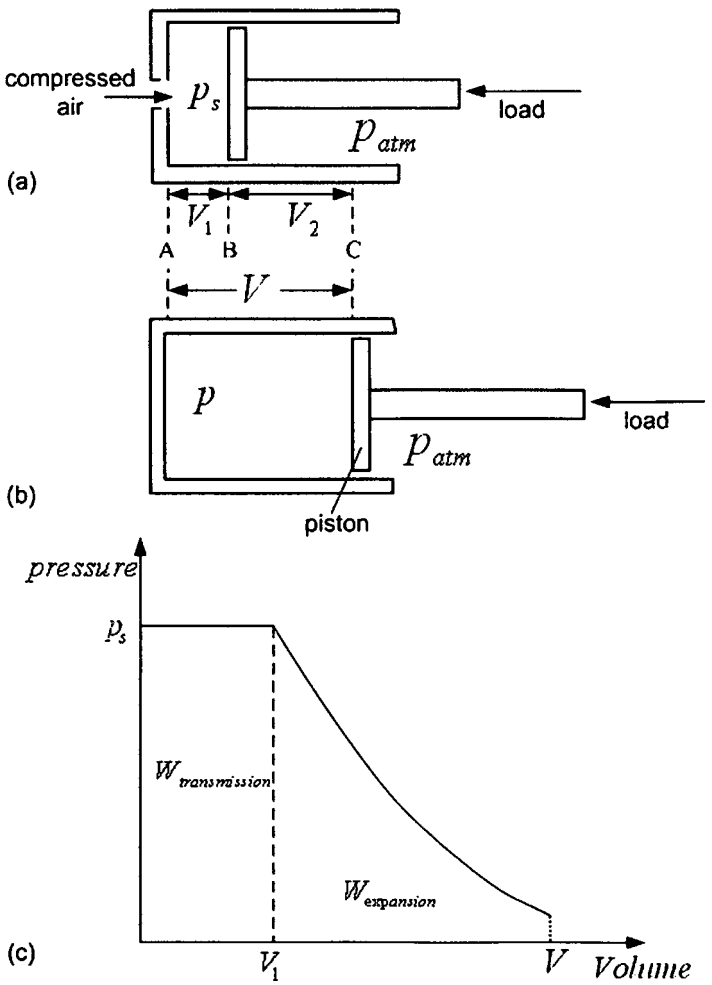

Figure 6.1 Ideal consumption of compressed air energy

Under the atmospheric temperature, the transmission power of air can be expressed by:

$$P_t = \dot{M}RT_{atm}\left(1-\frac{p_{atm}}{p}\right) \tag{6.4}$$

The expansion power of compressed air under atmospheric temperature can be expressed by:

$$P_e = \dot{M}RT_{atm}\left(\ln\frac{p}{p_{atm}} + \frac{p_{atm}}{p} - 1\right) \tag{6.5}$$

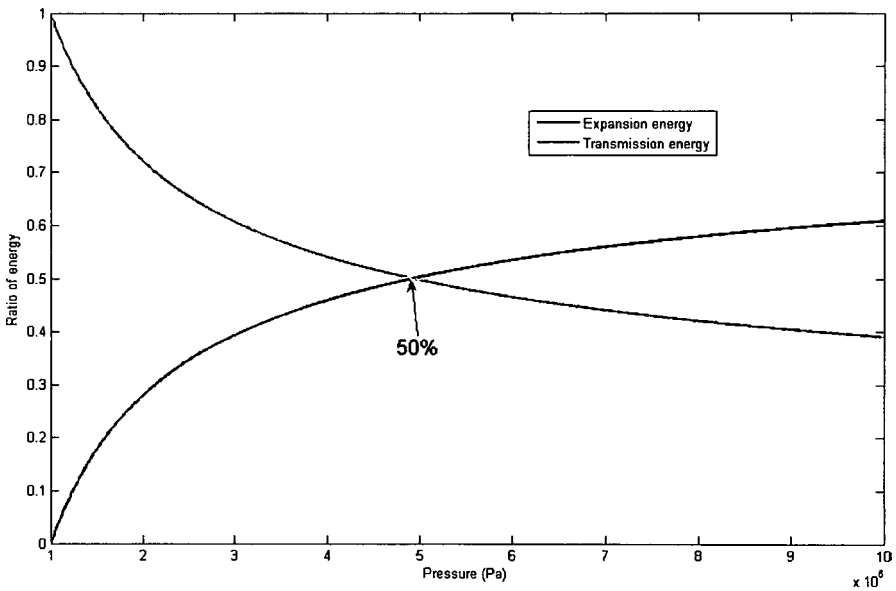

Figure 6.2. Composition of air energy

Assuming atmospheric pressure is $1x10^5$ Pascal, Figure 6.2 shows the percentage of expansion energy and that of transmission energy to total air energy vs. air pressure. In the figure, the black and grey curves show how the ratio of expansion energy and transmission energy vary respectively. The ratio of transmission energy goes down from 1 to below 0.4, while the ratio of expansion energy increases from zero to above 0.6. These two curves meet at the pressure is 4.9×10^5 Pa. The higher the air pressure is, the lager ratio of expansion energy is. Since the air supply pressure in

factories ranges from 6×10^5 Pa to 10×10^5 Pa, the ratio of expansion energy is typically larger than that of transmission energy, so how to utilise expansion energy of compressed air is very important to energy efficiency of a pneumatic system. It shows that savings of 30% air energy is quite normal (CADDET 1999).

The temperature of air hardly influences air energy when we are discussing energy efficiency of a pneumatic actuator because the air power increases about 15% when the temperature difference is 100 K (Cai, Kagawa & Kawashima 2002). Besides transmission energy and expansion energy, kinetic energy can also be converted into mechanical work. However it accounts for less than 5% of available energy when the average velocity is below 100 m/s at the pressure above 3×10^5 Pa. Therefore, kinetic energy can normally be neglected when the internal energy distribution in pneumatic components is not counted in.

6.1 Energy distribution of a pneumatic actuator system

Figure 6.3 shows how a pneumatic actuator system utilise the energy delivered by compressed air. As a pneumatic actuator system is driven by compressed air, all the energy goes into the system is from compressed air used to operate the system. As mentioned earlier, available energy of compressed air consists of transmission energy and expansion energy. A pneumatic actuator system converts energy carried by the compressed air

into mechanical energy and outputs it through the shaft. The output work is always less than the available energy. The energy loss includes mechanical losses due to friction and vibration, and the losses in the forms of leakage and heat transfer.

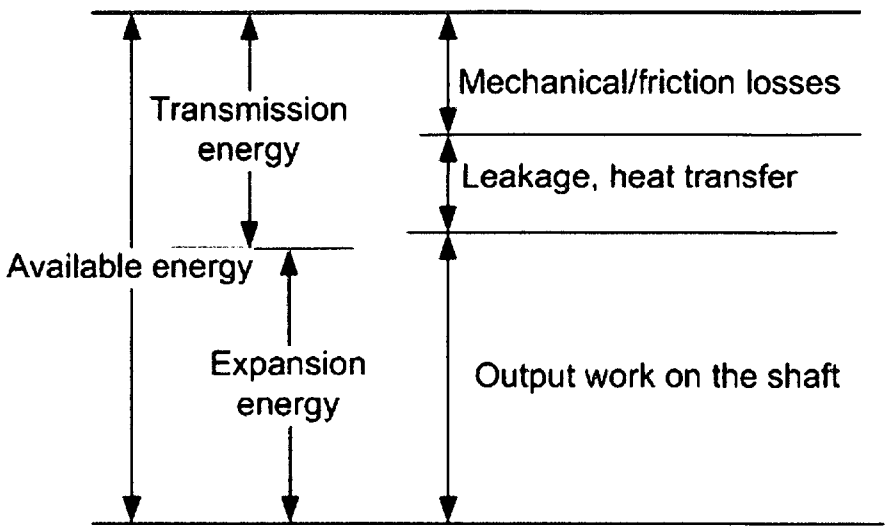

Figure 6.3 Energy distribution of a pneumatic actuator system

6.2 Ability of energy conversion of a scroll-type air motor

A pneumatic cylinder is a very popular and common actuator used around the world. A normal actuation mode of a cylinder is: in the driving stroke of a cylinder actuation, there is little pressure disturbance in the drive chamber. In the returning stroke, compressed air in the drive chamber will be exhausted. In this actuation mode, it can be seen that there is no work done by air expansion and supplied expansive energy is not utilised.

Chapter 6 Energy Transformation of a Scroll Air Motor and Energy Efficiency Comparison between a Scroll Air Motor and a Vane Type Air Motor

Generally, expansive power accounts for more than half of all power transmitted in airflow.

A scroll air motor utilises both transmission power and expansion power of compressed air. The central chamber works as a cylinder does. When a scroll air motor is running, compressed air directly and continuously goes into the central chamber. The section of moving scroll, which is one of the walls of central chamber, is pushed by the air. The pressure in the central chamber keeps roughly constant. Transmission power of air is utilised in charging phase. After the air goes into the side chambers, expansive energy is utilised to push corresponding sections on the moving scroll. The energy of the compressed air is utilised gradually as it goes from the central chamber through the most outer side chambers.

Using the parameters of a scroll-type air motor given in Chapter 3 and Chapter 4, at the supply pressure is 3 bar, the air pressures inside the chambers of the scroll-type air motor is shown in Figure 5.16. From the figure, we can see the three phases, charging phase, expansion phase and discharging phase, are happening simultaneously in different chambers, which is not convenient for analysing energy efficiency. If we focus on a certain mass of air and track the pressure variation of that air, the situation is clear. Figure 6.4 clearly shows how the pressure varies as a certain mass of air travels through the scroll-type air motor. The air goes into the central

chamber starting the charging phase at point **A.** The charging phase ends at point **B**, which is also the start of expansion phase. Through point **A** to point **B**, the pressure keeps constant at the value of the supply pressure. The curve between point **B** and **D** indicates pressure change through expansion process. The discharging phase starts at point **D**. The air exhausts into atmosphere thereafter.

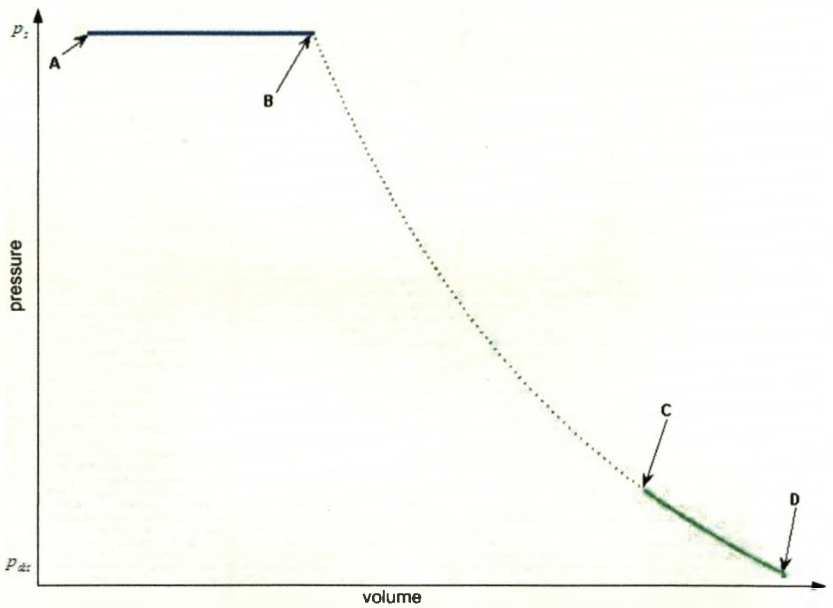

Figure 6.4. Pressure-volume diagram for a scroll air motor

Figure 6.5 shows the three types of expansion, normal expansion, (a), deficient expansion, (b), and over expansion, (c). Deficient expansion refers to the expansion that leads to the pressure after expansion is higher than the ideal exhaust pressure, which is normally atmospheric pressure, p_{atm}. When it is higher than the exhaust pressure, an isochoric expansion

loss will occur. Over expansion leads to the pressure after expansion lower than the ideal exhaust pressure and the gas in the exhaust chamber will flow backwards into the control volume and an isochoric compression loss will appear. In order to maximise the energy efficiency, a normal expansion is desired. The supply pressure should be set according to the expansion ratio of a scroll-type air motor. Ideally, the supply pressure should be set to the value that makes the discharge pressure is equal to the ambient pressure to make sure the maximum energy efficiency occurs. That is called normal expansion. However, in reality, deficient expansion is more feasible than normal expansion, which makes discharge pressure is higher than ambient pressure. It is called over expansion for a scroll-type air motor if the exhaust pressure is below atmospheric pressure, gas in atmosphere will flow.

The hatched area in Figure 6.5 represents the energy loss due to over or deficient expansion.

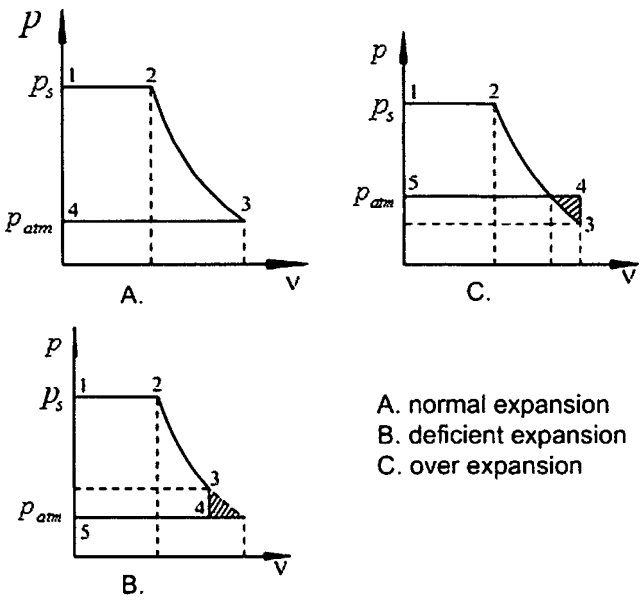

Figure 6.5 Three types of expansion

6.3 Power output of a scroll-type air motor

For a scroll-type air motor, the higher energy efficiency does not mean the high power. Air power is calculated by equation (6.3). Increasing the supply pressure can increase the air power. However, with the expansion ratio is fixed, the higher supply pressure may lead to deficient expansion and an isochoric expansion loss. Furthermore, as power of a scroll-type air motor is the product of the energy efficiency and the air power, very low energy efficiency could lead to lower output power of a scroll-type air motor.

Power of a rotary machine is calculated by:

$$\text{Power (kw)} = \frac{\text{Torque (Nm)} \cdot \text{Speed (rpm)}}{9550} \tag{6.6}$$

Substituting the simulation results into equation (6.6), power output from the scroll-type air motor is shown as the grey curve in Figure 6.6. The black curve stands for air power calculated by equation (6.3). Both air power and power generated by the scroll-type air motor increase while the supply pressure increases from 0.35 MPa to 3 MPa.

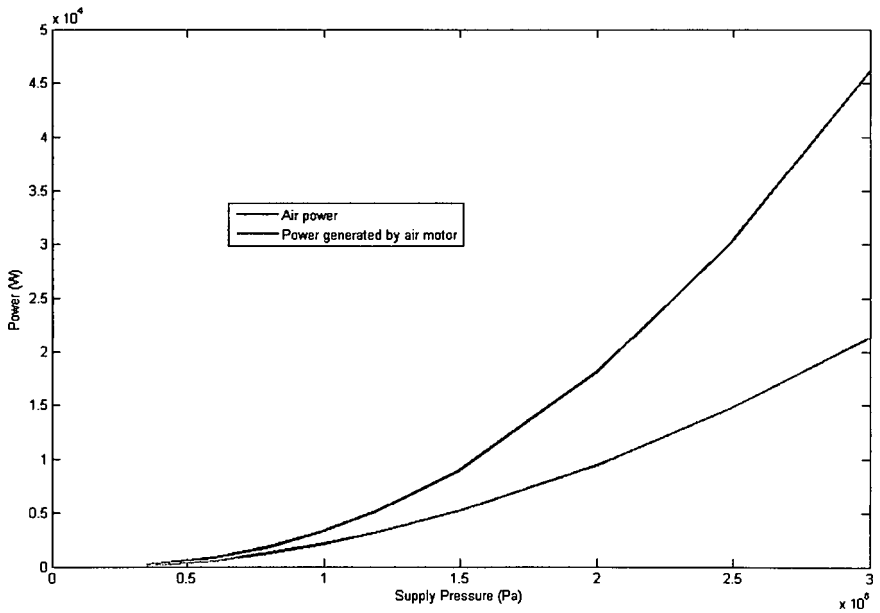

Figure 6.6. Air power and power generated by the scroll-type air motor

6.4 Energy efficiency comparison between a scroll-type air motor and a vane type air motor

Energy efficiency of a scroll-type air motor is calculated by:

$$\eta = \frac{\text{Power generated by the air motor}}{\text{Air power consumed by the air motor}} \tag{6.7}$$

Using the equation above and the mathematical model for the scroll air motor presented in the previous chapters, the energy efficiency of the scroll air motor can be calculated. Similarly, using the equation above and the mathematical model for a vane type air motor intriduced in Chapter 2, the energy efficiency of the vane type air motor can be calculated.

In order to compare the restults, the following standards must be introduced:

- These two models are simulated under same assumptions (Yang, Wang & Ke 2006) (Wang et al. 1998) (Yang et al. 2008b) (Yang, Wang & Nan 2007) .
- The displacement volume of the vane-type air motor and that of the scroll-type air motor are equal.
- The inertias and the loads of the air motors are same. And the air motors have same dynamic friction coefficients.
- The air supplies are constant and continuous with same pressure.
- The air motors respectively get same air energy in the same period of time.

Figure 6.7 shows that while the supply pressure increases as the supply pressure increase. It hits the peak of 76% at the supply pressure of 4.4 bar. Then the energy efficiency decreases as the supply pressure continues increasing.

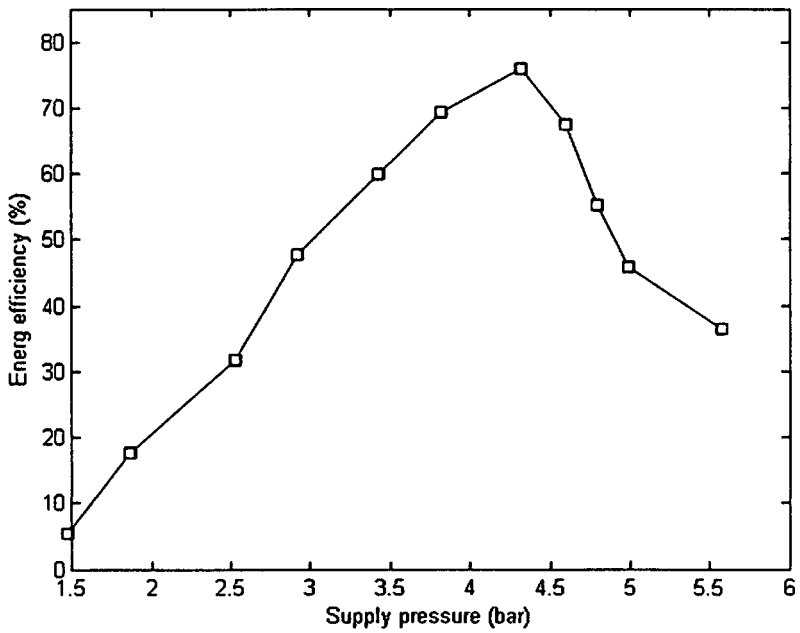

Figure 6.7. Energy efficiency v.s. supply pressure for the scroll air motor (simulation result)

Figure 6.8 shows the energy efficiency of the vane type air motor. It can be seen that the energy efficiency of the vane type air motor is much lower than that of the scroll air motor under same conditions. The simulation results in Chapter 3 indicate that the exhaust of the vane type air motor is much higher than that of the scroll motor under equivalent conditions. That

means that fact that most air energy is wasted in the exhaust of the vane type air motor.

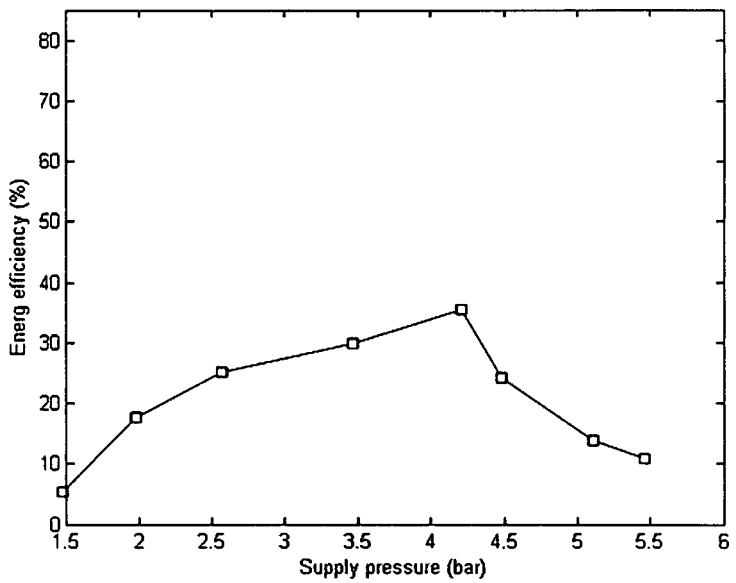

Figure 6.8 Energy efficiency v.s. supply pressure for the vane type air motor (simulation result)

(Yang et al. 2008a) discovered that using a by-pass valve to reuse exhaust of a pneumatic drive system can increase its energy efficiency and performance. However, this method only applies to pneumatic servo-control systems. For a pneumatic drive system that needs to run at a constant speed, a by-pass valve can not re-circulate the exhaust.

From the comparison, the scroll air motor is able to transform energy more efficiently than the vane type air motor, as the scroll air motor is able to utilise both transmission and expansion energy in the compressed air, while

the vane type air motor is able to utilise the transmission energy only. This can also be drawn from the pressure-volume diagrams of these two types of air motors. From the simulation result of the vane type air motor, Figure 3.5, the pressure-volume diagram of the vane type air motor is similar to that of the scroll air motor, Figure 6.4. However, the compressed air does not do any work once it enters Chamber **B,** Figure 3.2. Thus, the work done by the same amount mass of compressed air in the scroll air motor is much bigger than that of the vane type air motor.

6.5 Summary

The energy efficiency of the scroll-type air motors is much higher than the average energy efficiency of conventional pneumatic actuating systems, which is often lower than 30% (Cai & Kagawa 2001). In fact, irreversible processes such as friction, heat transfer, and air mixture will cause air power loss, so the actual energy efficiency of a scroll-type air motor should below the theoretical value.

In theory, energy efficiency of a scroll-type air motor mainly depends on supply air pressure, surrounding air pressure and ratio of expansion. Furthermore, high energy efficiency does not necessarily mean high power. However, it is still possible for a scroll type air motor to have both high

energy efficiency and high power, where high supply pressure is used to drive a scroll type air motor with proper expansion ratio.

In order to utilise air energy as much as possible, expansion ratio of side chambers is very important. Normal expansion is desired, as both deficient expansion an over expansion negatively affect the operating performance and energy efficiency of a scroll air motor.

Energy efficiency of the scroll air motor is compared with that of the vane type air motor. The vane type air motor has lower energy efficiency mainly due to its structure, which utilises transition energy of compressed air only.

Chapter 7

The Experimental System and Model Validation

In order to validate the mathematical model for the scroll air motor and analyse the energy efficiency of the scroll air motor, experimental investigations have been performed. The testing rig was constructed, including compressed air supply, the scroll air motor, the three phase AC generator, electrical loads, sensors, and data acquisition system. The scroll air motor driven by compressed air is used to drive the load, the three phase AC generator and bulbs. The supply pressure, exhaust pressure, air flow rate, angular speeds of the shaft, voltage and current outputs of the AC generator are measured to validate the model. Using the measured data, the air power is calculated and furthermore energy efficiency can be analysed.

7.1 Overview of the test rig

The test rig consists of three functional blocks, the pneumatic block, the mechanical block, and the electric/electronic block. Beside these three blocks, the data acquisition system is based on National Instruments® LabVIEW® and PCI-6024E data acquisition card. The pneumatic block includes an air compressor, the scroll type air motor, a control valve,

compressed air preparation equipments, a silencer and the links. The mechanical block consists of the scroll air motor, the encoder, and the alternator. The electric/electronic block consists of two pressure sensors, a flow rate metre, a voltage sensor, a current sensor, and the load. The diagram of the rig is shown in Figure 7.1. The orange lines stand for electronic circuit between the sensors and the PC or the electric circuit between the alternator and the load. The blue lines stand for pneumatic tubes between the pneumatic devices. The black columns stand for mechanical shafts between the encoder and the air motor, and the scroll air motor and the alternator.

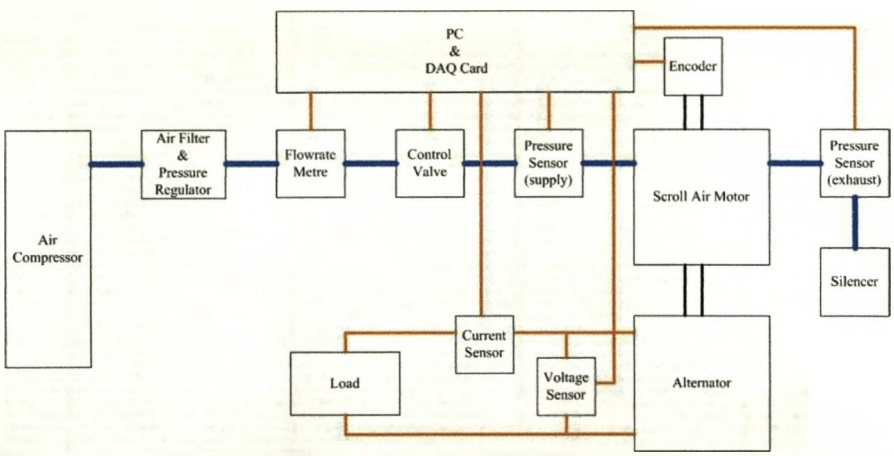

Figure 7.1 Functional blocks of the testing rig

The PC controls the scroll air motor to turn on with preset air pressure. The scroll air motor drives the alternator to generate electricity. Then the electricity drives the load, which is a group of bulbs in the system. The air compressor supplies the air motor with high pressure gas through the

regulator, the filter and the control valve. The exhaust goes out through the silencer. The block encoder in the figure represents an optical incremental encoder, which outputs fixed number of pulses every rotation. By measuring the frequency of the pulses from the encoder, the controller can work out the rotation speed of the air motor. The angular speed of the scroll air motor can also be figured out by measuring the frequency of the alternator output voltage. The voltage and current outputs from the alternator can be measured by the voltage sensor and the current sensor, and the RMS (Root Mean Square) values are calculated by the LabVIEW program. With the motion control card, the PC monitors and logs the speed of the air motor, supply and exhaust air pressure, outputs from the alternator and air flow rate.

The experimental data are used to calculate the air power and the output power from the scroll air motor. Then the energy efficiency can be derived from the data.

The data acquisition system can also be divided into three layers shown in Figure 7.2. The actual device layer includes all the sensors, meters, valves and the motion control card. This layer sends raw data to the virtual device layer and receives instruction from virtual device layer. The virtual device layer adapts the raw data, converts them into engineering units and sends the data in engineering units to the data processing layer. Also, the virtual device layer converts the instructions from the data processing layer into

physical voltage or current and sends them to the actual device layer. The data processing layer and the virtual device layer are performed by the software.

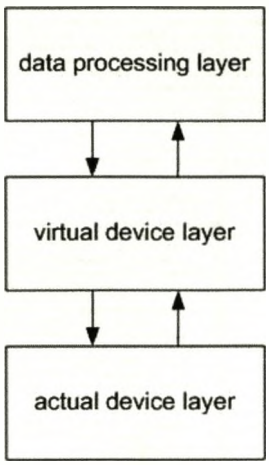

Figure 7.2 Layer model of the data acquisition system

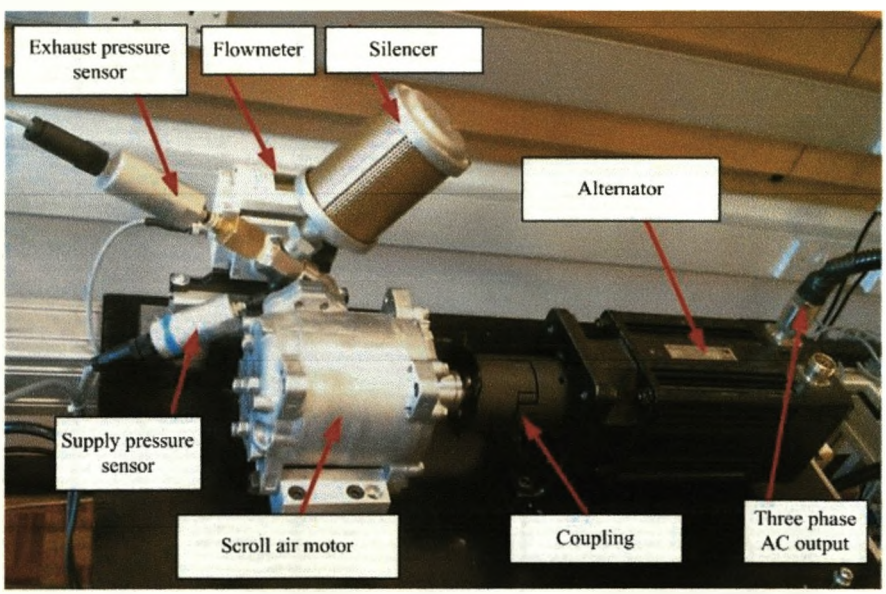

Figure 7.3 The testing rig

Figure 7.3 is the photograph of the test rig, in which the components are indicated. The specifications of these parts and calibration are in the following sectors.

7.2 The list of the devices and software

The devices and software used for the experiments are listed in the table below.

1.	Air motor	Modified TRS090 scroll compressor
2.	Alternator	Three phase AC brushless servo motor 3BRS-71-M4-3000
3.	Air compressor	Tiger® type 8/25; Output pressure: 0-6bar
4.	Compressed air tank	BOC compressed air tank, filled to 200 bar
5.	Regulator + filter + lubricator	FESTO LDE M2-G1/4-P
6.	Pneumatic valve	FESTO MPYE 5-1/8-HF-010B
7.	Pressure sensor	FESTO SDE-10-10v/20mA; measure range: 0-10bar; output: 0-10v DC or 4-20mA
8.	Flow meter (high flow rate)	FESTO MS6 SFE-F5-P2U-M12; measure range: 200-5000 l/min; analogue output: 0-10v DC
9.	Flow meter (low flow rate)	FESTO SFE-LF-F200-HQ8-P2I-M12; measure range: 0.5-200 l/min; analogue output: 4-20mA
10.	Current transducer	LEM LTS 6-NP; measure range: 0-6A DC/AC; output: 2.5±0.625v DC

11.	Voltage transducer	230V/9V transformer
12.	Encoder	British Encoder 775-1500; pulse per revolution: 1500
13.	Data acquisition card	National Instruments® PCI 6024E
14.	Data acquisition software	National Instruments® LabVIEW®
15.	Load	110V, 6w, bulbs x 9
16.	PC	Pentium 4, 1G ram, 160G HDD

Besides the devices listed above in the table, various cables, leads, tubes, adaptors, and sockets were used in the experiments. The sensor cables were supplied with the sensors. Normal AC leads rated 300AC/10A were used to connect the alternator and the load. 6mm-diameter tube was used between the air regulator and the scroll air motor. The scroll air motor was lubricated with SAE40 (*SANDEN TRS090 Specification* 1997) (Nieter & Gagne 1992).

7.3 Modification of the scroll

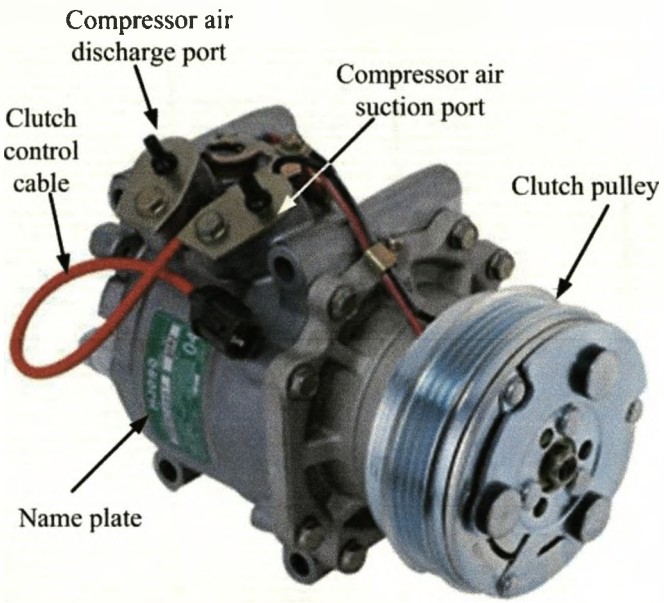

Figure 7.4 TRS090 air conditioner compressor

The scroll used for experiments is modified from a scroll type air compressor designed for car air conditioners. A TRS 090 auto air conditioner compressor is shown in Figure 7.4. The original pack comes with the main body, a compressor air suction port, a compressor air discharge port, a grooved pulley and a clutch control cable. When it is running as a compressor, the clutch engages, so that the moving scroll is driven by the shaft following the pulley powered by the car engine. And the compressor intakes air through the compressor air suction port then pressurises the air and finally discharges the compressed air through the compressor air discharge port.

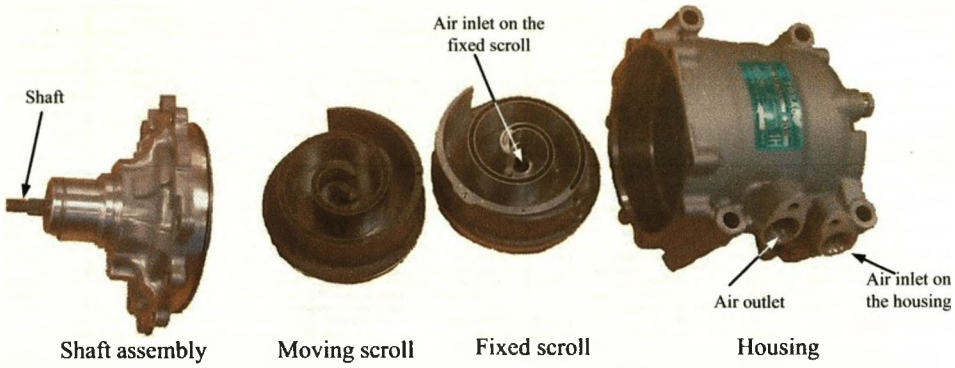

Figure 7.5 The main parts of the scroll air motor

Figure 7.5 shows the disassembly of the main parts of the scroll air motor, which are the shaft assembly, the moving scroll, the fixed scroll, and the housing. When the scroll air motor is assembled, the fixed scroll is fixed on the bottom of the housing with four bolts screwed into the back plate of the fixed scroll through the holes on the bottom of the housing. The air inlet and the air outlet are on the side wall of the housing. The scroll side of the moving scroll touches the scroll side of the fixed scroll in conjugacy. The back plate of the moving scroll connects to the shaft with the cam and ball bearing coupling.

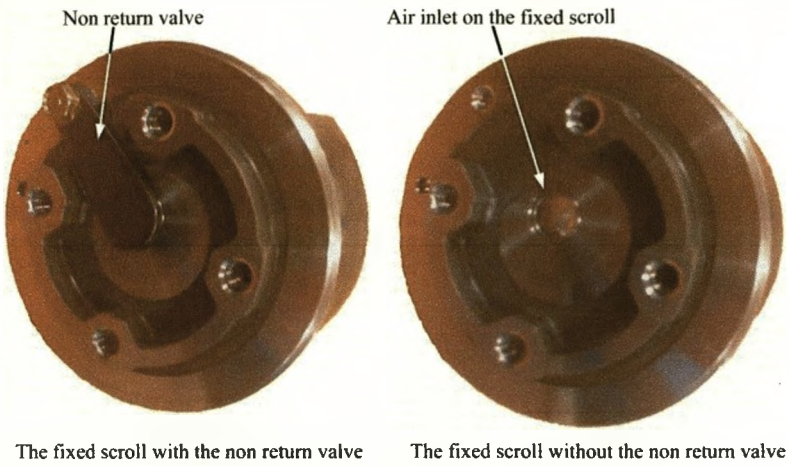

Figure 7.6 Fixed scroll modification

Because a scroll air motor is a scroll air compressor working backwards, it must be modified to make it work as a scroll air motor. The clutch pulley and the clutch control cable are removed from the main body. The compressor air suction port and compressor air discharge port work as air motor air outlet and air motor air inlet respectively. Inside the housing, the non return valve is removed from the fixed scroll to allow compressed air flow into the chambers formed by the scrolls, Figure 7.6.

7.4 The dimensions and characteristics of the scroll air motor

In order to validate the mathematical model described in the early chapters, the real value of the scroll air motor must be obtained and substituted into the equations. The nominal values from the datasheet are: displacement 85.7cc/rev; allowable continuous speed 10,000rpm; maximum downshift

speed 12,000rpm; weight 3.85kg; inertia $17.4\text{x}10^{-2}\text{kgm}^2$. (*TRS090 Datasheet* 1997)

The geometry dimensions of a scroll are measured by a venire calliper. It shows in Figure 7.7, $\phi_{backplate}$ stands for the diameter of the back plate; z stands for the height of the scroll wall; δ stands for the scroll wall thickness; $\delta + 2r$ is the pitch between 2π of scroll. The measured dimensions are: $\delta = 4mm$, $r = 6mm$, $z = 33.2mm$; $\phi_{backplate} = 112mm$; and the tangential angle $\varphi \in [0, 3.5\pi]$.

Substitute the measured values into equation (4.5) and (4.15), the scroll is constructed mathematically. Figure 7.8 shows the comparison between the real scroll and the computerised scroll created with the measured parameters. By projecting the real scroll and the mathematically constructed scroll on the same plane, it shows that the real scroll lies underneath the constructed scroll. The dark scroll in the back is the real scroll, and the transparent scroll in the front is the constructed scroll. The shapes and the trends are the same. However there are some differences between the scrolls. The major difference is at the inner end of the scrolls.

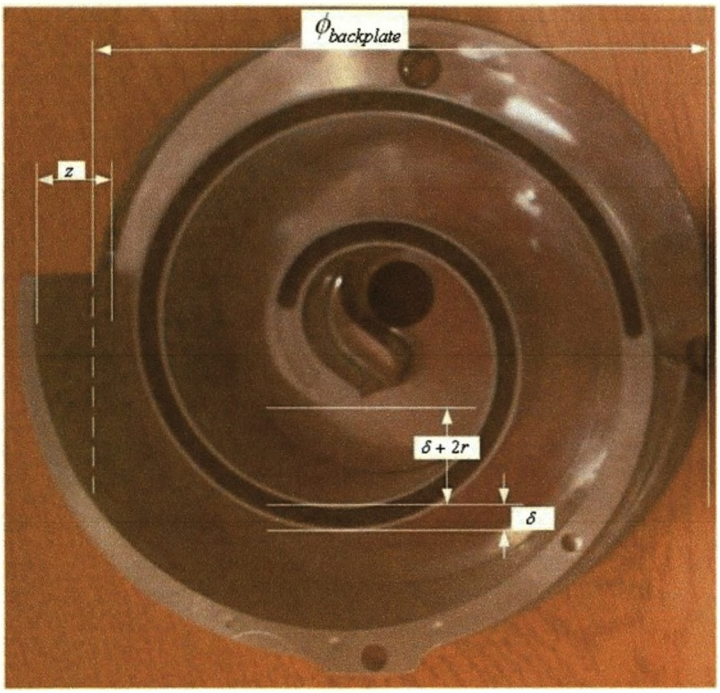

Figure 7.7 The dimension designators of a scroll

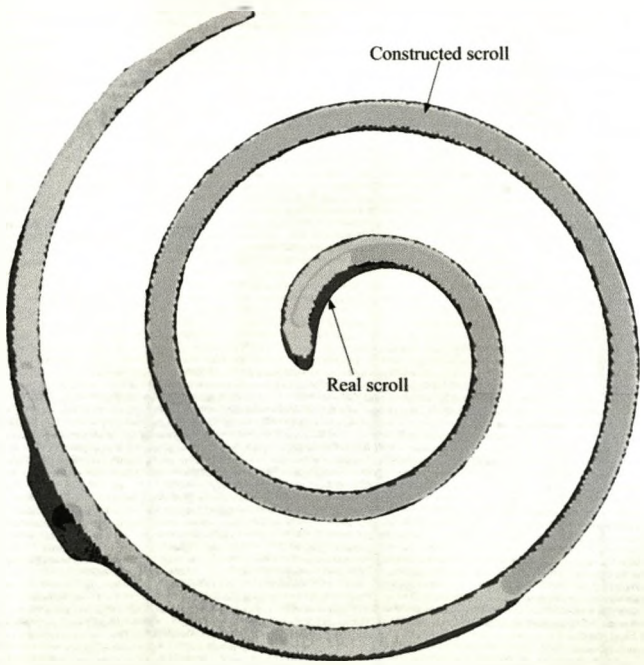

Figure 7.8 The comparison of the real scroll and the computerised scroll

From Figure 7.7 and Figure 7.8, the inner end of the real scroll is not just a simple spiral. In reality the inner end of the scroll is specially designed to decrease the volume of the discharging chamber of the scroll air compressor, so that the compression ratio is increased (Lee & Wu 1995).

7.5 The alternator in the system

The alternator used in the experiment system is a three phase synchronous brushless AC servomotor model 3BRS 71-M4-3000 (3EKM 71-M4-3000). It is a four-pole motor with maximum speed of 3000rpm, peak current 18.8A and maximum voltage 310V AC, stall torque 3.8Nm, rotor inertia $5\text{x}10^{-4}$ kgm^2 (*Handbook of AC Synchronous Servomotor 3BRS-71-M4-3000* 2005). The stator coils are Δ (delta) connected. Figure 7.9 is the equivalent circuit of the alternator stator. $\mathbf{E}_A$ is the induced voltage on each stator coil. R_{coil} stands for the copper resistance of each stator winding. jX_s is the reacted voltage on each coil. $\mathbf{V}_L$ represents line voltage. In a Δ configuration, the line voltage is equal to the phase voltage $\mathbf{V}_P$, and the line current $\mathbf{I}_L$ is $\sqrt{3}$ times as great as the phase current $\mathbf{I}_P$ in value. (Chapman 2005)

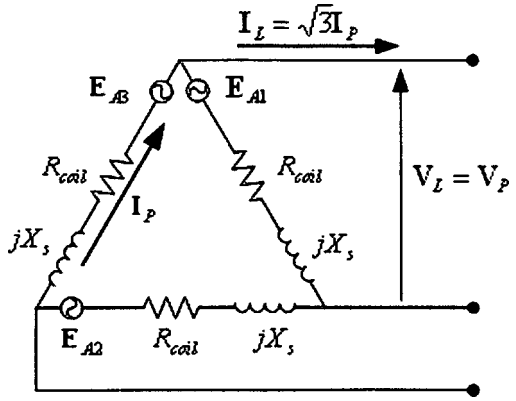

Figure 7.9 The alternator stator equivalent circuit

The torque constant $k_T = 0.81Nm/A$. The voltage constant $k_E = 54V/1000rpm$ (measured value); $k_E = 50V/1000rpm$ (nominal value). The resistance of a winding $R_{coil} = 3.2\Omega$ (measured value); $R_{coil} = 1.31\Omega$ (nominal value). The winding inductance $L_{coil} = 26mH$ (measured value); $L_{coil} = 7.1mH$ (nominal value).

7.6 NI PCI 6024E card and LabVIEW®

National Instruments® PCI 6024E is one of the low-cost E Series multifunction data acquisition. It provides Two 12-bit analogue outputs; 8 digital I/O lines; two 24-bit counters. The maximum sampling rate is 200kS/s. The analogue input range is programmable with the maximum ±10V. With National Instruments® LabVIEW®, it can operate real-time.

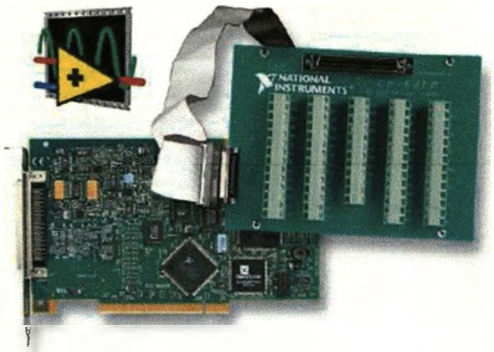

Figure 7.10 National Instruments PCI 6024E data acquisition card and CB-68LP terminal block

There are five analogue signals from the testing rig. They are supply pressure, 0-10V DC; exhaust pressure, 0-10V DC; air flow rate, 0-10V DC; AC voltage, 0-10V DC; and AC current, 2.5±0.625V DC. All these signals are sent to the data acquisition card via the terminal block, CB-68LP. (Figure 7.10)

LabVIEW® (short for Laboratory Virtual Instrumentation Engineering Workbench) is a platform and development environment for a visual programming language from National Instruments. The graphical language is named "G". It is commonly used for data acquisition, instrument control, and industrial automation on a variety of platforms including Microsoft Windows, various flavours of UNIX, Linux, and Mac OS.

In the system the sampling rate of the card is set to 1000Hz.

7.7 System calibration

Before carrying out the experiments, the system including all the sensors and the acquisition card must be calibrated to ensure the experimental data are true and accurate.

The data acquisition card, PCI 6024E, has onboard self calibration function. It is completely software controlled without any manual adjustment. The inputs and outputs are calibrated with onboard precise reference. The maximum absolute accuracy for the analogue inputs is 7.560mV at the measure range of ±10V (*National Instruments PCI 6024E datasheet* 2006).

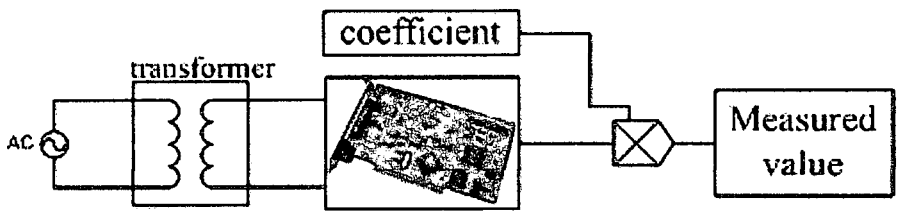

Figure 7.11 The voltage measurement circuit diagram

The voltage transducer is calibrated with the multi meter. Comparing the reading from the multi meter at the AC source with that from the data acquisition card at the output of the transformer, a coefficient is figured out. Due to linearity of the transducer output respect to its input, the real value of the AC voltage is the product of the analogue input and the coefficient (Figure 7.11).

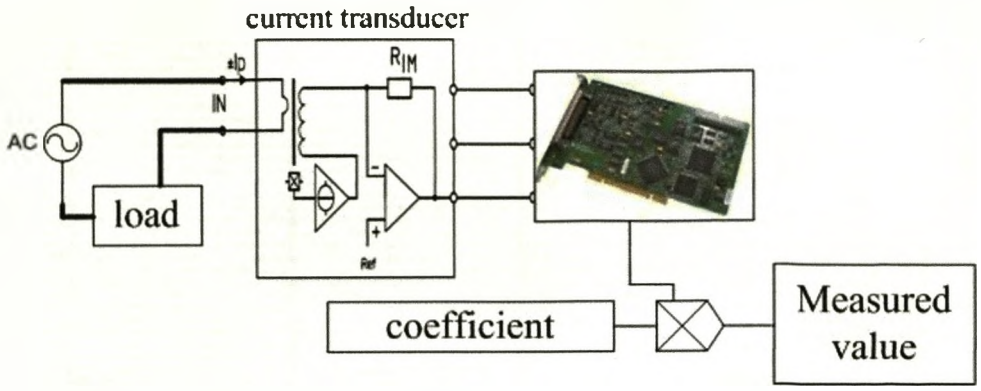

Figure 7.12 The current measurement circuit diagram

The current transducer is calibrated with the clamp multi-meter, ISO-TECH-ICM3090. The principle of calibrating the current transducer is the same as that of calibrating the voltage transducer. The difference is, in the current measurement circuit, the transducer is connected in serial with the source and a load, while the voltage transducer is parallel with the source with or without a load. (Figure 7.12)

The pressure sensors and the flow rate metres are calibrated with the reference instruments provided by the supplier.

7.8 The load of the system

The load in the system is bulbs, which can be considered as pure resistant components. The bulbs are Δ (delta) connected. And the load on one phase is equal to that on the other phases. The value of the load can be changed by adding or removing bulbs to or from the system. The voltage-ampere

characteristic of the bulb is measured under different voltage conditions and used in calculation and modelling.

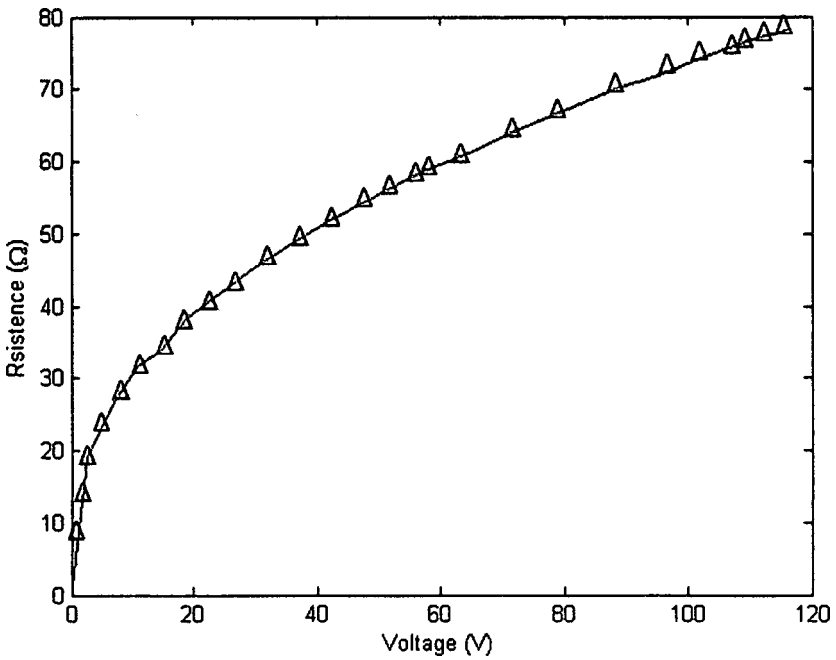

Figure 7.13 Resistance of a bulb derived from measured voltage-ampere value

The curve in Figure 7.13 shows how resistance of a bulb changes against supply voltage.

7.9 Experiments and experimental data processing

The experiments are designed to study the characteristics of the air motor-alternator, on which the energy efficiency of the air motor is analysed. In general, the system consists of three parts, the scroll air motor, the alternator and the load. And the scroll air motor and the alternator compose

the energy conversion sector. A "dry run" is useful to study the energy conversion sector. "Dry run" means running a system without the load. By running a "dry run" some parameters such as voltage constant k_E, friction characteristics and leakage can be calculated or predicted. Because the characteristics of the load are relatively simple than these of the energy conversion sector and they are not the topic of the thesis, a "dry run" is quite important for analysis of the whole system. After studying the energy conversion sector, the load is added into the system to analysis the energy efficiency. Experiments are done with the load of three bulbs (one on each phase), six bulbs (two on each phase), and nine bulbs (three on each phase). With different loads, the relationship between the input and the output are different, for example, the input pressure – rotational speed curve, the input flow rate – output voltage curve, and the most important issue, the input air power – output electric power relationship.

AC voltage, AC current, inlet pressure, exhaust pressure, and volumetric flow rate are acquired from with the data acquisition card directly. The AC wave and its frequency can be used to calculate the angular speed of the scroll air motor. The electric power generated by the alternator is the product of the RMS values of the AC voltage and the AC current. The air power is calculated by equation (6.3). The experimental data are analysed in this chapter.

7.9.1 Experiments without load

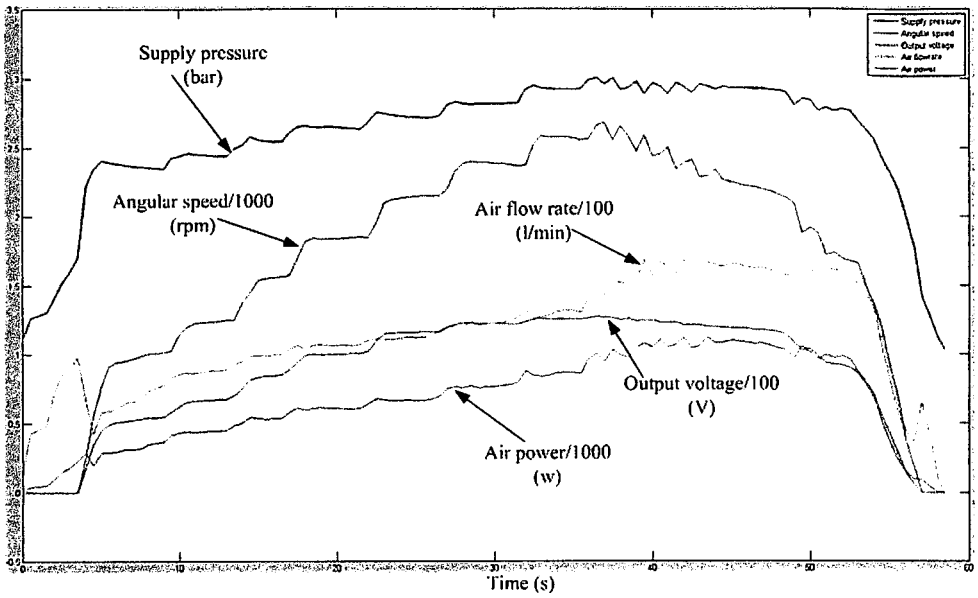

Figure 7.14 Experimental data (without load)

Figure 7.14 shows the experimental data of a "dry run". The supply pressure is absolute pressure. The output voltage is RMS value. During the experiment, the supply pressure is adjusted manually with the pressure regulator to set the operating points. At the start, the scroll air motor does not rotate until the compressed air overcomes the static friction. It is noticed that even when the scroll air motor is not in motion, the air flow exists and reaches the maximum value of 100 l/min. This flow is caused by the gap inside the air motor. Also that means the air leakage counts for a large portion of energy loses.

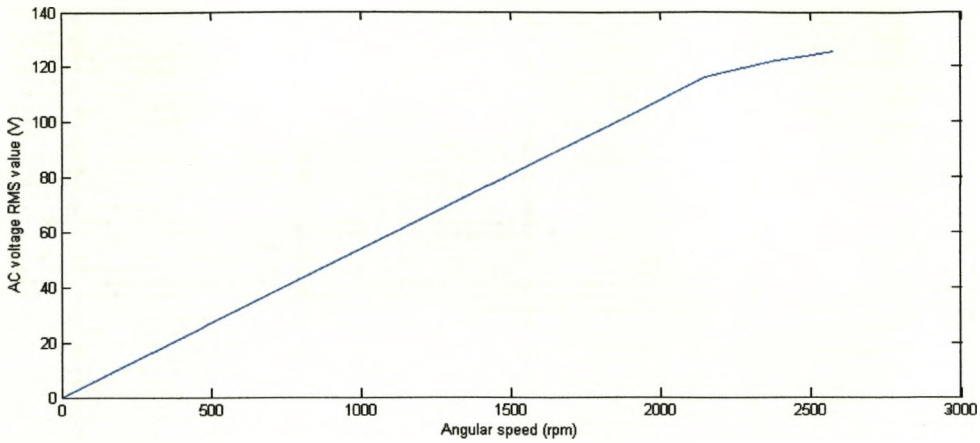

Figure 7.15 Angular speed vs AC voltage (without load)

Figure 7.15 shows the relationship between the angular speed and AC voltage, from which the constant $k_E = 0.054V/rpm$ can be derived.

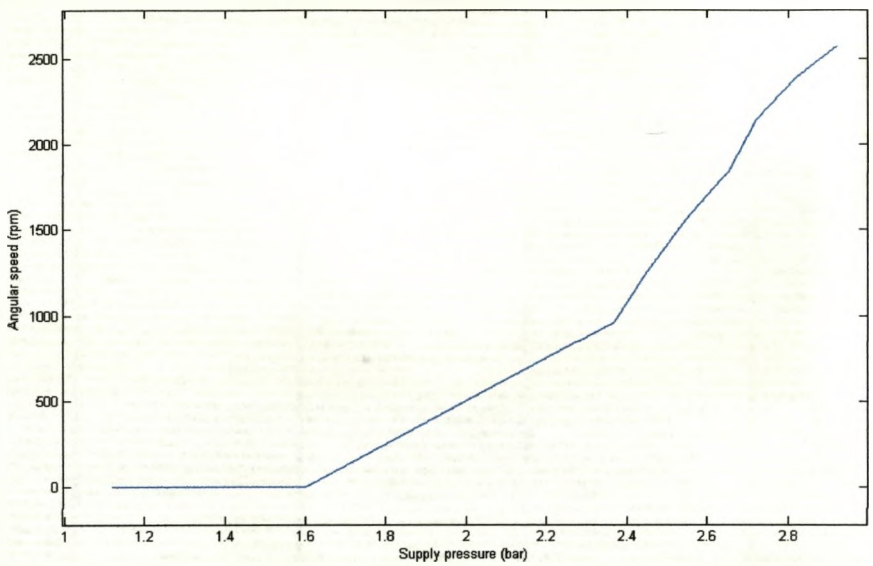

Figure 7.16 Experimental result of supply pressure vs angular speed without load

Figure 7.16 shows the relationship between the supply pressure and the angular speed of the scroll air motor. Once the system has overcome the static friction, the curve is quite linear. The experimental result is consistent with the simulation result shown in Figure 5.19.

At the condition of "dry run", there is no current output, so the electric power is zero.

7.9.2 Experiments with load

The characteristics of the system are tested with the load of three bulbs, six bulbs, and nine bulbs respectively. The open loop input of the system is supply pressure, and the measured values are AC voltage, AC current, air flow rate, supply pressure, and exhaust pressure. These experimental data are used to calculate angular speed, electric power, and air power.

Figure 7.17 shows the experimental for the system with three bulbs. The supply pressure is adjusted manually to some operating points. Due the nominal voltage of the bulbs is 110V AC, the operating point is up to the pressure, under which the AC voltage output is in the safe range.

Figure 7.18 indicates the angular speed respond to the supply pressure for three-bulb load and the simulation result using the mathematical model. Figure 7.19 shows the air power and the electric power generated by the system at different operating points for three bulb load. It is seen that the

leakage air power can be as high as 180W before the system turns in motion. Figure 7.20 gives the energy efficiency at the operating points. The experimental result shows the energy efficiency can be up to 55%, while the simulation result is higher than that.

Figure 7.24 and Figure 7.28 give energy efficiency at the operating points with the load of six bulbs and nine bulbs respectively. Comparing to Figure 7.20, the supply pressure ranges are extended as the loads are heavier. The trend of the curve in Figure 7.24 is similar that in Figure 7.28. After the system overcomes the static friction, the efficiency goes up as the supply pressure increase until the supply pressure is above 4bar. The energy efficiency reaches the peak at the supply pressure of 4 bar. Then it decreases as the supply pressure increases.

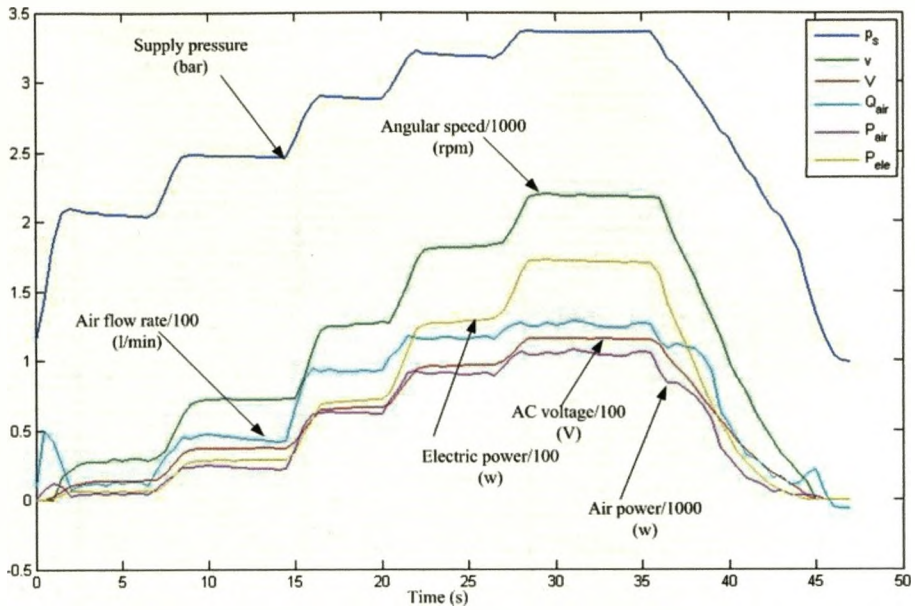

Figure 7.17 Experimental data (three-bulb load)

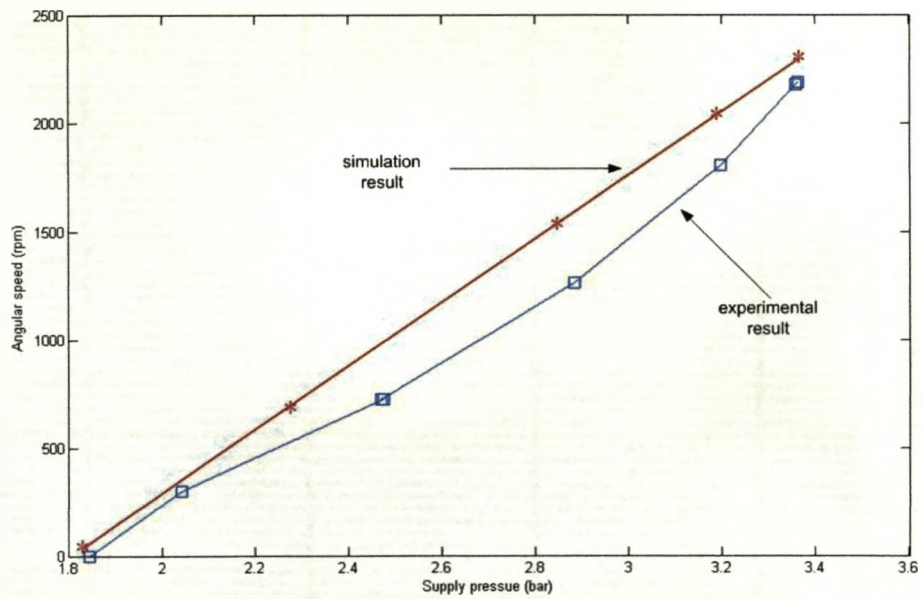

Figure 7.18 Supply pressure vs angular speed (three-bulb load)

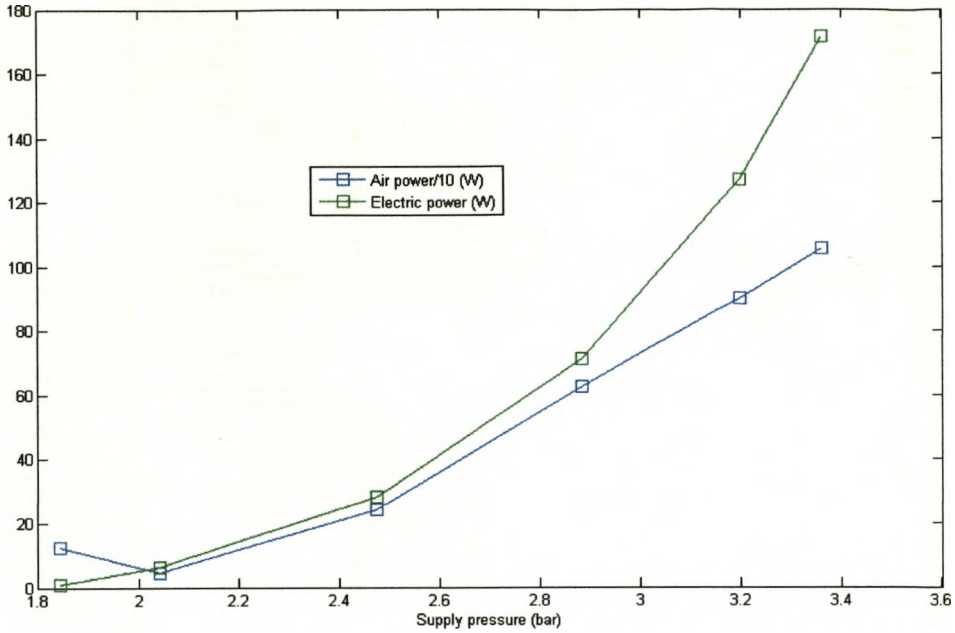

Figure 7.19 Supply pressure vs air power/electric power (three-bulb load)

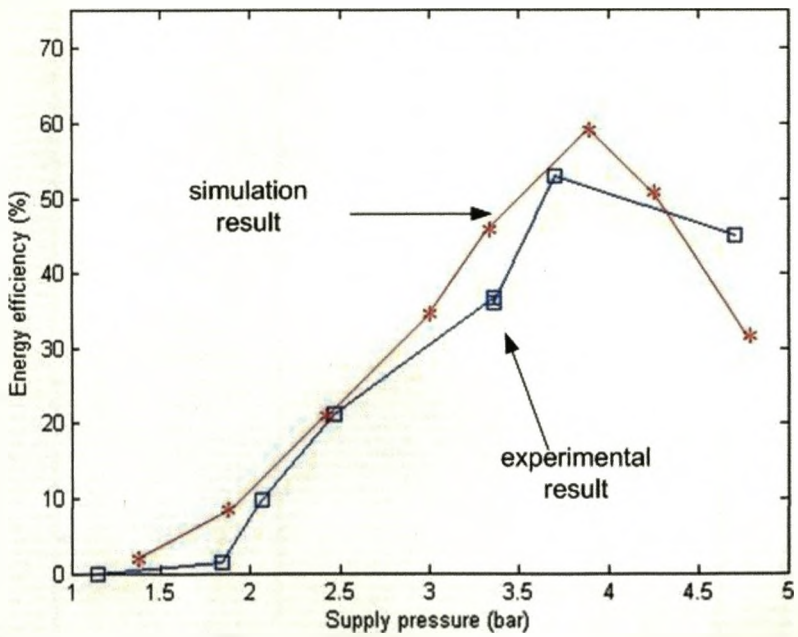

Figure 7.20 Supply pressure vs energy efficiency (three-bulb load)

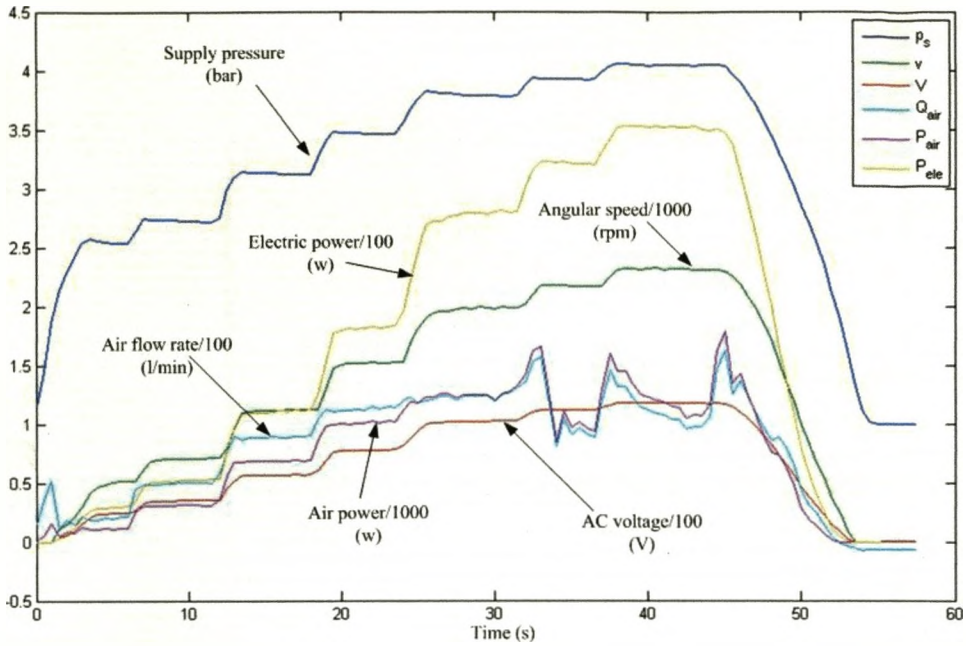

Figure 7.21 Experimental data (six-bulb load)

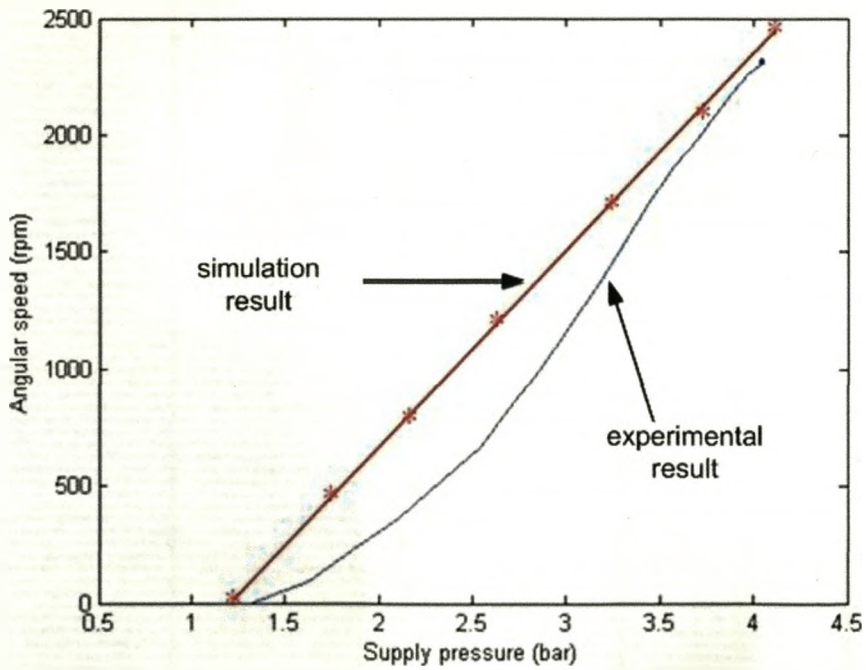

Figure 7.22 Supply pressure vs speed (six-bulb load)

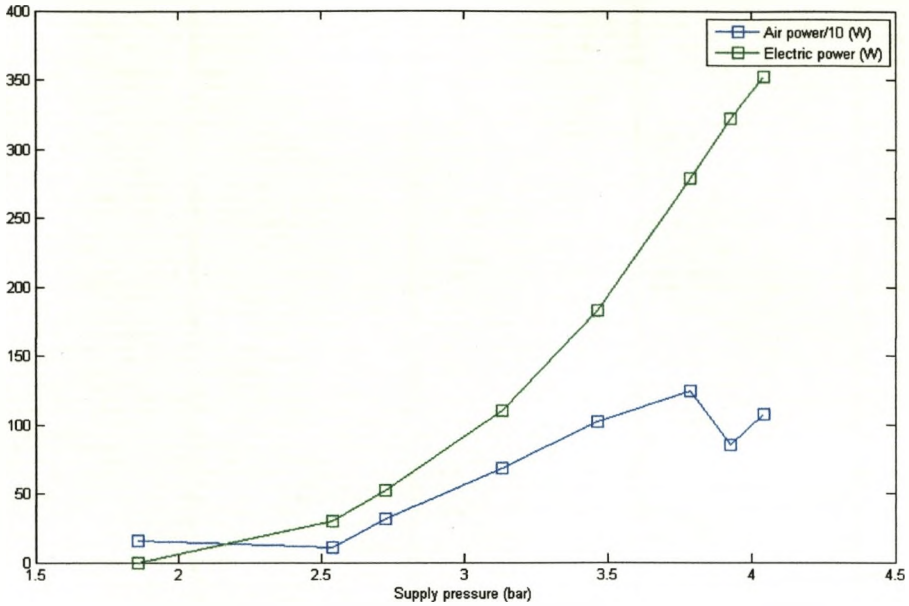

Figure 7.23 Supply pressure vs air power/electric power (six-bulb load)

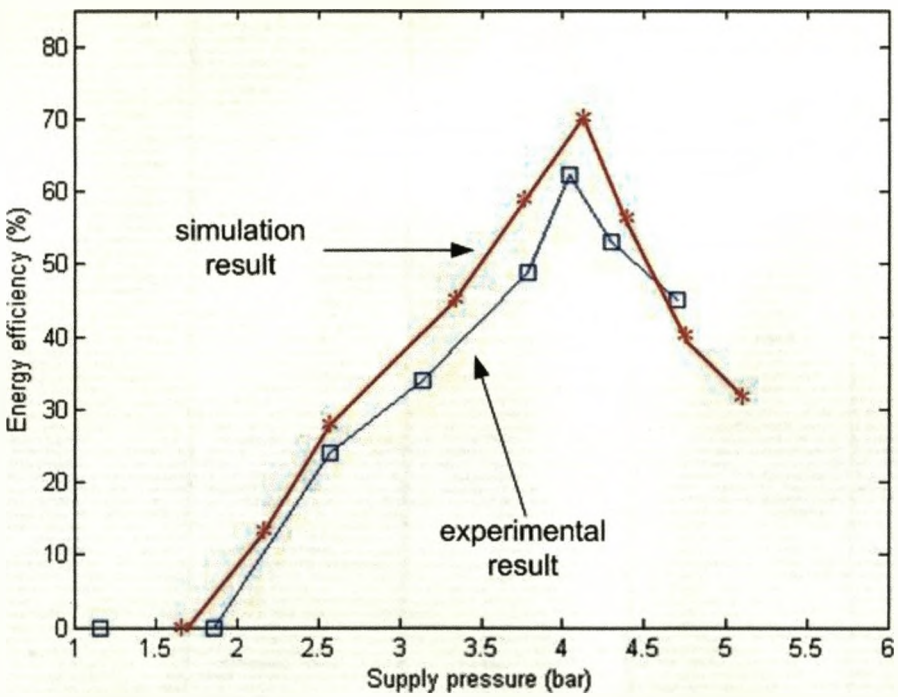

Figure 7.24 Supply pressure vs energy efficiency (six-bulb load)

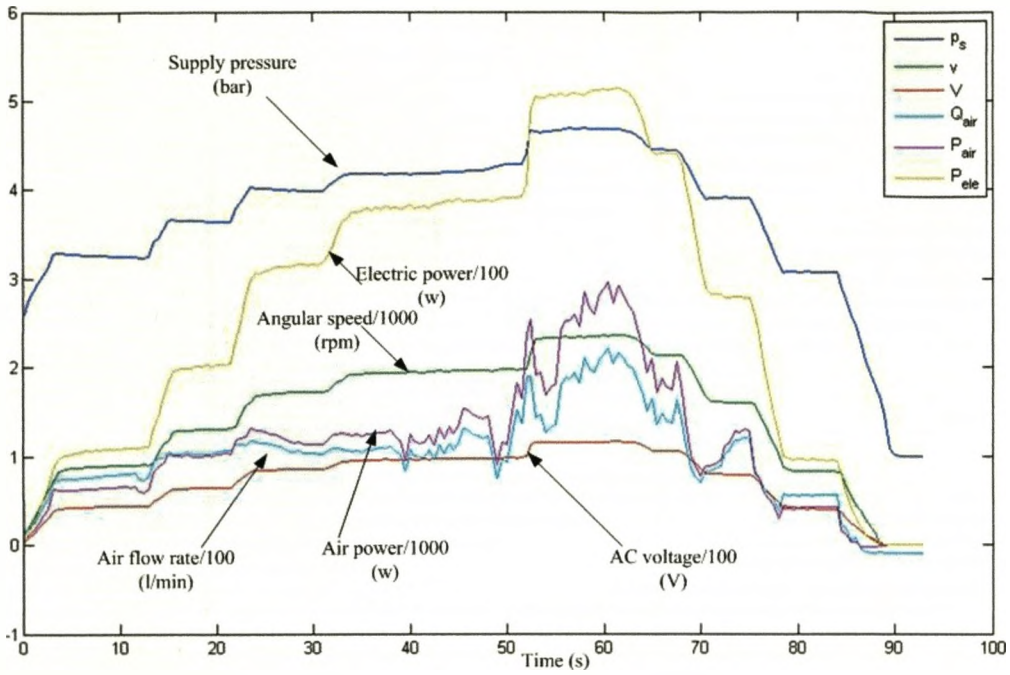

Figure 7.25 Experimental data (nine-bulb load)

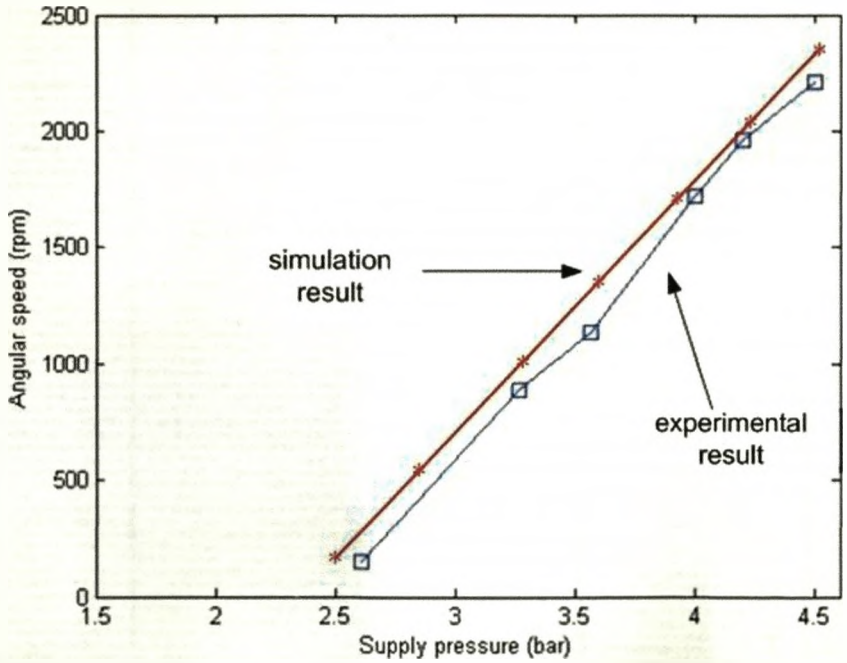

Figure 7.26 Supply pressure vs speed (nine-bulb load)

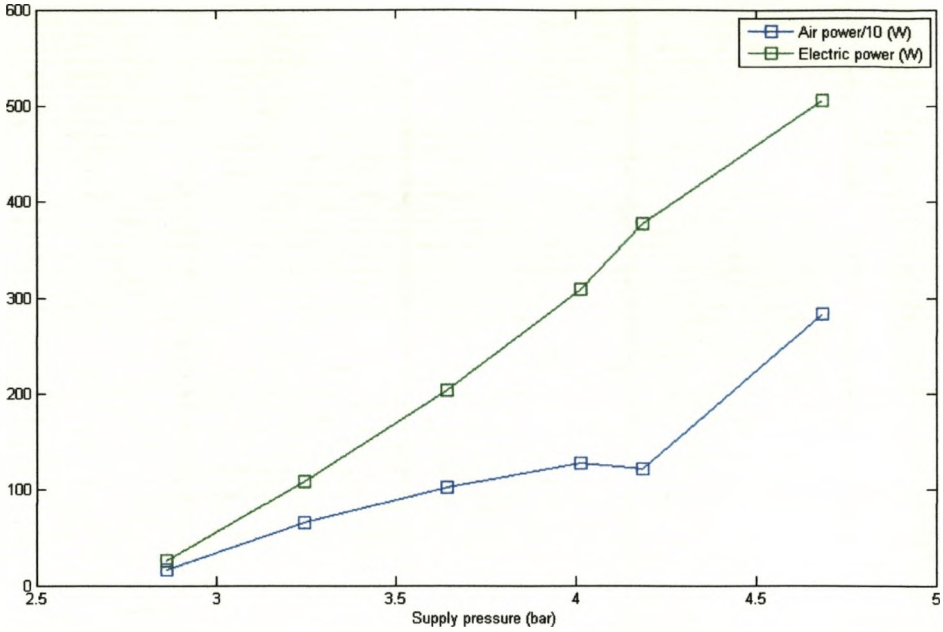

Figure 7.27 Supply pressure vs air power/electric power (nine-bulb load)

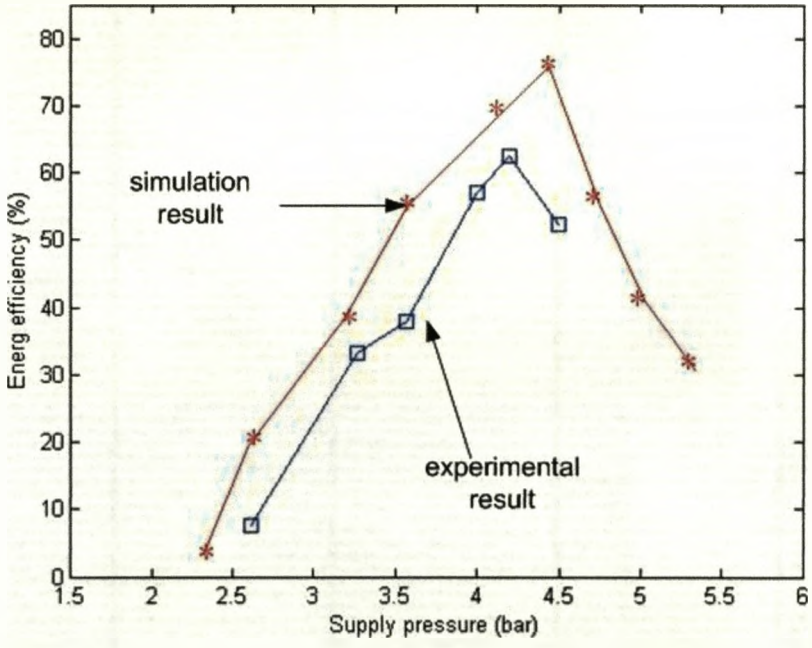

Figure 7.28 Supply pressure vs energy efficiency (nine-bulb load)

7.10 Summary

The experimental data are compared with the simulation results. It is shown that the scroll air motor's energy efficiency can be as high as 65%. The experimental data and the simulation results have the same trend and match each other. However, under same conditions, the angular speed and energy efficiency the simulation result are higher than those of the experimental result. This may be caused by imperfect assembling or other yet to be identified aspects.

Chapter8

Summary and Further Discussion

8.1 Summary

A mathematical model of a scroll type air motor is developed. It uses intrinsic equations to describe the scrolls. Green's Theorem is used to calculate the cross section area and volume of the chambers. The model uses the first law of thermodynamics for open control volumes to calculate the instantaneous states of compressed air as a function of the orbit angle. The geometrical model was given in generic format. It can be used to investigate the influence of the parameters on the scroll air motor performance. Leakage models describing flank leakage and radial leakage were developed. Drive torque generated by compressed air was calculated as the product of the orbit radius and the force on the direction of moving scroll movement. With the output torque and the angular speed, the output power was calculated. This model can simulate the working processes and predict the instantaneous states of the compressed air in each chamber. The mass flow rate and air pressure were used to calculate air power.

Based on the model, energy efficiency of a scroll type air motor is analysed with the definition of air power and available energy carried by the compressed air. A scroll type air motor is able to work at high energy

efficiency due to its special geometric structure and working processes, in which both transmission and expansion air power are utilised.

In order to validate the model, the experiment rig was constructed. The scroll type compressor, SANDEN TRS090, was modified and used as a scroll type air motor. The AC servo motor was used as an AC generator to power light bulbs. The output power of the AC generator was calculated with the measured values of current and voltage. Based on the manufacturer provided performance chart, the output power of the scroll type air motor was calculated. Supply pressure, exhaust pressure, air flow rate, AC voltage, and current were measured with National Instruments data acquisition card and manipulated with LabVIEW and MatLab.

The scroll type air motor described in this thesis is a comprehensive model for scroll type air motors and it is implemented in MatLab/Simulink simulation environment. The experimental results have compared with the simulation results and they agree to each other. It can be used to investigate the air motor's performance under different operating conditions and subject to design changes.

Using the scroll type air motor, a parametric study of the scroll type air motor was conducted. The influence of radial and flank leakage on the air motor's performance is investigated. Performance of the scroll air motor was also studied for scroll designs with geometrical variations. With the

definition of air power, energy efficiency of a scroll type air motor was investigated. The following conclusions can be drawn:

1) Leakage can have tremendous effects on the air motor's performance. Due to leakage, the energy efficiency decreases. It was found that radial leakage decreases the energy efficiency far more than flank leakage because of bigger cross section flow area and more leakage flow.

2) Air power consists of two parts, transmission power and expansion power. Expansion power takes more than 50% of air power with the pressure greater than 5 bar. In most applications of pneumatic cylinders, vane type air motor, and some other pneumatic drives, most expansion power of compressed air is exhausted and wasted.

3) A scroll type air motor is able to work at high energy efficiency under proper conditions. A scroll type air motor has dedicated mechanism, expansion chamber, to utilise the expansion power carried by compressed air. The charge chamber works like a pneumatic cylinder to utilise transmission power. Then both transmission power and expansion power of compressed air can be utilised simultaneously.

4) High energy efficiency does not necessarily mean high output power. In order to increase the output power of a scroll air motor, the supply pressure and flow rate can be increased. However, due to geometrical

structure of the scrolls and different types of expansion, the energy efficiency may be decreased as the supply pressure increases. Deficient and over expansion should try to be avoided in terms of energy efficiency.

5) Beside the geometrical parameters of a scroll type air motor, the supply pressure also has a big influence on the energy efficiency of a scroll type air motor. Supply pressure ideally should be set to satisfy normal expansion.

Based on the summary, further discussion towards model improvement and further energy efficiency analysis will be given in the next section.

8.2 Further discussion and suggestions

From the parametric study, it was found that the scroll air motor's performance is affected by the profile of the scrolls. The model can be used for future investigations to find an optimal geometry of the scrolls that maximises the energy efficiency and study the scroll's performance under the influence of frictions and other factors.

A simple model of frictions was used in the thesis. The parameters were tuned based on the references and experiences. It is too simple to predict the influence of frictions. A better model for the frictions needs to be developed.

Chapter 8 Summary and Further Discussion

In order to use the mathematical model and the energy efficiency analysis result developed in this thesis to future investigation on characteristics of a scroll type air motor, to following modifications are suggested and need to be conducted:

1) To use the mathematical model developed in this thesis to simulate and predict other scroll type air motors with different geometrical structure, the profile of the scrolls needs to be modified. The corresponding modifications need to be made based on the new scroll type air motor.

2) Better measurement equipments need to be used. Pressure sensors need to be fit on the base of the fit scroll to measure instantaneous pressure inside the chambers. Thermo couples need to be fit on the scroll air motor to measure heat transfer and other thermo effects.

3) The mathematical model developed in this thesis can be used to develop control methods for scroll air motor systems.

BIBLIOGRAPHY

Compressing Air Costs 1994, Energy Efficiency Office (London), UK.

SANDEN TRS090 Specification 1997, SANDEN International Corpration.

'Power from The People' 2003, *Power from The People*, viewed 27 March, 2007 <http://news.bbc.co.uk/1/hi/programmes/working_lunch/3231549.stm>.

'Saving Energy in Compressed Air Systems' 2003, *Saving Energy in Compressed Air Systems*, Energy Institution (UK), viewed 27 March 2007 <www.energyinst.org.uk/content/files/cpd/compressedair.pdf>.

'Wind Plus Compressed Air Equals Efficient Energy Storage in Iowa Proposal' 2003, *Wind Plus Compressed Air Equals Efficient Energy Storage in Iowa Proposal*, Energy Services Bulletin, Vol. 22, No. 4, viewed 27 March 2007 <http://www.wapa.gov/es/pubs/esb/2003/03Aug/esb084txt.htm>.

Handbook of AC Synchronous Servomotor 3BRS-71-M4-3000 2005, Motor Technology (UK).

'Powergen MicroCHP' 2005, *Powergen MicroCHP*, E. ON UK, viewed 27 March, 2007 <http://www.chpa.co.uk/news_downloads/2005/CHPA%20micro%20CHP.pdf>.

'Compressed Air Case Studies' 2006, *Compressed Air Case Studies*, IRISH ENERGY CENTRE, viewed 27 March 2007 <www.sei.ie/uploadedfiles/InfoCentre/casestudy11.pdf>.

'Counting the cost of compressed air' 2006, *Counting the cost of compressed air*, Champion Compressors, viewed 05 May 2009 <http://www.ferret.com.au/c/Champion-Compressors/Counting-the-cost-of-compressed-air-n677100>.

National Instruments PCI 6024E datasheet 2006, National Instruments.

'Pnu Power' 2006, *Pnu Power*, Energetix Group plc, viewed 01 April 2007 <http://www.energetixgroup.com/default.asp?id=156>.

Andersen, B.W. 1976, *The Analysis and Design of Pneumatic System*, Robert E.Krieger Publishing Company, New York.

Andrew, P.E. 1998, *Hydraulics and Pneumatics A Technician's and Engineer's Guide*, Butterworth Heinemann, Oxford.

Apostol, T.M. 1969, *Calculus*, 2 edn, John Wiley & Sons Inc.

Armstrong-Helouvry, B. 1991, *Control of Machines with Friction*, Kluwer Academic Publisher.

Astolfi, A., Limebeer, D.J.N., Vinter, R.B., Melchiorri, C. & Tornambè, A. 1997, 'Modelling and Control of Mechanical Systems', Imperial College Press.

Backe, W. 1986, 'The Application of Servo Pneumatic Drives for Flexible Mechanical Handling Techniques', *Robotics*, vol. 2, pp. 45-56.

Backe, W. 1993, 'The Present and Future of Fluid Power', *Journal of System and Control Engineering*, vol. 207, no. 4, pp. 193-212.

Barnes, M. 1996, 'Virtual Reality and Simulation', *Winter Simulation Conference*, pp. 101-110.

Blackburn, J.F., Reethof, G. & Shearer, J.L. 1960, *Fluid Power Control*, The Technology Press of MIT/John Wiley & Sons, New York.

Bo, J. 1995, 'Study of Oil-jet Air Compressor (柏杰, 喷油涡旋空气压缩机研究 in Chinese)', Master thesis, Xian Jiaotong University.

Burrows, C.R. & Webb, C.R. 1967, 'Simulation of an on-off Pneumatic Servomechanism', *Proceedings Institute Mechanism Engineers*, vol. 182.

Burrows, C.R. & Webb, C.R. 1969, 'Further Study of a Low Pressure on-off Pneumatic Servomechanism', *Proceedings Institute Mechanism Engineers*, vol. 184, pp. 849-858.

Bush, W., J., Beagle & P., W. 1992, 'Derivation of General

Relationship Governing the Conjugacy of Scroll Profiles', paper presented to the *Proceedings of International Compressor Engineering Conference at Purdue*.

CADDET 1999, *Compressed air: savings of 30% are quite normal*, CADDET Energy Efficiency, 26 March 2007.

Cai, M. & Kagawa, T. 2001, 'Energy Consumption Assessment of Pneumatic Actuating Systems Including Compressor', *IMechE Conference Transactions, ISS*, pp. 381-390.

Cai, M., Kagawa, T. & Kawashima, K. 2002, 'Energy Conversion Mechanics and Power Evaluation of Compressed Fluid in Pneumatic Actuator Systems', paper presented to the *37th Intersociety Energy Conversion Engineering Conference*.

Cai, M., Kawashima, K. & Kagawa, T. 2006, 'Power Assessment of Flowing Compressed Air', *Journal of Fluids Engineering*, vol. 128, pp. 402-405.

Caillat, J. 1988, 'A Computer Model for Scroll Compressors', *International compressor engineering conference at Purdue*.

Caillat, J., Weatherston, R. & Bush, J.1988, Scroll-Type Machine With Axially Compliant Mounting of Work, U.S. Patent, 4767293

Carmo, M.P.D. 1976, *Differential Geometry of Curves and Surfaces*, Prentice-Hall, Englewood Cliffs (N.J.).

Chadwick, B. 1997, *Design and Simulate Air Circuit on Your PC, Hydraulics & Pneumatics*, vol. 50, Penton Publishing USA.

Chapman, S.J. 2005, *Electric Manchinery Fundamentals*, 4th edn, McGraw Hill.

Chen, Y. 2000, 'Mathematical Modelling of Scroll Compressor', PhD. thesis, Perdue University.

Chen, Y., Groll, E.A., Halm, N.P. & Braun, J.E. 2002, 'Mathematical Modeling of Scroll Compressors-Part I: Compression Process Modelling', *International Journal of Refrigeration*, vol. 25, pp. 731-750.

Chen, Y., Halm, N.P., Braun, J.E. & Groll, E.A. 2002, 'Mathematical Modelling of Scroll Compressors-Part II: Overall Scroll

Compressor Modelling', *International Journal of Refrigeration*, vol. 25, pp. 751-764.

Conte, S.D. & DeBoor, C. 1980, *Elementary Numerical Analysis*, McGraw Hill, New York.

Crozier, T. & Jones, G. 2002, *The Potential Market for MicroCHP in the UK*, Energy for Sustainable Development Limited.

Cruex, L.1905, Rotary Engine of Work, U.S. Patent, 801182

DeBlois, R. 1988, 'Instrumentation and Data Analysis Techniques for Scroll Compressors', *International compressor engineering conference at Purdue*.

Dehoff, R.T. 1993, *Thermodynamics In Materials Science*, Mcgraw-Hill College

Etemad, S., Yannascoli, D. & Hatzikazakis, M.1989, Scroll Machine With Wraps Of Different Thicknesses of Work, U.S. Patent, 4834633

Gao, X. 1997, 'Study on Oil-jet Air Compressor (高秀峰, 喷油空压机研究 in Chinese)', Master thesis, Xian Jiaotong University.

Gao, X., Li, L., Zhao, Y., Shu, P. & Shen, J. 2004, 'Research on a Scroll Expander Used for Recovering Work in a Fuel Cell', *Int. J. Thermodynamics*, vol. 7, pp. 1-8.

Goldstein, M. & Goldstein, I.F. 1993, *The Refrigerator and the Universe: Understanding the Laws of Energy* Harvard University Press.

Gravesen, J., Heneiksen, C. & Howell, P. 1998, *Danfoss: Scroll Optimisation*, Department of Mathematics, Technical University of Denmark.

Gravesen, J. & Henriksen, C. 2001, 'The Geometry of the Scroll Compressor', *SLAM Review*, vol. 43, pp. 113-126.

Gu, Z. 1997, 'Study on Dual Scroll Compressor', PhD. thesis, Xian Jiaotong University.

Halm, N.P. 1997, 'Mathematical Model of Scroll Compressor', Master thesis, Purdue University.

Hayano, M., Sakata, H., Nagatomo, S. & Nurasaki, H. 1988, 'An Analysis of Losses in Scroll Compressor', *International Compressor Engineering Conference at Purdue*, pp. 189-197.

Hirano, T., Hagimoto, K. & Takeda, K.1989, Scroll-type Fluid Machine with Specific Inner Curve Segments of Work, US, 4856973

Hirano, T. & Haginoto, K.1987, Rotary Type Fluid Machine of Work, US, 4678415

Hirano, T., Mutsumura, N. & Takeda, K. 1988, 'Development of High Efficiency Scroll Compressors For Air Conditioners', *International Compressor Engineering Conference*.

Howell, P. 1999, *Fluid Mechanical Modelling of the Scroll Compressor*, Mathematical Institute, University of Oxford.

Ishii, N. 1987, 'Mechanical efficiency of various large capacity scroll compressors', *17th international congress of refrigeration*, Vienna.

Ishii, N. 1988, ' On the superior dynamic behavior of a variable speed scroll compressor', *International compressor engineering conference at Purdue*.

Ishii, N., Fukushima, M., Sano, K. & Sawai, K. 1986, 'A Study on Dynamic Behavioue of A Scroll Compressor', *International Compressor Engineering Conference at Purde*.

Ishii, N., Fukushima, M., sawai, K. & Imaichi, K. 1988, 'Dynamic Behavior of A Scroll Compressor', *JSME International Journal*, vol. 31, no. 1, pp. 58-67.

Kam W. Li 1995, *Applied Thermodynamics: Availability Method and Energy Conversion*, Taylor & Francis, London.

Kane, J.W. & Sternheim, M.M. 1980, *Physics, S. I. Version*, Wiley, New York.

Ke, J., Wang, J., Jia, N., Yang, L. & Wu, Q.H. 2005, 'Energy efficiency analysis and optimal control of servo pneumatic cylinders', paper presented to the *The Proceedings of 2005 IEEE Conference on Control Applications*, Toronto, Canada.

Ke, J., Wang, J. & Yang, L. 2006, 'A fast response energy efficient pneumatic cylinder', paper presented to the *Proceedings of the 12th Chinese Automation & Computing Society Conference in the UK*, Loughborough, England.

Kenmochi, Y. & Kimura, H.2005, Single-winding multi-stage scroll expander of Work, U. S. Patent, 6922999

Lambert, J.D. 1973, *Computational Methods in Ordinary Differential Equations*, John Wileym & Sons, New York.

Lee, Y.-R. & Wu, W.-F. 1995, 'On the Profile Design of a Scroll Compressor', *Int. J. Refrig.*, vol. 18, pp. 308-317.

Lemofouet, S., Rufer, A., Cyphelly, I., Barrade, P. & Grasser, F., *Principle of a Hybrid Compressed Air and Supercapacitors Energy Storage System with Maximum Efficiency Point Tracking*, Industrial Electronics Laboratory, Swiss Federal Institute of Technology, viewed 27 March, 2007 <http://leiwww.epfl.ch/publications/lemofouet_rufer_cyphelly_barrade_grasser_store_03.pdf>.

Li, L. 1989, 'Modelling and Computer Simulation of Thermodynamic Process of Scroll Compressor (李连生, 涡旋压缩机工作过程的热力学模型与计算机模拟 in Chinese)', Master thesis, Xian Jiaotong University.

Li, L. 1998, *Scroll Compressor*, Mechanical Industry Press, China.

Li, L. 2000, *Scroll Compressors and Scroll Mechanism*, Xi'an Jiaotong University Press.

Lin-Chen, Y.Y. 2001, 'Software Development for Pneumatic Actuator System Design and Simulation Using Component-based Methods', M.Phil. thesis, University of Liverpool.

Liu, Z., Du, G., Gu, J. & Cao, X. 1996, 'Optimisation of Dimensional Parameters of Scroll Compressor', *International Compressor Engineering Conference*, Perdue.

Liu, Z., Du, G., Qi, Z. & Gu, J. 1994, 'The Conjugacy Analysis of Modified Part of Scroll Profiles', *International Compressor Engineering Conference*, Perdue, p. 4790484.

Maxwell & Clerk, J. 2001, *Matter and Motion*, Electric Book Co.

Mayer, K. 2005, *Research, Development and Demonstration of Micro-CHP Systems for Residential Applications*, viewed 27 March, 2007 <http://www.energetics.com/depeerreview05/pdfs/presentations/tat/tat_b2-4.pdf>.

McCloy, D. & Martin, H.R. 1973, *The Control of Fuild Power*, Longman.

McCullough, J.E.1993, Scroll expander driven compressor assembly of Work, United States, 5247795

McCullough, J.E. & Hirschfeld, F. 1979, 'The Scroll Machine - An Old Principle with a New Twist', *Mech Eng*, vol. 101, pp. 46-51.

Muir, E.B., Griffith, R.W. & Lilienthal, G.W.1986, Scroll-type Machine with Rotation Controlling Means and Specific Wrap Shape of Work, US, 4609334

Nelson, D. 2003, *Dictionary of Mathematics*, Penguin Group.

Nieter, J. 1988, ' Dynamics of Scroll Suction Process', *International compressor engineering conference at Purdue*.

Nieter, J. & Gagne, D. 1992, 'Analytical Modelling of Discharge Flow Dynamics in Scroll Compressors', paper presented to the *Proceedings of international compressor engineering conference*, Purdue.

Ogata, K. 2002, *Modern Control Engineering*, Pearson Education International.

Puff, R. & Kruegger, M. 1992, 'Influence of the Main Constructive Parameters of a Scroll Compressor on its Efficiency', *International compressor engineering conference at Purdue*.

Richardson, J., Hubert.1989, Scroll Compressor With Orbiting Scroll Member Biased By Oil Pressure of Work, U.S., 4875838

Rodger, R.J. & Wanger, T.C. 1990, 'Scroll Compressor Flow Modeling: Experimental and Computational Investigation', *International Compressor Engineering Conference at Purde*.

Schein, C. & Radermacher, R. 2001, 'Scroll Compressor Simulation

Model', *Journal of Engineering for Gas Turbines and Power*, vol. 123, pp. 217-225.

Seggern, D.H.V. 1990, *Handbook of Curves and Surface*, CRC Press Inc.

Shaffer, R. 2006, *Patented Scroll Expander Produces Up to 1kW Quiet Power for Expansion Generators in Waste Heat Recovery Systems*, Air Squared viewed 26 March, 2007 <http://news.thomasnet.com/fullstory/479068/4201>.

Shearer, J.L. 1956, 'Study of Pneumatic Processes in the Continuous Control of Motion with Compressed Air', *Transactions of the ASME*.

Shearer, J.L. 1957, 'Nonlinear Analogue Study of a High Pressure Servomechanism', *Transactions of the ASME*.

Stroud, K.A. 1996, *Further Engineering Mathmatics*, Macmillan Press Ltd.

Szyperski, C. 1998, *Component Software Beyond Object-oriented Programming*, ACM Press, New York.

Teradhima, Y., Kawakami, Y., Arubaga, T. & Kawai, S. 2000, *An approach for energy-saving of pneumatic cylinders by meter-in circuit*, </http://www.callisto.si.usherb.ca/~fluo2000/PDF/FI_105.pdf>.

Terauchi, K.1966, Scroll Type Compressor Having Reinforced Spiral Elements of Work, US, 4594061

Terauchi, K. & Hirage, M.1985, Scroll Type Fluid Compressor with Thickened Spiral Elements of Work, US, 4547137

Tischer, J. & Utter, R.1985, Scroll Machine Using Discharge Pressure For Axial Sealing of Work, U.S. , 4522575

Tojo, K.1980, Scroll Compressor With Means For End Plate Bias And Cooled Gas Return To Sealed Compressor Spaces of Work, U.S. , 4216661

Tojo, K., Igekawa, M., Maeda, N., Machiela, S., Shiibayaski, M. & Uchikawa, N. 1986, 'Computer Modeling of Scroll Compressor with Self-adjusting Back-pressure Mechanism', *International Compressor Engineering Conference at*

Purdue, pp. 872-886.

Uebing, M. & Vaughan, N.D. 1997, 'On Linear Dynamic Modelling of a Pneumatic Servo System', paper presented to the *The fifth Scandinavian International Conference on Fluid Power*, Linkoping, Sweden.

Wang, B., Li, X. & Shi, W. 2005, 'A General Geometrical Model of Scroll Compressors Based on Discretional Initial Angles of Involute', *International Journal of Refrigeration*, vol. 28, pp. 958-966.

Wang, J., Lin-Chen, Y., Wang, J.D., Moore, P.R. & Pu, J. 2000, 'Modelling Study, validation and robust tracking control of pneumatic cylinder actuator system', *IEE Control 2000*.

Wang, J., P, J., Moore, P.R. & Zhang, Z. 1998, 'Modelling Study and Servo-control of Air Motor Systems', *Int. J. Control*, vol. 71, pp. 459-476.

Winandy, E., O., C.S. & Lebrun, J. 2002, 'Experimental Analysis and Simplified Modelling of a Hermetic Scroll Refrigeration Compressor', *Applied Thermal Engineering*, vol. 22, pp. 107-120.

Winnick, J. 1997, *Chemical Engineering Thermodynamics*, John Wiley & Sons Inc.

Wolansky, W.D., Nagohosian, J. & Henke, R.W. 1977, *Fundamentals of Fluid Power*, Houghton Mifflin Company.

Yanagisawa, T. 1990, 'Optimum Operating Pressure Ratio for Scroll Compressors', *International compressor engineering conference at Purdue*.

Yanagisawa, T., Cheng, M., Fukuta, M. & Shimizu, T. 1990, 'Optimum Operating Pressure Ratio for Scroll Compressor', *International Compressor Engineering Conference*.

Yang, A., Pu, J., Wong, C.B. & Moore, P.R. 2008, 'By-pass valve control to improve energy efficiency of pneumatic drive system', *Control Engineering Practice*, vol. 17, no. 6, pp. 623-628.

Yang, L., Wang, J. & Ke, J. 2006, 'Development of a Mathematical Model for a Scroll Type Air Motor', paper presented to the

Eighteenth International Conference on Systems Engineering (ICSE), Coventry University, England.

Yang, L., Wang, J., Mangan, S., Derby, J.W. & Lu, N. 2008, 'Mathematical Model and Energy Efficiency Analysis of a Scroll-type Air Motor', *IAENG International Journal of Applied Mathematics*, vol. 38, no. 1.

Yang, L., Wang, J. & Nan, L. 2007, 'Energy Efficiency Analysis of a Scroll-type Air Motor Based on a Simplified Mathematical Model', paper presented to the *The World Congress on Engineering 2007 (WCE 2007)*, London, UK.

Yong, H. 1994, 'Leakage Calculation Through Clearance', *International Compressor Engineering Conference at Purdue*, pp. 93-97.

Zhu, J. 1994, 'Analysis of Radial Flexibility of Scroll Compressor ', Master thesis, Xian Jiaotong University.

Zhu, J., Wang, G. & Li, Y. 1994, 'Geometrical Analysis of Scroll Compressor for High Pressure Ratio (朱杰, 旋转压缩机径向柔性机构的研究 in Chinese)', *International Compressor Engineering Conference*, Perdue, pp. 473-479.

APPENDICES

Appendix A

The screen shot of the NI LabView VI (Virtual Instrumentation) used for data acquisition is shown in Figure 8.1. The block diagram of the VI is shown in Figure 8.2.

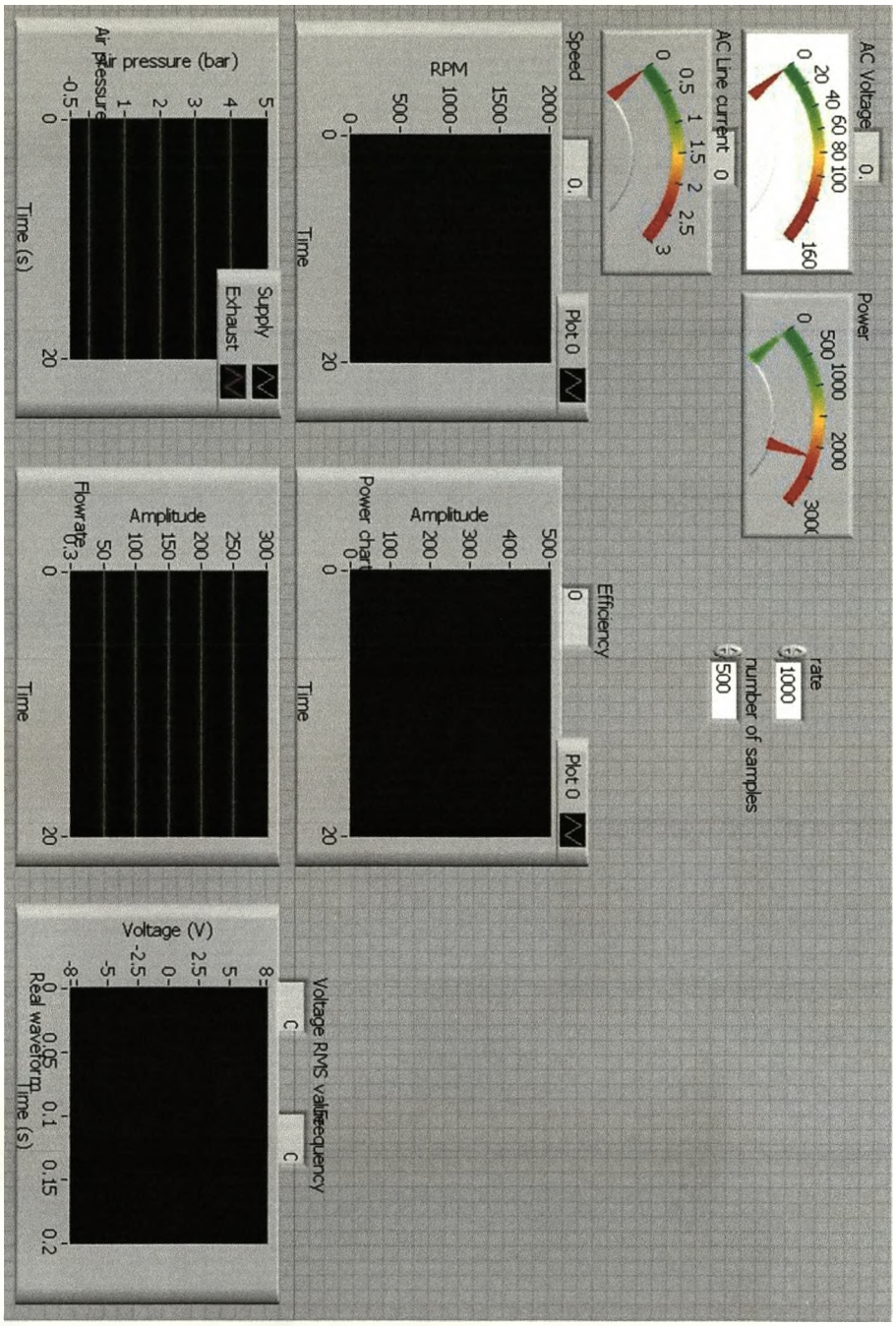

Figure 8.1 VI for data acquisition

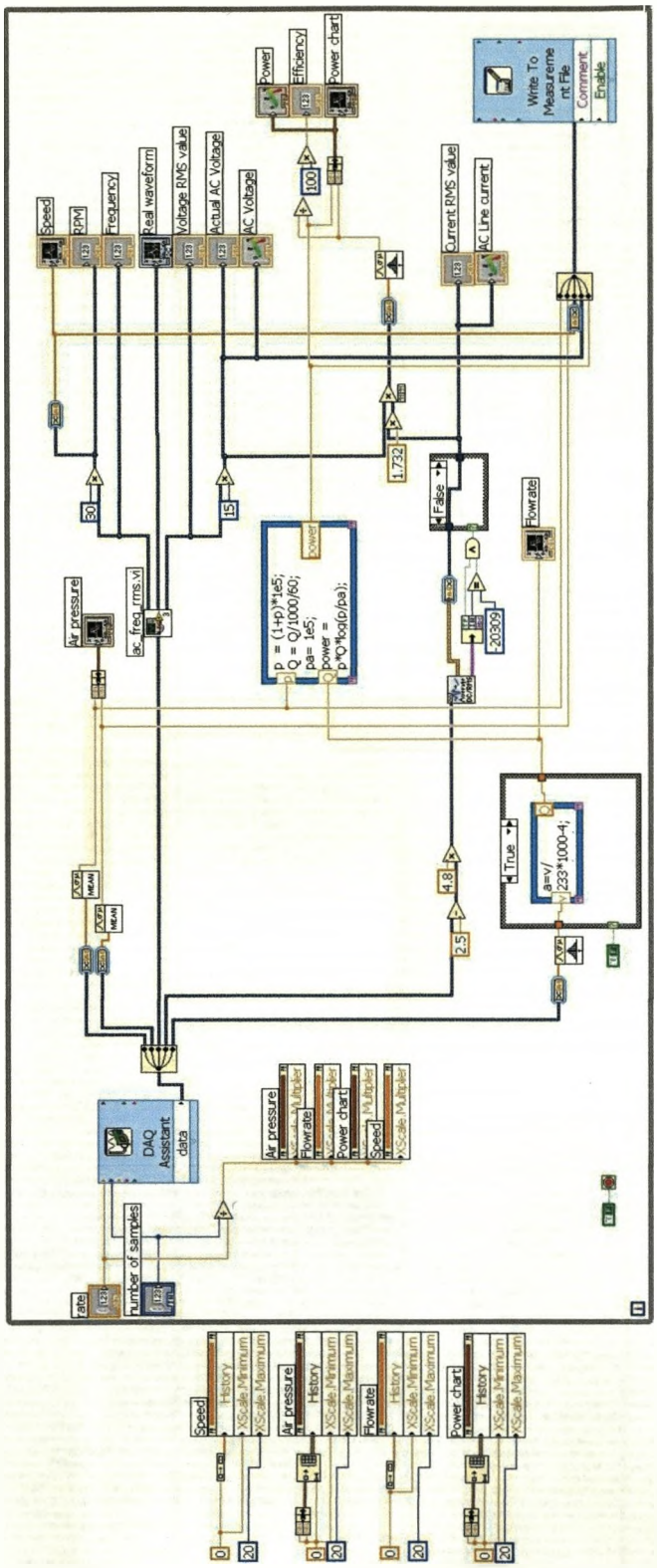

Figure 8.2 Block diagram of the VI

Appendix B

The experimental data recorded is given in the following tables. The measured pressures are gauge pressures. The measured AC voltage is expressed as RMS values.

Table 8.1 Experimental data (three-bulb load) - 1

Experimental Data (Three-bulb Load) - 1					
Time (s)	Supply Pressure (bar)	Exhaust Pressure (bar)	Volumetric Flow rate (L/min)	AC Voltage	AC Current (A)
0	0.031252	-0.003908	0	0	0.045764
0.5	0.031054	-0.003914	0	0	0.046045
1	0.030325	-0.00392	0	0	0.045829
1.5	0.029467	-0.003885	0	0	0.045845
2	0.02888	-0.003942	0	0	0.045412
2.5	0.028408	-0.004006	0	0	0.046008
3	0.006078	-0.00506	0	0	0.042835
3.5	-0.00659	-0.005692	0	0	0.041581
4	-0.006657	-0.005621	0	0	0.042116
4.5	-0.006767	-0.005583	0	0	0.042115
5	-0.006781	-0.005566	0	0	0.04259
5.5	-0.006753	-0.005598	0	0	0.0419
6	-0.00605	-0.005534	0	0	0.042336
6.5	0.009817	-0.004855	0	0	0.04449
7	0.03369	-0.00367	0	0	0.046567
7.5	0.07125	-0.002285	0	0	0.049862
8	0.098944	-0.001155	0	0	0.054327
8.5	0.135696	7.41E-05	0	0	0.056991
9	0.215984	0.002765	0	0	0.063157
9.5	0.345704	0.007081	0	0	0.070505
10	0.438745	0.010522	0	0	0.075179

10.5	0.503026	0.012698	0	0	0.078405
11	0.5846	0.015559	0	0	0.08231
11.5	0.692922	0.019203	0	0	0.088285
12	0.882524	0.018149	0	0	0.169437
12.5	1.453613	0.001226	264.33482	14.25755	0.623151
13	1.371186	0.004082	398.61753	22.09227	0.427526
13.5	1.345815	0.004533	505.35589	26.04227	0.383673
14	1.329485	0.005376	524.79723	26.90106	0.372649
14.5	1.328201	0.004726	546.28088	27.52373	0.373822
15	1.320774	0.005367	539.25691	27.69697	0.375935
15.5	1.324447	0.004732	554.00368	27.69075	0.373823
16	1.312885	0.005323	545.83994	28.2341	0.378651
16.5	1.31571	0.005373	563.55142	28.05396	0.380464
17	1.314246	0.004654	564.74686	28.58361	0.379994
17.5	1.306982	0.005428	554.56551	28.6142	0.380934
18	1.307656	0.005335	573.32839	28.774	0.382381
18.5	1.30976	0.004967	573.58714	28.92516	0.383864
19	1.303227	0.004786	563.84233	29.07051	0.385971
19.5	1.301157	0.005165	569.87075	29.10535	0.38796
20	1.301945	0.005158	583.37545	29.09806	0.382611
20.5	1.32459	0.00534	584.82641	29.81604	0.391456
21	1.493272	0.008429	639.77775	37.4262	0.457643
21.5	1.506281	0.01062	802.52336	42.16055	0.483305
22	1.500332	0.010621	835.32873	43.25262	0.484606
22.5	1.498469	0.010771	839.65721	43.34709	0.484805
23	1.497862	0.010735	834.52847	43.37992	0.484497
23.5	1.497237	0.010661	834.13902	43.40981	0.48499
24	1.496777	0.010753	836.71247	43.44469	0.486033
24.5	1.495089	0.010793	843.31234	43.46951	0.485726
25	1.493996	0.010729	846.05614	43.53465	0.484922
25.5	1.493498	0.010753	846.58619	43.64525	0.485258
26	1.492427	0.010963	846.89035	43.79374	0.486686
26.5	1.520393	0.011008	848.15473	44.15185	0.492641
27	1.70967	0.017169	918.80659	54.25613	0.560455
27.5	1.691395	0.019389	1109.8333	58.51933	0.580931
28	1.68781	0.019173	1132.9415	59.19764	0.58006
28.5	1.68586	0.01951	1131.1751	59.12478	0.580937
29	1.683357	0.019346	1138.1342	59.30474	0.581963
29.5	1.682509	0.019544	1137.493	59.5994	0.583874
30	1.679287	0.019262	1143.7342	59.69891	0.584768

30.5	1.678996	0.019389	1140.5987	59.82441	0.584632
31	1.677027	0.019162	1148.4997	59.88577	0.586041
31.5	1.675373	0.019745	1146.8297	59.88809	0.584821
32	1.732585	0.020543	1156.6062	61.57518	0.598416
32.5	1.872235	0.029081	1292.3539	72.84934	0.661127
33	1.844939	0.029777	1422.6307	74.86851	0.668656
33.5	1.840998	0.02957	1430.9842	75.4587	0.670631
34	1.837845	0.029304	1433.3555	75.56487	0.670955
34.5	1.835452	0.029564	1439.3303	75.60041	0.670971
35	1.834042	0.029687	1441.8632	75.72985	0.672279
35.5	1.831128	0.029388	1446.0631	75.81434	0.673121
36	1.828913	0.029474	1443.6552	76.15224	0.673965
36.5	1.826927	0.029377	1449.6554	76.61835	0.675551
37	1.825261	0.029446	1453.6728	76.50261	0.674318
37.5	1.821655	0.029869	1456.221	76.74703	0.680904
38	1.819005	0.029427	1463.374	77.11407	0.677054
38.5	1.811714	0.029646	1471.0409	77.40051	0.68069
39	1.806075	0.029674	1480.3601	78.19996	0.68121
39.5	1.801883	0.030083	1485.9141	78.12936	0.684419
40	1.802448	0.029858	1492.1698	78.61748	0.686749
40.5	1.802119	0.03001	1490.2003	78.43081	0.685195
41	1.800728	0.029436	1492.8364	78.26422	0.685712
41.5	1.800506	0.029401	1490.089	78.5545	0.687732
42	1.798355	0.029559	1493.3024	78.63476	0.684212
42.5	1.799369	0.029234	1494.6174	78.26059	0.681527
43	1.797606	0.029438	1487.812	78.31078	0.686883
43.5	1.797608	0.029358	1493.6854	78.60957	0.68604
44	1.797336	0.029573	1488.3833	78.24474	0.683208
44.5	1.798214	0.02932	1490.0618	78.15814	0.686424
45	1.794998	0.028885	1484.3574	78.21302	0.680773
45.5	1.666306	0.02419	1470.8854	72.48306	0.649846
46	1.664555	0.021081	1291.3424	66.77006	0.625895
46.5	1.664219	0.020931	1273.3869	66.67118	0.620963
47	1.66548	0.021134	1271.9252	66.76046	0.624786
47.5	1.665557	0.020844	1274.4706	66.49473	0.621317
48	1.662428	0.021098	1269.0706	66.7869	0.624421
48.5	1.664557	0.021028	1272.7445	66.40006	0.624053
49	1.661833	0.020883	1271.0617	66.45479	0.61998
49.5	1.663328	0.021061	1267.7373	66.65962	0.622302
50	1.533918	0.016974	1267.3006	60.81833	0.583985

50.5	1.533153	0.014411	1067.3104	55.3842	0.559214
51	1.537486	0.014541	1052.2519	54.77179	0.556064
51.5	1.538343	0.014536	1055.0801	54.72612	0.553892
52	1.538449	0.014331	1052.216	54.74212	0.557429
52.5	1.536991	0.014211	1053.3344	54.74713	0.555252
53	1.535849	0.014676	1047.6228	54.75505	0.558256
53.5	1.536707	0.014679	1050.8348	54.84178	0.553474
54	1.538241	0.014549	1056.5017	54.74945	0.55844
54.5	1.53848	0.014198	1051.8391	54.67639	0.553748
55	1.535645	0.014612	1045.7981	54.68765	0.558366
55.5	1.538025	0.014556	1048.532	54.63255	0.55271
56	1.45983	0.012904	1052.3769	52.45965	0.537682
56.5	1.376105	0.008992	899.09939	43.70344	0.481727
57	1.385131	0.008791	814.88329	41.87006	0.476528
57.5	1.387519	0.00866	814.71301	41.72679	0.471781
58	1.38922	0.008535	809.86446	41.602	0.473786
58.5	1.386097	0.008422	798.69065	41.39005	0.472755
59	1.337637	0.00806	803.13404	39.89184	0.460154
59.5	1.245536	0.005343	725.45777	34.86948	0.419691
60	1.108099	0.003477	576.11279	27.00393	0.354277
60.5	0.914885	0.000868	430.74507	17.27676	0.265248
61	0.670868	-0.001329	216.10628	6.913815	0.133721
61.5	0.391938	-0.002192	0	0	0.047954
62	0.074236	-0.004355	0	0	0.045741
62.5	0.00152	-0.005457	0	0	0.041925

Table 8.2 Experimental data (three-bulb load) - 2

Experimental Data (Three-bulb Load) - 2					
Time (s)	Supply Pressure (bar)	Exhaust Pressure (bar)	Volumetric Flow rate (L/min)	AC Voltage	AC Current (A)
0	0.149543	-0.00129	0	0	0.028165
0.5	0.41267	0.001851	0	0	0.031438
1	0.84359	-4.56E-05	0	2.342123	0.247105

1.5	1.067076	-0.00113	170.9308	6.538239	0.387304
2	1.098483	-0.00059	215.9128	10.17513	0.368783
2.5	1.079772	-0.00049	254.7909	11.50516	0.302777
3	1.067595	-0.00033	274.264	12.7416	0.277799
3.5	1.06213	-0.00021	268.1308	13.3529	0.257664
4	1.046789	-4.05E-05	275.885	13.71986	0.260222
4.5	1.04983	-0.00014	294.0565	13.58243	0.253294
5	1.044874	1.68E-05	280.2283	13.93415	0.25875
5.5	1.040535	-0.00022	296.4202	13.87689	0.249105
6	1.043693	-0.0002	297.6354	13.87492	0.255149
6.5	1.032084	1.07E-05	281.8626	14.01971	0.25726
7	1.073232	-0.00011	301.3698	14.5449	0.263774
7.5	1.216625	0.001413	350.7737	19.31147	0.32472
8	1.369272	0.003269	478.1887	26.35698	0.380396
8.5	1.462788	0.005154	601.5054	32.79756	0.425668
9	1.4814	0.006538	690.6558	35.79523	0.439654
9.5	1.476764	0.006491	709.338	36.78602	0.442087
10	1.47527	0.006437	721.5082	36.87777	0.441255
10.5	1.473305	0.006542	723.4139	37.00812	0.443266
11	1.471777	0.006503	729.1957	37.06597	0.442923
11.5	1.471541	0.00647	722.0778	37.05714	0.442347
12	1.470137	0.006425	721.6052	37.17253	0.442814
12.5	1.469349	0.006509	721.0659	37.15452	0.442303
13	1.467221	0.006455	720.8922	37.25909	0.443916
13.5	1.466539	0.00641	723.4183	37.2781	0.444585
14	1.46597	0.006454	720.86	37.16913	0.44421
14.5	1.464665	0.00649	724.973	37.16892	0.444271
15	1.582305	0.00843	725.2113	41.65466	0.480169
15.5	1.741021	0.012535	869.4414	50.23789	0.537887
16	1.844297	0.01689	1069.794	58.41157	0.579427
16.5	1.901196	0.021032	1219.224	64.91654	0.615191
17	1.894914	0.021183	1246.016	65.10641	0.615544
17.5	1.894487	0.0211	1249.184	65.72874	0.617663
18	1.88938	0.02117	1251.947	65.91563	0.618368
18.5	1.887122	0.021333	1263.028	66.06527	0.620129
19	1.882864	0.021144	1262.167	66.17442	0.620021
19.5	1.880621	0.021342	1267.286	66.79042	0.62183
20	1.876426	0.021557	1276.109	66.72032	0.624786
20.5	1.946275	0.023483	1274.505	69.17422	0.639085
21	2.055406	0.029984	1411.77	77.29211	0.682314

21.5	2.165003	0.037688	1550.334	85.74166	0.723126
22	2.222883	0.044913	1716.867	93.52575	0.758879
22.5	2.202778	0.045972	1798.311	95.051	0.764611
23	2.196027	0.045969	1807.813	95.62081	0.766724
23.5	2.193599	0.04602	1814.251	95.58051	0.769072
24	2.189776	0.045928	1815.012	95.88711	0.766892
24.5	2.187866	0.045837	1816.747	96.00746	0.770189
25	2.18583	0.045501	1815.978	96.45333	0.770721
25.5	2.183164	0.045267	1823.007	96.50146	0.769987
26	2.180016	0.045225	1827.056	96.7082	0.77284
26.5	2.171382	0.045717	1838.355	97.14293	0.775252
27	2.211333	0.047597	1846.642	99.32458	0.78453
27.5	2.289804	0.054379	1941.608	104.8429	0.81069
28	2.360653	0.062276	2066.961	111.768	0.841866
28.5	2.367372	0.066522	2175.647	115.7746	0.856985
29	2.35971	0.066238	2192.554	115.9057	0.857928
29.5	2.357827	0.066205	2199.956	116.2226	0.857862
30	2.362285	0.06611	2192.444	115.8622	0.857339
30.5	2.363218	0.065756	2185.734	115.7184	0.856909
31	2.362194	0.065547	2187.632	115.6719	0.85692
31.5	2.359158	0.065384	2191.362	115.8365	0.857277
32	2.360516	0.065417	2186.704	115.5609	0.857113
32.5	2.360592	0.065232	2184.215	115.6402	0.856696
33	2.360834	0.064809	2185.945	115.6998	0.856217
33.5	2.3603	0.064947	2180.645	115.5011	0.85411
34	2.35764	0.064416	2182.665	115.1851	0.854235
34.5	2.359404	0.064565	2175.911	115.5393	0.856279
35	2.35875	0.064636	2178.081	115.2364	0.852529
35.5	2.360004	0.064165	2174.881	115.1915	0.855072
36	2.272255	0.058616	2169.775	111.4248	0.835471
36.5	2.170883	0.048909	2015.72	102.7308	0.795816
37	2.108085	0.042136	1853.727	95.27764	0.764271
37.5	2.026272	0.035737	1734.339	88.40058	0.729395
38	1.938014	0.029648	1608.139	80.64704	0.69299
38.5	1.853297	0.024391	1466.469	72.73554	0.652243
39	1.761143	0.019208	1321.207	64.56559	0.608325
39.5	1.650873	0.015129	1175.941	56.73924	0.56105
40	1.59054	0.011622	982.8463	49.60517	0.520814
40.5	1.481172	0.008244	874.3487	41.80373	0.467247
41	1.36915	0.006282	770.3466	35.51758	0.423946

41.5	1.307925	0.004448	620.4317	29.88112	0.381795
42	1.179145	0.002408	523.0834	23.30845	0.328166
42.5	1.091108	0.001403	431.3225	19.02152	0.286895
43	1.029492	0.000671	327.6716	14.87663	0.254088
43.5	0.915738	-0.00021	263.259	10.99775	0.200319
44	0.787084	-0.00037	183.1252	6.925208	0.14961
44.5	0.556836	0.004569	130.9323	2.637719	0.079829
45	0.3416	0.005171	0	0	0.028761
45.5	0.174859	0.001702	0	0	0.028498
46	0.041027	-0.00184	0	0	0.028206
46.5	-0.00279	-0.00323	0	0	0.028436
47	-0.0072	-0.00347	0	0	0.028134

Table 8.3 Experimental data (six-bulb load) - 1

Experimental Data (Six-bulb Load) - 1					
Time (s)	Supply Pressure (bar)	Exhaust Pressure (bar)	Volumetric Flow rate (L/min)	AC Voltage	AC Current (A)
0	0.033268	-0.0051	0	0	0.043816
0.5	0.111077	-0.00385	0	0	0.047655
1	0.186316	-0.00263	0	0	0.050785
1.5	0.268829	-0.0015	0	0	0.053727
2	0.362184	-0.00016	0	0	0.056912
2.5	0.415314	0.000702	0	0	0.058294
3	0.515715	0.001992	0	0	0.062188
3.5	0.622248	0.002972	0	0	0.083001
4	0.708617	0.004629	0	0	0.205685
4.5	0.56826	0.010262	0	0	0.074908
5	0.554635	0.010312	0	0	0.075034
5.5	0.548463	0.010338	0	0	0.075652
6	0.545741	0.010488	0	0	0.075914
6.5	0.593426	0.011888	0	0	0.0786
7	0.590997	0.012244	0	0	0.078534
7.5	0.586992	0.012199	0	0	0.078811

8	0.646215	0.013792	0	0	0.081656
8.5	0.655704	0.014183	0	0	0.081745
9	0.652188	0.014192	0	0	0.081364
9.5	0.760195	0.017122	0	0	0.088338
10	0.764854	0.017925	0	0	0.0868
10.5	0.75589	0.0178	0	0	0.086257
11	0.751363	0.01776	0	0	0.086495
11.5	0.748174	0.017852	0	0	0.086152
12	0.807113	0.019419	0	0	0.089524
12.5	0.854376	0.019172	0	0	0.083023
13	1.353753	0.000848	136.6229	4.587734	0.713137
13.5	1.412651	-0.00013	176.9548	7.823077	0.762264
14	1.402253	0.000176	256.6554	11.45076	0.708509
14.5	1.370952	0.001345	289.386	14.37478	0.623599
15	1.364758	0.00138	345.0177	15.92766	0.602387
15.5	1.353667	0.001562	365.0014	16.89967	0.581486
16	1.348112	0.001627	373.8431	17.25922	0.573113
16.5	1.346699	0.001557	378.6574	17.70287	0.576718
17	1.346397	0.001581	382.2691	17.49063	0.576143
17.5	1.346154	0.001675	384.2635	17.98993	0.581512
18	1.345705	0.001688	385.274	17.6326	0.578267
18.5	1.346137	0.001509	370.9997	18.11467	0.585449
19	1.341264	0.001941	373.2484	18.12726	0.581644
19.5	1.336148	0.001964	373.1682	17.87752	0.580796
20	1.339269	0.001585	390.1231	18.0789	0.583269
20.5	1.340229	0.001618	392.227	18.31362	0.591278
21	1.341884	0.001675	392.1323	18.33792	0.583581
21.5	1.33824	0.001937	377.4336	18.23806	0.583084
22	1.330896	0.002013	378.8028	18.20083	0.586052
22.5	1.336225	0.001562	393.6808	18.2011	0.583651
23	1.337871	0.001611	394.3579	18.34762	0.594227
23.5	1.339285	0.001702	380.4522	18.39544	0.587036
24	1.330405	0.002168	378.7197	18.37352	0.59222
24.5	1.332651	0.001489	394.3359	18.40079	0.584753
25	1.52557	0.003578	409.8438	23.08723	0.697388
25.5	1.572007	0.005285	556.5674	27.40334	0.752473
26	1.561963	0.005681	567.1541	28.19229	0.757644
26.5	1.560246	0.005772	572.2947	28.1744	0.757113
27	1.561236	0.0057	573.5914	28.20402	0.746893
27.5	1.561312	0.005922	582.3799	28.5081	0.756662

28	1.562525	0.005747	584.074	28.41855	0.760131
28.5	1.561179	0.005563	574.5665	28.21186	0.7482
29	1.557284	0.005822	576.1277	28.55608	0.755183
29.5	1.558139	0.005824	574.2489	28.41922	0.761416
30	1.558771	0.005799	585.0669	28.20929	0.748463
30.5	1.558615	0.00601	584.2722	28.61478	0.757953
31	1.558674	0.005843	586.6602	28.42629	0.761459
31.5	1.728494	0.008192	591.3808	32.77831	0.840507
32	1.785139	0.011306	758.7685	38.7566	0.914619
32.5	1.776514	0.011173	791.3049	39.11368	0.909069
33	1.776814	0.011474	784.4375	39.53425	0.911578
33.5	1.776414	0.011162	795.089	39.42724	0.91567
34	1.773385	0.011271	786.3783	39.24037	0.908848
34.5	1.775398	0.011439	793.4607	39.71526	0.917075
35	1.771407	0.011298	789.4277	39.32421	0.916504
35.5	1.773093	0.011392	788.6575	39.60779	0.910822
36	1.77177	0.011218	798.237	39.5629	0.918249
36.5	1.769456	0.011278	790.4061	39.42783	0.908482
37	1.771292	0.011364	796.7097	39.7489	0.923082
37.5	1.768006	0.011311	791.0066	39.37159	0.911207
38	1.768509	0.011312	790.5815	39.86845	0.91891
38.5	1.804012	0.011707	800.4689	40.18084	0.925655
39	2.007271	0.017637	865.3742	48.74394	1.057206
39.5	1.994072	0.019351	1029.101	51.92393	1.071071
40	1.991897	0.019275	1031.229	52.40807	1.08156
40.5	1.990129	0.019797	1039.987	52.46405	1.077187
41	1.985977	0.019711	1039.334	52.34676	1.081174
41.5	1.985629	0.019427	1038.222	52.69943	1.083526
42	1.982725	0.019865	1047.117	52.86451	1.087554
42.5	1.98115	0.01944	1049.505	52.84266	1.081295
43	1.98038	0.019349	1041.689	52.7409	1.081825
43.5	1.979368	0.019515	1048.372	52.77184	1.083283
44	1.979753	0.019716	1052.063	52.88415	1.08495
44.5	1.981678	0.019725	1045.881	52.85807	1.086159
45	2.160796	0.025577	1059.928	59.46518	1.17311
45.5	2.15729	0.028301	1247.942	63.45335	1.210117
46	2.153933	0.028189	1255.162	63.81485	1.212135
46.5	2.153115	0.028731	1258.65	63.93955	1.213358
47	2.149509	0.028048	1259.931	64.0633	1.213028
47.5	2.148301	0.028804	1265.91	64.24083	1.214383

48	2.145595	0.028583	1262.975	64.39685	1.217268
48.5	2.146703	0.028569	1267.407	64.39734	1.221208
49	2.144482	0.028588	1268.034	64.33592	1.21885
49.5	2.143195	0.028771	1269.844	64.93601	1.221176
50	2.139499	0.02881	1279.718	64.66029	1.222005
50.5	2.13634	0.028751	1277.082	65.22986	1.229634
51	2.134948	0.028934	1283.438	65.26351	1.224044
51.5	2.128798	0.029201	1288.429	65.386	1.228625
52	2.125399	0.029434	1291.828	65.9004	1.236533
52.5	2.125255	0.029132	1291.424	65.76889	1.235317
53	2.121322	0.028952	1297.194	66.04296	1.230327
53.5	2.121859	0.029188	1297.741	66.09724	1.237458
54	2.122107	0.029018	1300.082	65.85144	1.237048
54.5	2.100294	0.028199	1293.57	65.13023	1.221303
55	2.008269	0.024553	1268.894	61.34514	1.179853
55.5	1.869716	0.018995	1148.255	54.32042	1.089813
56	1.698064	0.013074	981.5583	44.8726	0.966676
56.5	1.523045	0.007764	786.7997	34.93225	0.833138
57	1.369173	0.003951	599.0056	26.69382	0.699216
57.5	1.190386	0.001883	446.352	19.87044	0.576711
58	0.970012	-0.00087	280.2033	11.27864	0.39559
58.5	0.70693	-0.00213	158.0671	5.336604	0.225194
59	0.572579	-0.00389	0	0	0.060154
59.5	0.12109	-0.00343	0	0	0.04848
60	0.009156	-0.00536	0	0	0.042864
60.5	-0.00435	-0.0056	0	0	0.042751
61	-0.00541	-0.00558	0	0	0.04207

Table 8.4 Experimental data (six-bulb load) - 2

Experimental Data (Six-bulb Load) - 2					
Time (s)	Supply Pressure (bar)	Exhaust Pressure (bar)	Volumetric Flow rate (L/min)	AC Voltage	AC Current (A)

0	0.151163	-0.00181	0	0	0.028716
0.5	0.445949	0.001098	0	0	0.029458
1	0.856289	-0.00028	0	0	0.385187
1.5	1.135683	-0.00187	119.4014	3.408559	0.608333
2	1.282366	-0.00144	140.1514	5.464418	0.671343
2.5	1.416764	-0.00042	211.4604	9.554223	0.73407
3	1.539996	0.000874	299.4645	15.63434	0.763361
3.5	1.571489	0.002344	411.6932	20.97448	0.722571
4	1.551575	0.002887	462.3979	23.15186	0.699576
4.5	1.543516	0.003078	485.5971	23.873	0.699523
5	1.539284	0.003028	503.5295	24.5569	0.698779
5.5	1.534729	0.003146	514.4922	24.71417	0.700529
6	1.533397	0.003088	518.6528	24.84287	0.701078
6.5	1.620137	0.003938	510.7005	26.7985	0.737961
7	1.741331	0.006068	616.9532	32.25163	0.835425
7.5	1.739359	0.006909	680.6705	34.1517	0.845774
8	1.736741	0.006756	694.4974	34.58373	0.843184
8.5	1.733015	0.007005	704.9597	34.96761	0.854766
9	1.730535	0.007134	701.495	34.65531	0.84835
9.5	1.727119	0.007172	707.5322	35.35375	0.858623
10	1.72417	0.007135	707.5246	35.2713	0.851572
10.5	1.721873	0.007203	708.0086	35.21163	0.855831
11	1.71955	0.007245	708.9183	35.40977	0.860187
11.5	1.717638	0.007344	711.3151	35.61386	0.861525
12	1.750211	0.007529	713.7284	35.90531	0.866004
12.5	1.995506	0.012766	796.497	45.1478	1.010089
13	2.099329	0.017185	956.8466	51.33942	1.076627
13.5	2.141881	0.020374	1097.933	56.02275	1.122268
14	2.138203	0.020499	1105.925	56.1691	1.121669
14.5	2.135098	0.0211	1112.172	56.24672	1.123586
15	2.132599	0.020786	1117.709	56.39106	1.122336
15.5	2.130609	0.020886	1116.857	56.73106	1.124605
16	2.128706	0.021321	1119.9	56.79595	1.130607
16.5	2.126528	0.021045	1122.255	56.60673	1.126572
17	2.125003	0.021017	1122.318	57.18227	1.131536
17.5	2.122876	0.021341	1126.232	56.79367	1.129525
18	2.123645	0.020743	1125.153	57.32098	1.135059
18.5	2.261691	0.024855	1126.844	60.97446	1.185457
19	2.415407	0.033057	1309.169	69.352	1.273713
19.5	2.48627	0.041624	1477.424	76.29863	1.344029

20	2.476968	0.04058	1502.206	77.06581	1.344997
20.5	2.470954	0.041016	1513.998	77.44336	1.354833
21	2.470594	0.04057	1513.769	77.3055	1.345897
21.5	2.469703	0.039854	1515.028	77.52631	1.355086
22	2.464709	0.040962	1521.113	77.87882	1.35422
22.5	2.465641	0.040632	1517.923	77.46995	1.34942
23	2.463508	0.039908	1519.316	77.76078	1.356049
23.5	2.460843	0.040398	1527.592	78.01517	1.358078
24	2.56052	0.04404	1529.435	81.02398	1.39017
24.5	2.671	0.053691	1683.764	87.886	1.459284
25	2.758252	0.062047	1803.741	93.9433	1.511859
25.5	2.828993	0.070307	1897.529	99.68732	1.563763
26	2.812265	0.069941	1949.038	100.303	1.569444
26.5	2.806275	0.070013	1958.287	100.3805	1.568721
27	2.800469	0.069406	1958.549	101.2216	1.575831
27.5	2.792982	0.068673	1972.335	101.4294	1.577282
28	2.787095	0.069737	1982.309	101.8064	1.582373
28.5	2.78493	0.06891	1976.569	101.9437	1.58538
29	2.78326	0.069192	1990.201	101.8282	1.582634
29.5	2.782582	0.068338	1985.973	101.8896	1.580871
30	2.782732	0.067869	1979.273	102.192	1.58337
30.5	2.77707	0.068235	1991.779	102.2566	1.588046
31	2.774626	0.067839	1986.285	102.013	1.583519
31.5	2.787081	0.068478	1989.606	102.2958	1.5845
32	2.878106	0.076186	2016.897	106.7652	1.63008
32.5	2.937477	0.082448	2095.855	109.9105	1.655443
33	2.929197	0.083428	2173.192	111.7138	1.665984
33.5	2.927207	0.083366	2174.575	111.5945	1.670118
34	2.924794	0.083072	2170.807	111.5809	1.664626
34.5	2.926926	0.083021	2174.1	111.5949	1.66714
35	2.928421	0.082852	2168.459	111.216	1.665306
35.5	2.922898	0.082775	2165.145	111.1984	1.665043
36	2.918686	0.082851	2164.873	111.3739	1.663182
36.5	2.925885	0.082068	2166.503	111.086	1.662405
37	2.983968	0.086658	2161.38	113.2826	1.684819
37.5	3.035385	0.092226	2245.997	115.593	1.707783
38	3.052139	0.096415	2307.673	117.5229	1.728933
38.5	3.050472	0.095747	2319.844	117.6705	1.729995
39	3.046982	0.096295	2315.919	117.6054	1.731634
39.5	3.046501	0.096102	2307.606	117.4768	1.730826

40	3.039693	0.096038	2319.116	117.4631	1.72961
40.5	3.042594	0.09704	2325.476	117.638	1.728609
41	3.047288	0.097004	2304.921	117.5163	1.728203
41.5	3.043705	0.096901	2314.043	117.5489	1.730379
42	3.044554	0.095726	2314.134	117.4856	1.729519
42.5	3.043615	0.095601	2315.148	117.3472	1.728058
43	3.039432	0.095255	2307.485	117.4764	1.730735
43.5	3.044035	0.094782	2305.994	117.205	1.722839
44	3.04659	0.094919	2306.825	116.9016	1.722066
44.5	3.046256	0.095451	2306.909	117.148	1.725867
45	3.031176	0.094301	2297.913	116.6276	1.715247
45.5	2.967739	0.088102	2259.978	114.8532	1.694785
46	2.890908	0.079436	2181.832	109.583	1.648493
46.5	2.800918	0.070309	2084.905	104.1008	1.595969
47	2.700557	0.060652	1983.925	97.79406	1.545273
47.5	2.573223	0.050646	1866.958	90.76817	1.475374
48	2.442469	0.041328	1710.296	82.79095	1.395718
48.5	2.306961	0.032278	1537.086	73.61994	1.303806
49	2.173707	0.025534	1366.654	65.7361	1.218192
49.5	2.018481	0.018209	1183.801	56.03523	1.103694
50	1.85441	0.012738	999.7389	46.28003	0.984633
50.5	1.69484	0.008186	826.7096	37.66182	0.867105
51	1.545244	0.005451	666.8964	30.31252	0.764804
51.5	1.347352	0.002444	533.409	22.39875	0.620339
52	1.106837	0.000594	363.8878	14.68229	0.463181
52.5	0.888974	-0.00052	245.6944	8.258012	0.314677
53	0.628053	-0.00017	94.79076	2.806947	0.150599
53.5	0.315052	0.000502	0	0	0.02737
54	0.107726	-0.0018	0	0	0.027846
54.5	0.013053	-0.00302	0	0	0.027844
55	-0.00167	-0.00324	0	0	0.027852
55.5	-0.00604	-0.0033	0	0	0.027907
56	-0.00686	-0.00326	0	0	0.027948
56.5	-0.00725	-0.00326	0	0	0.027848
57	-0.0074	-0.00326	0	0	0.02794
57.5	-0.00746	-0.0033	0	0	0.027621

Table 8.5 Experimental data (nine-bulb load) - 1

Experimental Data (Nine-bulb Load) - 1					
Time (s)	Supply Pressure (bar)	Exhaust Pressure (bar)	Volumetric Flow rate (L/min)	AC Voltage	AC Current (A)
0	0.005188	-0.0054	0	0	0.043574
0.5	0.095004	-0.00392	0	0	0.048105
1	0.1797	-0.00242	0	0	0.04958
1.5	0.356894	0.000377	0	0	0.056779
2	0.506923	0.002717	0	0	0.061978
2.5	0.519587	0.003012	0	0	0.064029
3	0.608937	0.004289	0	0	0.076277
3.5	0.884783	0.000796	0	0	0.320197
4	0.930257	-0.0003	0	0	0.26896
4.5	1.033023	-0.00318	0	0	0.573836
5	1.022305	-0.00231	0	0	0.264084
5.5	0.942705	-0.0013	0	0	0.439059
6	1.05446	-0.00311	0	0	0.435232
6.5	0.915414	-0.00091	0	0	0.417494
7	1.047966	-0.00295	0	1.638836	0.422645
7.5	0.906877	-0.00081	0	0	0.396038
8	1.031244	-0.00249	0	1.827338	0.417444
8.5	0.931274	-0.00136	0	1.788401	0.413955
9	0.975587	-0.00119	0	1.559241	0.377815
9.5	0.982711	-0.00252	0	2.180144	0.468172
10	0.905546	-0.00013	0	0	0.302489
10.5	1.051253	-0.00364	98.83056	2.606353	0.461867
11	0.888637	-0.00045	0	1.545244	0.331797
11.5	1.010829	-0.00146	0	2.581815	0.414303
12	1.012966	-0.0027	0	2.955947	0.46021
12.5	0.928512	-0.00078	0	1.848836	0.344254
13	0.989376	-0.00087	80.25327	2.855781	0.412122
13.5	1.056922	-0.00301	120.018	3.333644	0.441596
14	0.988733	-0.00145	101.2343	3.394661	0.440139
14.5	1.001466	-0.0011	82.5536	3.232126	0.407268
15	1.011528	-0.00114	98.96945	3.36782	0.438952

15.5	1.012365	-0.00101	100.3624	3.771229	0.418098
16	1.095552	-0.00141	139.0112	4.347723	0.475267
16.5	1.278793	-0.0012	194.5311	7.11216	0.665628
17	1.230722	4.97E-05	166.028	7.201364	0.617193
17.5	1.27119	-0.0008	216.8366	8.051936	0.636578
18	1.233815	-0.00041	200.1233	8.235826	0.627285
18.5	1.231483	7.29E-05	186.2624	8.523651	0.596342
19	1.247808	-1.21E-05	232.7557	8.824285	0.621249
19.5	1.253052	-0.00094	207.9947	8.896399	0.60761
20	1.228987	-0.00022	209.7272	8.753628	0.602039
20.5	1.229742	0.000155	195.9062	8.848007	0.588096
21	1.232767	0.000151	219.2872	9.102091	0.606399
21.5	1.251042	-0.0003	238.7797	9.348263	0.611851
22	1.24018	-0.00085	212.5165	9.144224	0.613586
22.5	1.226451	-0.00023	197.4654	8.863415	0.598792
23	1.227323	-2.47E-06	198.4144	8.947354	0.584716
23.5	1.228853	0.000126	221.8996	9.242324	0.604609
24	1.244367	-0.00012	240.4123	9.377297	0.619369
24.5	1.243126	-0.00086	212.9768	9.104102	0.603031
25	1.225332	-0.00016	213.3012	9.022593	0.597011
25.5	1.225262	-3.72E-05	199.0047	9.096487	0.588252
26	1.225393	-1.18E-06	222.4779	9.253456	0.611724
26.5	1.23511	9.99E-05	240.4879	9.143777	0.616023
27	1.249849	-0.00071	240.7818	9.272186	0.595275
27.5	1.436648	0.001159	237.513	12.42041	0.765442
28	1.515395	0.002389	348.3721	15.03292	0.849608
28.5	1.510168	0.002316	364.2536	15.96498	0.83688
29	1.505792	0.002474	351.22	16.16893	0.830997
29.5	1.503354	0.002482	354.6098	16.27186	0.829117
30	1.502834	0.002519	355.5823	16.29532	0.828016
30.5	1.50206	0.002533	375.7488	16.32458	0.825809
31	1.501939	0.002404	376.1141	16.36573	0.82532
31.5	1.501457	0.002475	376.7615	16.42941	0.825271
32	1.501542	0.002461	376.1221	16.47974	0.826984
32.5	1.501487	0.002457	376.6305	16.51386	0.829512
33	1.501439	0.002414	376.5508	16.47764	0.832721
33.5	1.50099	0.002515	376.9303	16.41186	0.830468
34	1.500638	0.002448	376.9849	16.36728	0.827841
34.5	1.500284	0.002451	371.6881	16.3987	0.82585
35	1.500027	0.002536	371.8237	16.50441	0.826888

35.5	1.500417	0.002528	372.6746	16.62287	0.83304
36	1.66982	0.004137	376.4985	19.50826	0.948278
36.5	1.748927	0.006232	490.8695	23.51912	1.048092
37	1.748545	0.006278	527.1245	24.37076	1.052984
37.5	1.750343	0.006573	528.9341	24.42404	1.032089
38	1.740657	0.006599	520.0082	24.67458	1.050549
38.5	1.747104	0.006384	534.9475	24.53956	1.036958
39	1.744454	0.006872	518.0581	24.67963	1.052571
39.5	1.742866	0.006276	534.9573	24.637	1.031127
40	1.747651	0.006446	532.6365	24.65397	1.050774
40.5	1.738298	0.00662	523.3315	24.90893	1.046664
41	1.744293	0.006481	536.9233	24.61353	1.041283
41.5	1.74107	0.006901	521.745	24.84888	1.055113
42	1.740148	0.006341	538.741	25.01072	1.044746
42.5	1.743972	0.006695	536.8719	24.8641	1.043241
43	1.735558	0.006443	527.7273	24.78312	1.048635
43.5	1.743448	0.006647	538.9159	25.10291	1.059352
44	1.784512	0.00712	528.1817	25.65688	1.068707
44.5	1.987098	0.010691	607.1043	31.45841	1.23473
45	2.064459	0.01404	736.8709	36.73323	1.337202
45.5	2.059896	0.014366	780.8477	37.42889	1.332247
46	2.056677	0.014447	774.8045	37.52577	1.332432
46.5	2.057158	0.014311	788.1292	37.67143	1.337351
47	2.054194	0.014326	778.0568	37.61317	1.334178
47.5	2.056275	0.0144	786.6928	37.66143	1.334696
48	2.051679	0.014294	783.2493	37.76231	1.332323
48.5	2.054593	0.014559	789.2241	38.029	1.34116
49	2.049644	0.014475	784.3945	37.94468	1.345614
49.5	2.051477	0.014612	792.4942	37.77712	1.339318
50	2.050024	0.014193	793.964	37.97766	1.334119
50.5	2.048982	0.014348	784.7594	38.19813	1.345573
51	2.050102	0.014371	796.0799	37.88781	1.341527
51.5	2.070787	0.014929	787.6696	38.59865	1.353018
52	2.265503	0.020189	841.5861	44.27773	1.489802
52.5	2.277609	0.022398	979.9982	47.78967	1.541071
53	2.274291	0.022897	987.0537	48.06376	1.540779
53.5	2.274145	0.022549	989.7139	48.11961	1.537356
54	2.272914	0.022509	985.3696	48.1851	1.54156
54.5	2.2698	0.022248	988.0018	48.21642	1.540609
55	2.269108	0.022572	995.0802	48.23385	1.544385

55.5	2.269653	0.022382	988.9384	48.29754	1.539184
56	2.266282	0.022541	991.5262	48.42763	1.544258
56.5	2.265167	0.022191	1001.176	48.7061	1.548557
57	2.265777	0.022622	1000.251	48.6016	1.554348
57.5	2.263757	0.023117	994.8024	48.44053	1.547488
58	2.263743	0.022713	1004.108	48.90614	1.549406
58.5	2.263832	0.022702	1006.442	48.7805	1.558399
59	2.260402	0.022855	1001.465	48.90602	1.549495
59.5	2.26065	0.02278	1008.448	48.94121	1.561891
60	2.267511	0.022792	1004.137	49.35567	1.558898
60.5	2.37785	0.026061	1020.565	52.40368	1.627317
61	2.446972	0.031012	1133.27	56.79925	1.706782
61.5	2.442267	0.030941	1173.346	57.79444	1.711817
62	2.440394	0.030903	1180.903	57.74325	1.717933
62.5	2.438663	0.031792	1185.281	57.6924	1.711089
63	2.43733	0.031335	1186.284	58.1343	1.718883
63.5	2.435546	0.031354	1179.662	57.70435	1.713502
64	2.433159	0.031539	1181.535	58.14555	1.717858
64.5	2.433761	0.031438	1178.933	57.82508	1.720801
65	2.433533	0.031236	1179.9	58.1372	1.712383
65.5	2.431299	0.031209	1188.259	57.95359	1.721274
66	2.427971	0.031807	1189.051	58.48439	1.725871
66.5	2.424966	0.031706	1196.59	58.40933	1.722102
67	2.422541	0.031465	1198.766	58.49551	1.727601
67.5	2.420705	0.031389	1201.249	58.65464	1.730107
68	2.417664	0.031368	1205.453	58.90215	1.732627
68.5	2.41726	0.031223	1205.457	58.95015	1.733939
69	2.413195	0.031771	1207.881	59.19149	1.741514
69.5	2.409569	0.03172	1214.012	59.0968	1.739405
70	2.38055	0.031684	1211.567	59.05679	1.731427
70.5	2.194129	0.024348	1152.639	52.97342	1.609548
71	2.038759	0.018125	995.9953	45.83179	1.476002
71.5	1.885928	0.013206	850.9325	38.75233	1.331409
72	1.686629	0.008402	694.4609	31.06871	1.162149
72.5	1.527502	0.005025	570.0109	24.98889	1.009812
73	1.313061	0.002374	425.7922	17.80443	0.807871
73.5	1.094977	5.35E-05	304.9273	12.13519	0.630657
74	0.898422	-0.00242	223.7897	7.054546	0.438137
74.5	0.708562	-0.00245	81.21733	3.552648	0.262922
75	0.551173	-0.00327	0	2.369452	0.210506

75.5	0.17852	-0.00361	0	0	0.048528
76	0.042137	-0.00513	0	0	0.043247
76.5	0.000932	-0.00559	0	0	0.042015
77	-0.00391	-0.00561	0	0	0.042346
77.5	-0.00526	-0.00561	0	0	0.042908
78	-0.00584	-0.0056	0	0	0.042572

Table 8.6 Experimental data (nine-bulb load) - 2

Experimental Data (Nine-bulb Load) - 2					
Time (s)	Supply Pressure (bar)	Exhaust Pressure (bar)	Volumetric Flow rate (L/min)	AC Voltage	AC Current (A)
0	1.608289	0.000617	149.1262	4.717838	0.949046
0.5	1.749807	0.002055	183.4756	8.077468	1.040971
1	1.863328	0.003385	295.2067	13.28225	1.11826
1.5	1.956017	0.005144	394.3743	19.94048	1.102382
2	2.042953	0.007846	506.516	25.92257	1.148229
2.5	2.12964	0.010458	630.3815	31.3009	1.227743
3	2.282875	0.013915	696.0041	37.34895	1.349691
3.5	2.293891	0.015933	828.458	40.44988	1.387283
4	2.286774	0.016082	845.5559	40.87468	1.39681
4.5	2.282186	0.016321	856.557	41.44704	1.397843
5	2.276988	0.016402	865.2079	41.73412	1.413213
5.5	2.275036	0.016295	864.8441	42.19895	1.418267
6	2.269886	0.016434	869.525	42.53778	1.423936
6.5	2.267019	0.016695	878.6818	42.72397	1.432933
7	2.264365	0.016465	885.3938	42.60246	1.426455
7.5	2.261393	0.01669	880.9714	43.1963	1.436983
8	2.258057	0.016986	889.1654	42.85932	1.430092
8.5	2.257199	0.016794	887.1492	43.28488	1.444691
9	2.254	0.016945	892.9505	43.42636	1.438868
9.5	2.251675	0.0169	896.4801	43.37161	1.438131
10	2.248168	0.01699	892.6445	43.44114	1.442262

10.5	2.246181	0.017358	900.8591	43.61463	1.446231
11	2.244116	0.017166	896.1194	43.6308	1.446191
11.5	2.242446	0.017329	902.8101	43.70021	1.447248
12	2.239469	0.017303	898.3403	43.80143	1.449229
12.5	2.238222	0.017334	905.6739	43.91879	1.4529
13	2.245272	0.017555	900.4453	44.01641	1.457235
13.5	2.410377	0.021404	927.6044	48.67292	1.56145
14	2.465283	0.024455	1046.094	52.27166	1.610371
14.5	2.562619	0.028523	1134.303	56.71855	1.693836
15	2.654146	0.033095	1170.165	60.2369	1.75867
15.5	2.667333	0.034403	1274.574	63.119	1.797893
16	2.661203	0.035533	1286.385	63.30916	1.796578
16.5	2.657198	0.035909	1288.284	63.54448	1.802923
17	2.654977	0.035707	1291.155	63.62924	1.805619
17.5	2.653398	0.035683	1294.953	63.80526	1.802401
18	2.649575	0.036399	1301.527	64.28352	1.813667
18.5	2.648125	0.036548	1304.265	63.98096	1.812194
19	2.645948	0.036308	1308.473	64.55981	1.816988
19.5	2.645127	0.036286	1308.507	64.12907	1.809409
20	2.6433	0.036353	1307.892	64.53214	1.822164
20.5	2.641091	0.036486	1305.976	64.49004	1.813041
21	2.638816	0.036393	1308.171	64.33596	1.817016
21.5	2.64266	0.0364	1310.348	64.69623	1.825041
22	2.793577	0.042671	1326.587	69.4352	1.908626
22.5	2.866519	0.049092	1466.608	73.6035	1.964317
23	2.953301	0.05609	1567.579	78.88079	2.052236
23.5	3.028703	0.062043	1613.693	82.27573	2.094952
24	3.021438	0.063365	1685.223	83.70777	2.117159
24.5	3.021711	0.063292	1686.626	83.42144	2.114663
25	3.015538	0.06349	1697.285	84.13455	2.117689
25.5	3.013335	0.063766	1701.358	84.13581	2.120568
26	3.002364	0.064922	1709.423	84.56325	2.128789
26.5	3.00381	0.064615	1712.384	84.82519	2.131917
27	3.003285	0.064695	1712.691	84.92962	2.13625
27.5	2.997435	0.065296	1725.229	84.9274	2.13535
28	2.998874	0.06545	1717.555	85.37459	2.135379
28.5	2.996084	0.065122	1724.271	85.20043	2.142293
29	2.992731	0.066163	1726.719	85.57139	2.138937
29.5	2.995768	0.064869	1722.677	85.14145	2.140665
30	2.994467	0.065358	1726.744	85.56522	2.140006

30.5	2.993584	0.065999	1728.157	85.19911	2.139732
31	2.989902	0.065287	1729.158	85.73756	2.147798
31.5	3.045067	0.069269	1732.385	87.15671	2.166089
32	3.083651	0.072731	1790.43	89.00203	2.194041
32.5	3.118163	0.077248	1836.628	91.21595	2.229231
33	3.163071	0.082014	1849.122	93.26085	2.254216
33.5	3.16835	0.082861	1898.056	93.89072	2.262251
34	3.187227	0.083865	1912.227	94.97646	2.278273
34.5	3.186427	0.083331	1917.792	95.20206	2.278451
35	3.185001	0.083526	1922.859	95.50021	2.281308
35.5	3.181385	0.08466	1929.038	95.69673	2.290444
36	3.182299	0.08482	1929.289	95.43598	2.282659
36.5	3.182821	0.085309	1934.142	95.9898	2.289369
37	3.183325	0.085827	1938.842	95.49808	2.284931
37.5	3.179995	0.08654	1937.021	96.22786	2.2946
38	3.18133	0.087225	1939.458	95.75734	2.285005
38.5	3.181906	0.086345	1937.09	95.9758	2.294303
39	3.18501	0.085716	1937.084	95.78918	2.283044
39.5	3.184914	0.086346	1933.04	95.86388	2.29407
40	3.176489	0.086367	1946.703	96.36188	2.295438
40.5	3.181779	0.085833	1942.743	95.87639	2.284769
41	3.185704	0.086825	1934.896	95.79406	2.293492
41.5	3.180556	0.087277	1932.795	96.23681	2.291913
42	3.180118	0.086189	1942.698	95.7873	2.286612
42.5	3.188304	0.086971	1940.225	96.3552	2.298452
43	3.192473	0.087761	1956.359	96.79039	2.300341
43.5	3.196904	0.089735	1953.157	96.92559	2.304134
44	3.20195	0.089303	1953.219	96.94801	2.308579
44.5	3.199607	0.08921	1962.635	97.06812	2.30254
45	3.203755	0.090284	1963.67	97.38853	2.31241
45.5	3.206805	0.089222	1957.922	96.97386	2.304744
46	3.208387	0.087618	1966.933	97.27265	2.306004
46.5	3.213358	0.088359	1961.981	96.92933	2.307553
47	3.213922	0.087705	1954.996	96.90093	2.302051
47.5	3.218462	0.087652	1959.854	97.13803	2.304848
48	3.223432	0.08967	1958.089	96.91881	2.307096
48.5	3.2396	0.08902	1953.207	96.78015	2.303777
49	3.26054	0.088499	1962.447	97.11087	2.302352
49.5	3.271144	0.089353	1971.877	97.3497	2.314626
50	3.279301	0.088041	1970.226	97.70866	2.312198

50.5	3.278603	0.088498	1979.61	97.53444	2.310431
51	3.286249	0.087796	1966.48	97.35635	2.31483
51.5	3.283405	0.087488	1972.576	97.7779	2.316442
52	3.405671	0.094617	1975.532	99.83394	2.34954
52.5	3.660094	0.126094	2155.977	111.9501	2.511923
53	3.649494	0.131632	2313.216	114.4781	2.540736
53.5	3.641005	0.130805	2317.775	114.3133	2.536903
54	3.646821	0.13168	2318.871	114.4369	2.533866
54.5	3.650189	0.129359	2327.761	114.9075	2.544923
55	3.656902	0.129474	2324.386	114.605	2.53827
55.5	3.669159	0.127042	2323.305	115.0392	2.547966
56	3.677573	0.128557	2333.172	114.7675	2.538841
56.5	3.685951	0.128537	2327.572	114.8818	2.547964
57	3.679001	0.127437	2331.766	115.2444	2.548627
57.5	3.680576	0.128216	2332.916	115.0292	2.543035
58	3.68538	0.127942	2328.832	114.7873	2.544264
58.5	3.675544	0.131135	2339.059	115.3264	2.551655
59	3.672803	0.129734	2339.89	115.4872	2.552657
59.5	3.675827	0.129419	2342.078	115.5709	2.555375
60	3.677768	0.127947	2346.125	115.598	2.558479
60.5	3.676558	0.12931	2345.019	115.4495	2.557697
61	3.671016	0.128591	2354.514	115.7028	2.554408
61.5	3.674091	0.127003	2347.82	115.8786	2.563945
62	3.665342	0.126599	2359.746	115.5191	2.554603
62.5	3.651728	0.122573	2345.108	115.3063	2.550767
63	3.631946	0.120394	2323.952	114.5072	2.534133
63.5	3.595323	0.115582	2298.075	113.1912	2.516551
64	3.550892	0.10962	2253.022	110.8388	2.486473
64.5	3.499247	0.106858	2209.394	108.6832	2.457259
65	3.453762	0.098498	2145.024	105.6436	2.418618
65.5	3.455732	0.099124	2128.078	105.1766	2.415397
66	3.448725	0.097969	2129.484	105.3818	2.417829
66.5	3.444319	0.096651	2126.848	105.4445	2.418677
67	3.44476	0.097118	2127.139	105.4071	2.417987
67.5	3.438392	0.097762	2135.735	105.4606	2.418425
68	3.379312	0.092561	2130.955	103.6883	2.395949
68.5	3.296418	0.083616	2072.138	100.2523	2.341213
69	3.195719	0.075553	1994.21	95.66572	2.287176
69.5	3.084758	0.066158	1885.262	90.64181	2.21135
70	2.974051	0.056362	1780.987	85.42839	2.130722

70.5	2.892853	0.049943	1669.483	80.46704	2.067556
71	2.906919	0.048426	1614.596	79.62965	2.054358
71.5	2.906005	0.049488	1615.179	79.44054	2.057659
72	2.908975	0.048754	1605.934	79.56331	2.055613
72.5	2.915279	0.048558	1596.224	78.77494	2.046765
73	2.910856	0.04965	1602.173	78.90194	2.044242
73.5	2.912951	0.048844	1596.044	79.06056	2.04717
74	2.909951	0.048605	1598.121	78.94553	2.050371
74.5	2.908937	0.049345	1597.121	78.74508	2.048019
75	2.908563	0.049087	1593.663	78.71121	2.04271
75.5	2.802231	0.044414	1589.026	75.64231	1.988857
76	2.697761	0.037475	1466.304	70.70215	1.913499
76.5	2.569983	0.031312	1380.191	64.99912	1.819287
77	2.446186	0.025763	1266.552	59.14858	1.722033
77.5	2.308335	0.020304	1145.302	53.06206	1.608798
78	2.167669	0.015838	1017.658	47.6091	1.504078
78.5	2.073048	0.011813	865.3193	41.08382	1.39243
79	2.075301	0.011747	834.7951	40.39748	1.38207
79.5	2.076277	0.011598	829.4309	39.90729	1.375909
80	2.073364	0.011567	829.6104	40.19571	1.389323
80.5	2.073251	0.011557	829.0306	40.29068	1.382354
81	2.07421	0.011196	832.0609	39.77414	1.373038
81.5	2.072774	0.011596	832.2493	40.09592	1.386385
82	2.071015	0.011681	828.3495	39.99121	1.373739
82.5	2.069656	0.011697	829.8706	39.85005	1.383787
83	2.073066	0.011628	826.013	39.76359	1.367563
83.5	2.071602	0.011719	820.2853	39.74287	1.381402
84	2.070319	0.011868	818.8086	39.54307	1.368062
84.5	1.909679	0.009272	817.8034	36.06439	1.276233
85	1.756363	0.006211	664.368	29.87176	1.139551
85.5	1.587477	0.004119	562.9536	24.45129	0.994722
86	1.459877	0.002197	432.91	19.25685	0.869598
86.5	1.284356	0.00109	377.3915	15.32655	0.741335
87	1.076535	-0.00015	277.665	10.31112	0.570208
87.5	0.920912	-0.00065	192.5223	7.181233	0.459681
88	0.777301	-0.00132	125.9529	4.440943	0.328862
88.5	0.661404	-0.00193	0	1.992887	0.193126
89	0.456818	-0.00121	0	0	0.126449
89.5	0.078664	-0.00147	0	0	0.026084
90	0.003414	-0.0023	0	0	0.026264

90.5	-0.00412	-0.00237	0	0	0.025836
91	-0.00572	-0.00241	0	0	0.025939
91.5	-0.00661	-0.00243	0	0	0.025895
92	-0.00693	-0.00234	0	0	0.026275
92.5	-0.00708	-0.00237	0	0	0.025692
93	-0.00712	-0.00232	0	0	0.025841